

W. HANKEY

Re-Entry Aerodynamics

 **AIAA**
Education Series

J. S. PRZEMIENIECKI EDITOR-IN-CHIEF

Re-Entry Aerodynamics

Wilbur L. Hanky
Wright State University
Dayton, Ohio



AIAA EDUCATION SERIES
J. S. Przemieniecki
Series Editor-in-Chief
Air Force Institute of Technology
Wright-Patterson Air Force Base, Ohio

Published by
American Institute of Aeronautics and Astronautics Inc.,
370 L'Enfant Promenade SW, Washington, DC 20024

Text Published In the AIAA Education Series**Re-Entry Vehicle Dynamics**

Frank J. Regan, 1984

Aerothermodynamics of Gas Turbine and Rocket Propulsion

Gordon C. Oates, 1984

Aerothermodynamics of Aircraft Engine Components

Gordon C. Oates, Editor, 1985

Fundamentals of Aircraft Combat Survivability Analysis and Design

Robert E. Ball, 1985

Intake Aerodynamics

J. Seddon and E. L. Goldsmith, 1985

Composite Materials for Aircraft Structures

Brian C. Hoskin and Alan A. Baker, Editors, 1986

Gasdynamics: Theory and Applications

George Emanuel, 1986

Aircraft Engine Design

Jack D. Mattingly, William Heiser, and Daniel H. Daley, 1987

An Introduction to The Mathematics and Methods of Astrodynamics

Richard H. Battin, 1987

Radar Electronic Warfare

August Golden Jr., 1988

Advanced Classical Thermodynamics

George Emanuel, 1988

Aerothermodynamics of Gas Turbine and Rocket Propulsion, Revised and Enlarged

Gordon C. Oates, 1988

American Institute of Aeronautics and Astronautics, Inc.**Washington, DC****Library of Congress Cataloging in Publication Data**

Hankey, Wilbur, L.

Re-entry aerodynamics.

(AIAA education series)

Includes index.

I. Space vehicles—Atmospheric entry. I. Title.

II. Series.

TL1060.H36 1988 629.4' 152 87-37369

ISBN 0-930403-33-9

Copyright © 1988 by the American Institute of Aeronautics and Astronautics, Inc. All rights reserved. Printed in the United States of America. No part of this publication may be reproduced, distributed, or transmitted, in any form or by any means, or stored in a data base or retrieval system, without the prior written permission of the publisher.

FOREWORD

Wilbur L. Hankey's text, *Re-Entry Aerodynamics*, which grew from his lectures in a graduate-level course on hypersonics at the Air Force Institute of Technology, summarizes current theories for the analysis of aerodynamic flow about bodies or vehicles re-entering the Earth's atmosphere. It represents a welcome addition to the AIAA Education Series because of the renewed interest in extending the sustained flight regime well into the hypersonic range—as in the National Aerospace Plane (NASP) project. Hankey's book is a companion volume to the first text published in the AIAA Education Series, *Re-Entry Vehicle Dynamics* by Frank J. Regan.

Dr. Hankey's first chapter treats the kinetic theory of gases as an introduction to the transport phenomena in re-entry, including three flight regimes: continuum flow, slip flow, and free molecule flow. His second chapter discusses some of the fundamental concepts for trajectory analysis of re-entering vehicles. The third chapter introduces hypersonics, including the various approximations used to simplify the Navier-Stokes equations characterizing aerodynamic flow. The fourth chapter deals extensively with the re-entry heating and means of alleviating its effects.

Dr. Hankey has written a textbook that provides the overall background for analysis of aerodynamic flow of re-entering bodies and vehicles throughout the whole range of flow regimes. The text reflects his extensive knowledge of the field and his many years of experience as a senior research scientist in his previous positions with the Aerospace Research Laboratories and the Air Force Flight Dynamics Laboratory at Wright-Patterson Air Force Base, Ohio.

J. S. PRZEMIENIECKI
Editor-in-Chief
AIAA Education Series

This page intentionally left blank

TABLE OF CONTENTS

vii Preface

1 Nomenclature

3 Chapter 1. Re-Entry Flight Regimes

- 1.1 Introduction
- 1.2 Atmosphere
- 1.3 Kinetic Theory of Gases
- 1.4 Dimensional Analysis
- 1.5 Free Molecule Flow Heating
- 1.6 Slip Flow Regime

Problems

23 Chapter 2. Flight Mechanics

- 2.1 Trajectory Analysis
- 2.2 Range Modulation
- 2.3 Stability Analysis

Problems

51 Chapter 3. Hypersonic Aerodynamics

- 3.1 Governing Equations
- 3.2 Aerodynamic Prediction Methods
- 3.3 Hypersonic Aerodynamic Characteristics
- 3.4 Hypersonic vs Subsonic Aerodynamics

Problems

81 Chapter 4. Re-Entry Heating

- 4.1 Simplified Analysis
- 4.2 Component Heating
- 4.3 Boundary-Layer Equations
- 4.4 Aerothermochemistry
- 4.5 Fay-Riddell Solution
- 4.6 Interference Heating
- 4.7 Ablation
- 4.8 Hot-Gas Radiation
- 4.9 Combined Forms of Heating

Problems

143 Index

This page intentionally left blank

PREFACE

Interest in re-entry phenomena arose suddenly in 1958 when the Russians launched the satellite Sputnik I. Hypersonic groups were formed throughout the country in DOD, NASA, and industry. Universities offered courses in hypersonics, rarefied gasdynamics, super-aerodynamics, celestial mechanics, and aerothermochemistry. Government, industry, and universities developed hypersonic facilities. Most existing hypersonic textbooks were written shortly afterwards, during the early '60s, including some of the chapters of this text. Then, just as suddenly, not long after the lunar landings, the nation became disenchanted with aerospace. Projects were canceled, fiscal budgets slashed, wind-tunnel facilities closed down, engineers laid off, and hypersonic groups disestablished. Students were advised not to enter engineering, and enrollments plummeted.

But in the '80s, with the Shuttle on line, a space station in the offing, a surge of funding for the Strategic Defense Initiative (SDI) and, more recently, goals set for a National Aerospace Plane (NASP), space developments and hypersonics regained their luster. Engineering enrollments have reached the highest level in history, and courses are again being taught in high-speed flight.

This renewed interest plus the encouragement of the Editor-in-Chief of the Education Series, John S. Przemieniecki, prompted the rewriting of *Re-Entry Aerodynamics*. The text, although introductory in nature, focuses attention on the critical aspects of re-entry, such as flight mechanics from low speed to orbital velocities, stability at high speeds, hypersonic aerodynamics, and re-entry heating.

For assistance in developing this modern text I want to thank professional associates at the Air Force Flight Dynamics Laboratory, Wright-Patterson Air Force Base, Ohio.

WILBUR L. HANKEY
Wright State University
Dayton, Ohio

NOMENCLATURE

a	= speed of sound, ft/s
a	= acceleration, ft/s ²
A	= area, ft ²
C_f	= skin-friction factor
C_D	= drag coefficient
C_L	= lift coefficient
C_i	= species concentration by mass
C_V	= specific heat at constant volume (air 4290), ft ² /s ² ·°R
C_p	= specific heat at constant pressure (air 6006), ft ² /s ² ·°R
C_1	= constant
D	= drag, lb
D	= diffusion coefficient, ft ² /s
e	= specific internal energy, ft ² /s ² , = $C_V T + V^2/2$
E	= total energy, ft · lbf = frequency, s ⁻¹
F	= force, lb
g	= acceleration on gravity, ft/s ²
h	= altitude, ft
h	= specific enthalpy, ft ² /s ²
H	= total enthalpy, ft ² /s ² , = $h + V^2/2$
i, j, k	= Cartesian unit vectors
J	= conversion factor 778, ft · lb/Btu
K	= thermal conductivity, Btu/ft · s · °R
Kn	= Knudsen number
L	= lift, lb
L	= length, ft
Le	= Lewis number
m	= mass, slug
\dot{m}	= mass flow rate, slug/s
M	= total mass, slug
M	= Mach number
\mathcal{M}	= molecular weight
N	= total number
Nu	= Nusselts number
p	= pressure, lb/ft ²

NOMENCLATURE

P	= period, s
\underline{P}	= stress tensor, lb/ft ²
Pr	= Prandtl number
\dot{q}	= heating rate/unit area, Btu/ft ² · s
Q	= heat energy, Btu
R	= gas constant (air 1716), ft ² /s ² · °R
R	= radius, ft
Re	= Reynolds number
S	= reference area, ft ²
St	= Stanton number
t	= time, s
T	= temperature, °R
u, V, w	= Cartesian velocity components, ft/s
V	= velocity, ft/s
V	= volume, ft ³
W	= weight, lb
x, y, z	= Cartesian coordinates, ft
α	= angle of attack, rad
α	= atmospheric altitude factor, ft ⁻¹
β	= ballistic coefficient, slug/ft ³
γ	= specific heat ratio (air 1.4), = C_p/C_V
γ	= flight path angle, rad
δ	= boundary-layer thickness, ft
ϵ	= emissivity
r, θ	= polar coordinates, ft · rad
λ	= mean free path, ft
λ	= second viscosity coefficient, = $-\frac{2}{3}\mu$, lb · s/ft ²
Λ	= sweep angle, rad
μ	= viscosity, lb · s/ft ²
ν	= kinematic viscosity, = μ/ρ , ft ² /s
ρ	= density, slug/ft ³
σ	= diameter of molecule, ft
σ	= Stephan-Boltzmann constant, = 0.481×10^{-12} , Btu/ft ² · s · °R ⁴
σ_{ij}	= normal stress, lb/ft ²
τ	= shear stress, lb/ft ²
ϕ	= potential function, ft ² /s
ω	= angular velocity, rad/s

1

**RE-ENTRY
FLIGHT REGIMES****1.1 INTRODUCTION**

Today, successful re-entry of space vehicles has become commonplace. This was not always so. John Glenn's first manned re-entry in 1962 was accomplished only after considerable research in high-speed aerodynamics and after many parametric studies to select the optimum design concept. This required a detailed study of the following areas: 1) aerodynamic heating and air loads, 2) vehicle stability, 3) guidance and control system to attain a specified landing site, and 4) landing characteristics.

The design analysis for both ballistic and lifting manned re-entry configurations is the main subject of this text. To achieve this end, several engineering disciplines must be covered, such as: flight mechanics, trajectory analysis, heat transfer, real gases and aerothermochemistry, ablation and hot gas radiation, stability analysis, hypersonics, and numerical analysis.

Thermal Barrier

Originally, the major concern of re-entry was to find a way to survive the aerodynamic heating.^{1,2} Many technologists believed it to be impossible and coined the label "thermal barrier," analogous to the "sonic barrier" of the previous generation of technologists who believed that flight beyond the speed of sound was not possible. Their fears may be comprehended by calculating the kinetic energy (KE) of an orbiting satellite from the expression

$$\text{KE} = \frac{1}{2} m V_c^2 \quad (1.1)$$

where m is the satellite mass and V_c its velocity. During re-entry, all this kinetic energy must be dissipated and converted into heat to decelerate the vehicle to zero velocity. This energy balance is

$$Q = \text{KE} = \frac{1}{2} \frac{W}{g} V_c^2 \text{ or } \frac{Q}{W} = \frac{V_c^2}{2g}$$

where Q is the dissipated heat, W the satellite weight, and g the gravitational constant.

Table 1.1 Energy Required to Vaporize Some Typical Materials

Material	Energy to vaporize, Btu/lb	Melting temperature, °R
Tungsten	1,870	6500
Titanium	3,865	3700
Beryllium oxide	13,400	2900
Graphite	28,700	6800

For V_c equal to the circular or orbital speed (26,000 ft/s)

$$Q/W = 1.05 \times 10^7 \text{ ft} \cdot \text{lb/lb} = 13,500 \text{ Btu/lb} \quad (1.3)$$

(Note: 1 Btu = 778 ft · lb.)

Table 1.1 shows the energy required to vaporize different materials. From this table, it is apparent there would not be much left of a re-entering vehicle (except for a solid graphite object) if all the heat went into the vehicle during re-entry.

Another condition to examine is the stagnation temperature T_0 on the nose of a re-entry vehicle as depicted in Fig. 1.1. The energy equation for this case is given by

$$C_p T_0 = C_p T_\infty + V_\infty^2/2 \quad (1.4)$$

where C_p is the specific heat at constant pressure and other quantities are defined in Fig. 1.1.

A hypersonic approximation to this equation is ($T_0 \gg T_\infty$)

$$T_0 = V_\infty^2/2C_p \quad (1.5)$$

The stagnation temperatures T_0 have been computed in Table 1.2 for several values of V_∞ for $C_p = 6006 \text{ ft}^2/\text{s}^2 \cdot ^\circ\text{R}$ representing a typical value for air. From this table, it is evident that the temperatures encountered are higher than any material can sustain.

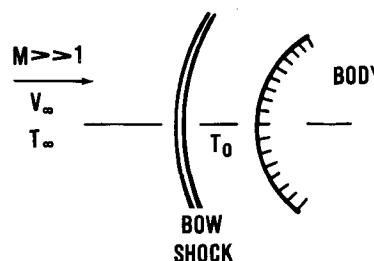


Fig. 1.1 Stagnation temperature on the nose of a re-entry vehicle.

RE-ENTRY FLIGHT REGIMES

Table 1.2 Stagnation Temperatures

V_∞ , ft/s	T_0 , °R
10,000	8,325
20,000	33,300
26,000	56,277

If this is the case, one concludes that a “thermal barrier” does exist. But, this is an erroneous conclusion. First, it was assumed that all the heat energy went into the body. When you briskly rub your hands together, both hands get warm. Similarly, during re-entry, both the vehicle and the surrounding air (which “rubs” over the body) get hot. The question is, how much energy goes into the body and how much goes into the wake of the air behind the body. To perform this analysis, one must examine the boundary layer through which the heat must pass into the body, as shown in Fig. 1.2. For this case, the heat flow is expressed as

$$\dot{Q}_B = A \left(k \frac{\partial T}{\partial y} \right)_w = St \rho A V (H_s - H_w) \quad (1.6)$$

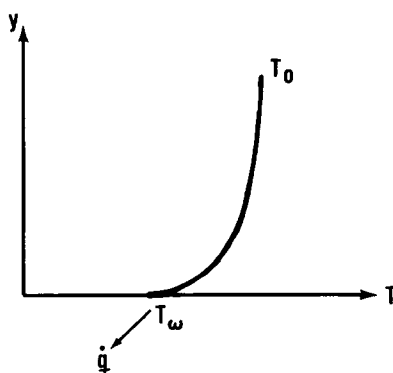
where A is the area, k the thermal conductivity, ρ the air density, V the air velocity, H_s the total enthalpy, H_w the wall enthalpy, and St the Stanton number.

The thermal energy flow rate of the airstream \dot{Q}_A is given by

$$\dot{Q}_A = \dot{m} H_s = \rho A V H_s \quad (1.7)$$

The ratio of these two heat-transfer rates is

$$\frac{\dot{Q}_B}{\dot{Q}_A} = \frac{St \rho A V (H_s - H_w)}{\rho A V H_s} \approx St \quad (1.8)$$

**Fig. 1.2 Boundary layer over the body vs temperature.**

From Reynolds analogy (the relationship between the Stanton number St and the friction coefficient C_f),

$$St = C_f/2 \approx 10^{-3} \quad (1.9)$$

Hence,

$$\dot{Q}_B = 10^{-3} \dot{Q}_A \quad (1.10)$$

This means that only a very small percentage of heat goes into the body since most of the energy is absorbed by the atmosphere.

This does not mean that there is no heating problem, because a small percentage of a big number still is appreciable. But it does show that it is possible to survive the re-entry heating. It is possible to design a thermal protection system from a wide variety of materials and successfully re-enter the atmosphere. There is no "thermal barrier," but there is a "thermal obstacle." The major problem is generally not the global amount of heat transfer into the vehicle, but the local "hot spots" that exist on the re-entry vehicle.

Thermal Protection Systems

In designing a thermal protection system, one must choose from two general approaches: *absorb* the energy that comes through the boundary layer or *reject* it. The absorbing systems include the *heat sink* method and the *ablation method*. In the heat sink method, the heat capacity of a large block of material is used to absorb the heat energy and the temperature rise ΔT is designed to remain below the melting point of the material so that no degradation of strength properties occurs. Hence, the energy balance is

$$Q = C_V m \Delta T \quad (1.11)$$

where C_V is the specific heat at constant volume. Materials are selected that have a high heat capacity and a high melting point. In addition, a high thermal diffusivity is necessary for the heat to rapidly flow into the block of material in order to minimize temperature gradients and prevent local surface melting. Beryllium and copper possess the necessary characteristics for good heat sink materials.

Ablation is also an absorbing method, although in this case, material is destroyed. The heat absorbed results in a change of phase of the substance. The equation for the energy balance in this case is

$$Q = h_V \Delta m \quad (1.12)$$

where h_V is the "heat of vaporization" of the material and Δm the mass loss through ablation. Materials having a high heat of vaporization are selected to minimize the amount of material ablated. Graphite and phenolics are current materials used on ballistic re-entry vehicles.

RE-ENTRY FLIGHT REGIMES

As a numerical example, the energy required to raise the temperature of water from just above freezing temperature until it is entirely boiled away will be computed. For water,

$$C_V = 1 \text{ Btu/lb} \cdot ^\circ\text{F}, h_V = 970 \text{ Btu/lb}$$

To raise 1 lb of liquid water from 32 to 212°F,

$$Q = C_V m \Delta T = \frac{(1 \text{ Btu})}{\text{lb} \cdot ^\circ\text{F}} (1 \text{ lb})(212 - 32)^\circ\text{F} = 180 \text{ Btu}$$

To boil this water at constant temperature,

$$Q = h_V \Delta m = 970 \frac{\text{Btu}}{\text{lb}} (1 \text{ lb}) = 970 \text{ Btu}$$

Note that over five times the energy is required to change the phase of the water from liquid to vapor as to raise the temperature from freezing to boiling. Likewise, ablation is a much more effective means of absorbing the heat as opposed to the heat sink method.

To *reject* the heat, we allow the temperature of the surface to rise until the thermal radiation leaving the surface equals the convective heat transfer coming in, i.e.,

$$\dot{q}_{in} = \dot{q}_{out} = \epsilon \sigma (T_2^4 - T_1^4) = \epsilon \sigma T_w^4 \quad (1.13)$$

where ϵ is the emissivity, σ the Stephan–Boltzmann constant, and $T_2 = T_w \gg T_1$. T_2 is referred to as the “radiation equilibrium temperature.” A possible design approach is to select a material having a high melting temperature and coat it with a substance having a high emissivity.

Refractory materials have high melting temperatures, as indicated in Table 1.3. In practice, these materials cannot be used much beyond 3000°R, since they oxidize and therefore must be coated. The coatings limit the temperature to well below the melting point. In addition, strength falls off rapidly at high temperatures, again limiting the application.

Using an upper limit of 4000°R and an upper limit on ϵ of 1.0, the maximum heating rate permitted for radiation equilibrium is:

$$\dot{q}_{max} = 1 \left(0.481 \times \frac{10^{-12} \text{ Btu}}{\text{ft}^2 \cdot \text{s} \cdot ^\circ\text{R}^4} \right) (4000^\circ\text{R})^4 = 123 \text{ Btu}/\text{ft}^2 \cdot \text{s}$$

Table 1.3 Melting Temperature of Refractory Materials

Material	Melting temperature, °R
Molybdenum	5200
Columbium	4000
Zirconium	3900

RE-ENTRY AERODYNAMICS

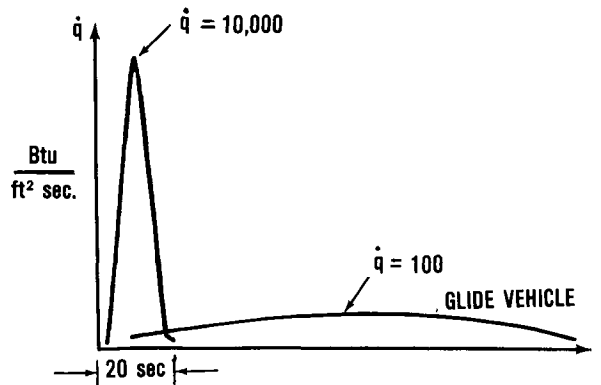


Fig. 1.3 Heating rate on the noses of different re-entry vehicles.

This constraint greatly limits the use of a *rejection*-type thermal protection system.

Histograms of the heating rate on the nose of two different types of re-entry vehicles are shown in Fig. 1.3. A ballistic missile has a profile of short duration with an intense heating rate peak. On the other hand, a glide vehicle re-entry is of a long duration with a relatively low peak heating rate. It should be observed, however, that the total heat energy can be comparable for both cases. A map of the domain where each thermal system applies for different applications is shown in Fig. 1.4 to help establish a better perspective.

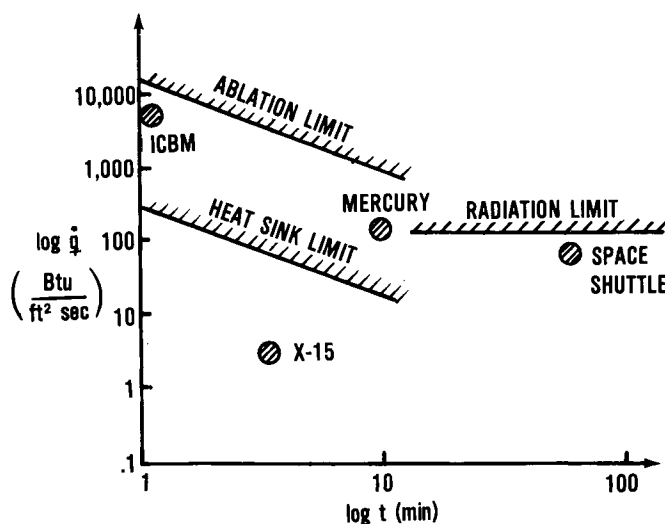


Fig. 1.4 Thermal system domains.

RE-ENTRY FLIGHT REGIMES

1.2 ATMOSPHERE

The U.S. Standard Atmosphere³ will be used to determine the upper atmospheric properties. A description of the primary features of the atmosphere will be presented in this section. Air is composed of the elements shown in Table 1.4.

The average molecular weight of this mixture of perfect gases is

$$\bar{M} = \sum C_i M_i = 28.966$$

The atmosphere is extremely thin, relative to the Earth radius ($R = 3959$ miles). At a 60 mile altitude, $\rho/\rho_{sl} = 10^{-6}$ and $\Delta h/R = 60/3959 = 0.015$, which is thinner relatively than an apple peel, compared to its core size.

Air can be analyzed as a long column that must obey Archimedes' principle of fluid statics. The incremental pressure dp can be expressed in terms of the density ρ and the gravitational constant g by the equation

$$dp = -\rho g dh \quad (1.14)$$

The pressure p is also expressible by

$$p = \rho RT \quad (1.15)$$

where R is the gas constant and T the temperature. Elimination of ρ in Eqs. (1.14) and (1.15) leads to

$$dp = -p \frac{g}{RT} dh \quad (1.16)$$

which can be integrated to give

$$\ell n\left(\frac{p}{p_{sl}}\right) = - \int \frac{g}{RT} dh \quad (1.17)$$

where p_{sl} is the sea level pressure. Thus, for a given temperature T as a function of the altitude h , the right-hand side of Eq. (1.17) can be integrated.

Table 1.4 Properties of Air

Element	Mass concentration C_i	Molecular weight M_i
N ₂	0.7809	28.016
O ₂	0.2095	32.000
Ar	0.0093	39.944
CO ₂	0.0003	44.010
ΣC_i	1.0000	

As an approximation, an isothermal case ($T = \bar{T}$) can be considered for which Eq. (1.17) becomes

$$\ln(p/p_{\text{sl}}) = -\alpha h \quad (1.18)$$

where

$$\alpha = g/R\bar{T} = 4.4 \times 10^{-5}/\text{ft} \quad (1.19)$$

Also from Eq. (1.15)

$$\frac{p}{p_{\text{sl}}} = \frac{\rho}{\rho_{\text{sl}}} \frac{R\bar{T}}{RT} = \frac{\rho}{\rho_{\text{sl}}} \quad (1.20)$$

Hence,

$$\rho/\rho_{\text{sl}} = e^{-\alpha h} \quad (1.21)$$

Clearly, the isothermal case ($T = \bar{T}$) may be used as an approximation for any subsequent re-entry computations.

1.3 KINETIC THEORY OF GASES

In dealing with the flow of air, information is needed concerning the thermodynamic properties of density, pressure, and temperature (ρ, p, T), as well as the air transport properties of diffusivity, viscosity, and thermal conductivity (D, μ, k). The basis for the understanding of these air properties, produced by many gas molecules in random motion, is contained in this section.

The approach used here⁴ to develop the concepts is classically described as the "Ultrasimplified Kinetic Theory of Gases." In this theory, one should appreciate that, although appropriate relationships will be derived, the numerical value of coefficients will be only approximate.

First, consider a cube of air with sides of length L containing N molecules. The velocity distribution is known to *Maxwellian*, in which all speeds are possible (see Fig. 1.5). Most molecules, however, are traveling

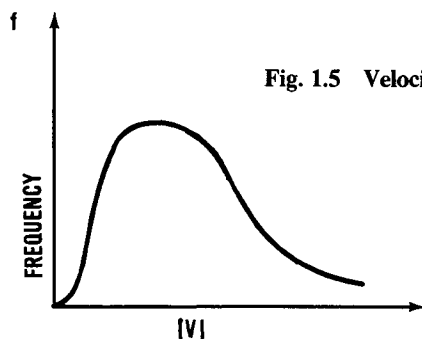


Fig. 1.5 Velocity distribution of molecules in a cube of air.

RE-ENTRY FLIGHT REGIMES

11

within $\pm 50\%$ of the most probable speed. Based upon this observation, a simple model of this molecular motion can be derived. The assumptions are

- 1) All molecules are identical rigid spheres of diameter σ and mass m .
- 2) All molecules possess the same speed \bar{V} , i.e., average molecular speed.
- 3) The molecules move equally in only three axes (x , y , z), i.e., $1/6N$ in each direction ($\pm x$, $\pm y$, $\pm z$), where N is the number of molecules.

Based on these simplifying assumptions, relationships for ρ , p , and T will now be derived.

The mass in the cube of air (or gas) is $M = N \times m$ and its volume is $V = L^3$. Hence, the density ρ is given by

$$\rho = M/V = Nm/V \quad (1.22)$$

Newton's second law for the collision of all the particles on one wall is given by

$$F\Delta t = M\Delta\bar{v} \quad (1.23)$$

where F is the total force acting on one wall and \bar{v} the average particle velocity.

Equaling the impulse to the change in momentum

$$F(L/\bar{v}) = (1/6)Nm[\bar{v} - (-\bar{v})]$$

Hence,

$$F = (Nm/3L)\bar{v}^2 \quad (1.24)$$

The pressure p can be expressed as

$$p = F/L^2 \quad (1.25)$$

Hence, substituting Eqs. (1.22) and (1.24) into Eq. (1.25) results in

$$p = \frac{1}{3}\rho\bar{v}^2 \quad (1.26)$$

The equation for the gas temperature T is derived from the equation of state $p = \rho RT$ and Eqs. (1.15) and (1.26), i.e.,

$$\rho RT = \frac{1}{3}\rho\bar{v}^2$$

Hence,

$$T = \bar{v}^2/3R \quad (1.27)$$

(A more precise analysis produces a result that $T = 0.392\bar{v}^2/R$.) The speed of sound a is related to temperature by the well-known expression

$$a = \sqrt{\gamma RT} \quad (1.28)$$

which can be used to determine the ratio of \bar{v}/a from Eq. (1.27). This leads to

$$\bar{v}/a = \sqrt{3/\gamma} = 1.35 \quad (1.29)$$

Therefore, the average molecular speed is approximately equal to the speed of sound.

Collision Frequency

To obtain the transport properties for the transport of mass, momentum, and energy, the collision frequency of the molecules is required. It is primarily through collisions that these basic quantities may be transported.

First, only collisions between molecules moving in the z direction will be considered, as depicted in Fig. 1.6. Any molecule moving inside the cylinder of radius σ at velocity $+2\bar{v}$ will collide with the stationary molecule. All others moving in the $+z$ direction will never collide with this molecule, as illustrated in Fig. 1.7. The number of molecules in this cylinder at any one time is

$$n(+z) = \frac{1}{6} N \frac{\pi \sigma^2 L}{L^3}$$

The frequency of these collisions is given by

$$f(+z) = \frac{n(+z)}{\Delta t} = \frac{(\pi/6)(N\sigma^2/L^2)}{L/2\bar{v}}$$



Fig. 1.6 Collisions between molecules moving in the z direction.

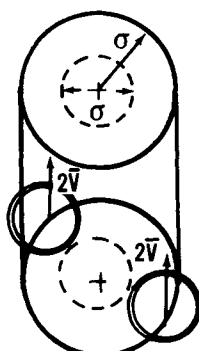


Fig. 1.7 Molecules moving inside the cylinder of radius σ at velocity $2\bar{v}$.

RE-ENTRY FLIGHT REGIMES

13

or

$$f(+z) = \frac{\pi \rho \sigma^2 \bar{v}}{3m} \quad (1.30)$$

Now consider collisions of this particle with molecules moving in the $+x$ direction (see Fig. 1.8). The frequency of these collisions is then given by

$$f(+x) = \frac{n(+x)}{\Delta t} = \frac{(\pi/6)(N\sigma^2/L^2)}{L/\sqrt{2}\bar{v}}$$

or

$$f(+x) = \frac{\sqrt{2}\pi\rho\sigma^2\bar{v}}{6m} \quad (1.31)$$

From symmetry $f(+x) = f(-x) = f(+y) = f(-y)$; therefore, the total collision frequency f is the sum of collision frequencies in all six directions,

$$\begin{aligned} f &= \sum f_i = f(-z) + f(+z) + 4f(+x) \\ f &= 0 + \frac{\pi\rho}{3m}\sigma^2\bar{v} + \frac{4\sqrt{2}}{6m}\pi\rho\sigma^2\bar{v} \end{aligned}$$

(Note that no molecules can collide with particles moving in a $-z$ direction since all travel at the same speed.) Hence,

$$f = \frac{\pi}{3}(1+2\sqrt{2})\frac{\rho\sigma^2\bar{v}}{m} \quad (1.32)$$

Of interest is the mean free path λ defined as the average distance traveled between collisions. The mean free path is also related to the mean molecular velocity and frequency of collision through the expression

$$\bar{v} = \lambda f \quad (1.33)$$

Hence, substituting Eq. (1.32) into Eq. (1.33)

$$\lambda = \frac{\bar{v}}{f} = \frac{m/\sigma^2}{(\pi/3)(1+2\sqrt{2})\rho} \quad (1.34)$$



Fig. 1.8 Molecules moving in the $+x$ direction.

or

$$\lambda = C_1 / \rho \quad (1.35)$$

where

$$C_1 = 3m/\pi\sigma^2(1 + 2\sqrt{2}). \quad (1.36)$$

This shows that the mean free path is inversely proportional to density. Examples of the actual values for the mean free path of air are the following: at sea level, $\lambda = 2.2 \times 10^{-7}$ ft; at 335,000 ft altitude, $\lambda = 1.0$ ft.

Transport Phenomena

Next, the transport properties of diffusivity, viscosity, and thermal conductivity (D, μ, k) will be evaluated.⁵ The methods for handling these three phenomena are so similar that they are most conveniently discussed as a group; they are often referred to under the title of *transport phenomena*. Table 1.5 lists the important features for the transport coefficients.

The exchange of momentum will be examined first. Consider a flow with a velocity gradient in the z direction of magnitude $\partial u / \partial z$ in which particles are moving across the field A in the xy plane as shown in Fig. 1.9.

The exchange of momentum as the particles pass through the field represents the impulse, i.e.,

Impulse = Δ Momentum

$$F\Delta t = M(U_b - U_a) \quad (1.37)$$

$$\tau L^2 \frac{L}{\bar{v}} = \frac{1}{6} Nm \left[\left(U_0 + \lambda \frac{\partial u}{\partial z} \right) - \left(U_0 - \lambda \frac{\partial u}{\partial z} \right) \right]$$

or

$$\tau = \frac{\lambda}{3} \frac{Nm}{L^3} \bar{v} \frac{\partial u}{\partial z} = \frac{\rho \bar{v} \lambda}{3} \frac{\partial u}{\partial z} \equiv \mu \frac{\partial u}{\partial z} \quad (1.38)$$

Table 1.5 Transport Properties

Conservation Relationship	Phenomenon	Gradient	Equation	Result
Mass	Diffusion D	Concentration $\frac{\partial C_i}{\partial z}$	$\dot{m}_i = \rho D_{ij} \frac{\partial C_i}{\partial z}$	Mass flux \dot{m}_i
Momentum	Viscosity μ	Velocity $\frac{\partial u}{\partial z}$	$\tau = \mu \frac{\partial u}{\partial z}$	Shear stress τ
Energy	Thermal conductivity k	Temperature $\frac{\partial T}{\partial z}$	$\dot{q} = k \frac{\partial T}{\partial z}$	Heat transfer \dot{q}

RE-ENTRY FLIGHT REGIMES

15

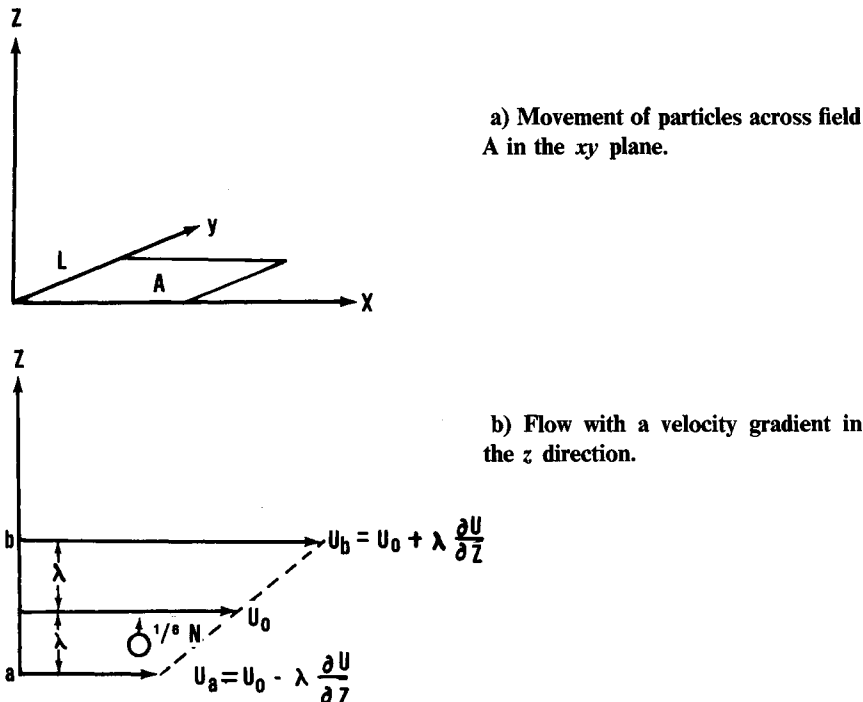


Fig. 1.9 Example of the exchange of momentum.

where the viscosity μ is defined as

$$\mu = \rho \bar{v} \lambda / 3 \quad (1.39)$$

Consider next a temperature gradient in place of a velocity gradient (see Fig. 1.10). As particles move across the field A,

Heat transfer = Change in internal energy

$$Q = M(e_b - e_a) \quad (1.40)$$

$$\dot{q}A \Delta t = (1/6)Nm(C_v T_b - C_v T_a)$$

$$\dot{q} = \frac{1}{6} \frac{Nm\bar{v}C_v}{L^3} \left[\left(T_0 + \lambda \frac{\partial T}{\partial z} \right) - \left(T_0 - \lambda \frac{\partial T}{\partial z} \right) \right]$$

$$\dot{q} = \frac{\rho \bar{v} \lambda C_v}{3} \frac{\partial T}{\partial z} \equiv k \frac{\partial T}{\partial z} \quad (1.41)$$

where the thermal conductivity k is defined as

$$k = (\rho \bar{v} \lambda / 3) C_v = \mu C_v \quad (1.42)$$

A gradient in species concentration can be examined in a similar manner (see Fig. 1.11). As particles move across the field A, they will transport mass of one species into a new region. The governing equation becomes

$$\text{Flux rate} \times \Delta t = \text{change of mass}$$

$$\dot{m}_i A \Delta t = M(C_{ib} - C_{ia}) \quad (1.43)$$

$$\dot{m}_i = \frac{1}{6} \frac{Nm}{L^3} \bar{v} \left[\left(C_{i0} + \lambda \frac{\partial C_i}{\partial z} \right) - \left(C_{i0} - \lambda \frac{\partial C_i}{\partial z} \right) \right]$$

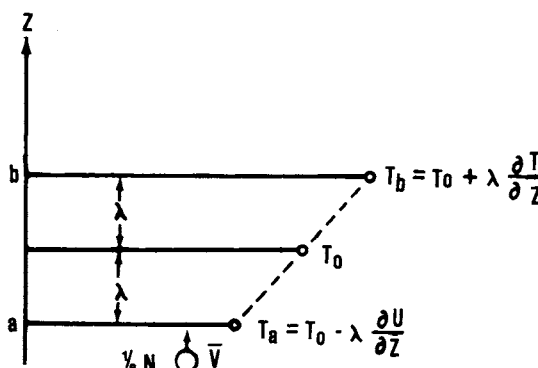


Fig. 1.10 Temperature gradient in the z direction.

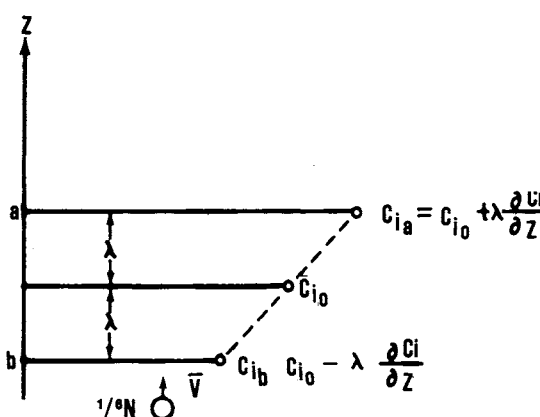


Fig. 1.11 Gradient in species concentration in the z direction.

RE-ENTRY FLIGHT REGIMES

17

$$m_i = \left(\rho \frac{\bar{v}\lambda}{3} \right) \frac{\partial C_i}{\partial z} \equiv \rho D \frac{\partial C_i}{\partial z} \quad (1.44)$$

where the diffusion coefficient D is given by

$$D = \bar{v}\lambda/3 = \mu/\rho = \nu \quad (1.45)$$

The various properties of air and several gases found in the Earth's atmosphere are given in Tables 1.6 and 1.7.

Table 1.6 Comparison of "Ultrasimplified" Results with Actual Values for Air

Simple results	Actual values for air
$\bar{v}^2/RT = \frac{1}{3} = 0.333$	0.392
$\mu = \frac{\rho \bar{v} \lambda}{3} = \frac{m/\sigma^2 \sqrt{3RT}}{\pi(1 + 2\sqrt{2})}$	
$\mu = C\mu\sqrt{T}$	$\frac{C\mu\sqrt{T}}{1 + S/T}$ where: $S = 198.6^\circ R$ $C\mu = 2.270 \times 10^{-8} \text{ lb} \cdot \text{s}/\text{ft}^2$
Prandtl number	
$Pr = \frac{\mu C_p}{k} = \frac{\mu C_p}{\mu C_v} = \gamma$	0.72
Lewis number	
$Le = \frac{\rho D C_p}{k} = \frac{\mu C_p}{k} = \gamma$	1.40

Table 1.7 Properties of Gases

Gas	M	γ	$\bar{v},$ 10^3 cm/s	$a,$ 10^3 cm/s ($T = 15^\circ \text{C}$)	$\mu,$ $10^{-7} \text{ dyne} \cdot \text{s/cm}$	$k,$ $10^{-3} \text{ cal} \cdot \text{m/s} \cdot \text{K}$	$Pr =$ $\mu C_p/k$
He	4.002	1.660	123.5	99.67	1875	0.344	0.68
Ar	39.94	1.67	39.08	31.64	2100	0.0387	0.69
H ₂	2.016	1.410	174.0	129.4	840	0.416	0.68
N ₂	28.02	1.406	46.67	34.67	1664	0.0566	0.74
O ₂	32.00	1.395	43.66	32.31	1918	0.0573	0.73
CO ₂	44.00	1.31	37.24	26.70	1377	0.0340	0.80

1.4 DIMENSIONAL ANALYSIS

By knowing only the units of the parameters involved in a physical process, useful information can be deduced by forming grouping of these parameters as *dimensionless* ratios. This technique is called “dimensional analysis” and is a very powerful engineering *tool*. It is an important part of the judgment process necessary to make engineering decisions and help eliminate errors.

Following is a list of such dimensionless ratios, important in fluid mechanics, which bear the names of early investigators:

$$M = V/a = \text{Mach number} \quad (1.46)$$

$$Re = \rho VL/\mu = \text{Reynolds number} \quad (1.47)$$

$$Pr = \mu C_p/K = \text{Prandtl number} \quad (1.48)$$

$$Le = \rho DC_p/K = \text{Lewis number} \quad (1.49)$$

$$Nu = h^*L/K = \text{Nusselt number} \quad (1.50)$$

$$Kn = \lambda/L = \text{Knudsen number} \quad (1.51)$$

where h^* is the heat-transfer coefficient.

The ratios of different forms of energy in fluid flows will be summarized next. This provides physical interpretation of the dimensionless numbers,

$$\frac{\text{Ordered energy}}{\text{Random energy}} = \frac{\frac{1}{2}mu^2}{\frac{1}{2}m\bar{v}^2} = \frac{u^2}{3RT} = \frac{\gamma}{3} \frac{u^2}{a^2} = \frac{\gamma}{3} M^2 \quad (1.52)$$

$$\frac{\text{Inertial force}}{\text{Viscous force}} = \frac{\dot{m}v}{\tau A} = \frac{\rho AV^2}{\mu \frac{V}{L} A} = \frac{\rho VL}{\mu} Re \quad (1.53)$$

$$\frac{\text{Viscous dissipation energy}}{\text{Energy conducted}} = \frac{\tau AV}{\dot{q}A} = \frac{\mu V^2/L}{kT/L} = \frac{\mu C_p}{k} \frac{V^2}{C_p T} = Pr \frac{M^2}{\gamma - 1} \quad (1.54)$$

$$\begin{aligned} \frac{\text{Heat diffused}}{\text{Heat conducted}} &= \frac{\dot{m}iH}{\dot{q}A} = \frac{\rho D \frac{\partial C_i}{\partial z} AH}{k \frac{\partial T}{\partial z} A} = \frac{\rho DH}{kT} \\ &= \frac{\rho DC_p}{k} \left(\frac{H}{C_p T} \right) = Le \left(\frac{H}{C_p T} \right) \end{aligned} \quad (1.55)$$

$$\frac{\text{Heat convected}}{\text{Heat conducted}} = \frac{h^*T}{kT/L} = \frac{h^*L}{k} = Nu \quad (1.56)$$

$$\frac{\text{No. of collisions with body}}{\text{No. of collisions with another molecule}} = \frac{f_L}{f_\lambda} = \frac{\bar{v}/L}{\bar{v}/\lambda} = \frac{\lambda}{L} = Kn \quad (1.57)$$

1.5 FREE MOLECULE FLOW HEATING

For free molecule flow (FM) $K_n \gg 1$. For this case,⁶ a collision between an air molecule and a surface will be examined (see Fig. 1.12). The energy balance for the exchange during the collision is given by

$$Q = E_i - E_r \equiv \alpha(E_i - E_w) \quad (1.58)$$

where

$$\alpha = \frac{E_i - E_r}{E_i - E_w} = \text{thermal accommodation coefficient} \quad (1.59)$$

This coefficient can be determined experimentally. With reference to Fig. 1.13, if $E_r \approx E_w$, then $\alpha \approx 1$. Based upon this value for α the rate of heat transfer can be computed, i.e.,

$$\dot{Q} = \alpha(\dot{E}_i - \dot{E}_w) = \alpha(\dot{m}H_s - \dot{m}H_w) \quad (1.60)$$

$$\dot{q}_A = \alpha\rho AV(H_s - H_w) \quad (1.61)$$

$$\dot{q}_{FM} = \alpha\rho V(H_s - H_w) \equiv St\rho V(H_s - H_w) \quad (1.62)$$

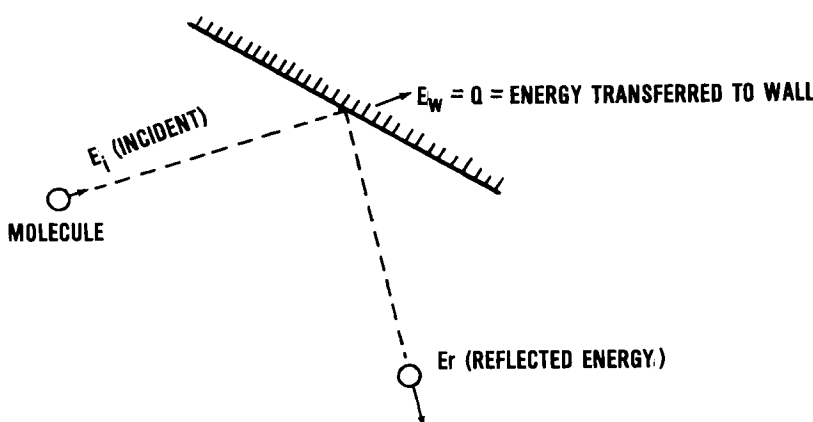


Fig. 1.12 Collision between air molecules and a surface.

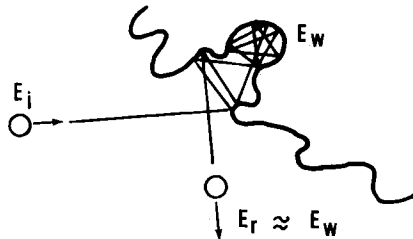


Fig. 1.13 Energy transition between a molecule and the surface.

Hence,

$$St = \alpha \approx 1 \quad (1.63)$$

The transition between free molecule and continuum heating is, for flight cases where $K_n \gg 1$,

$$\dot{q} = \dot{q}_{FM} \quad (1.64)$$

and, for flight cases where $K_n \ll 1$,

$$\dot{q} = \dot{q}_{\text{continuum}} \quad (1.65)$$

Little is known about the transition from one regime to the other where $K_n \approx 1$. As will be explained later, little information is needed, fortunately, in this region so that an ad hoc interpolation may be used as follows:

$$\dot{q}_{\text{transitional}} = \frac{\dot{q}_{\text{continuum}} + Kn\dot{q}_{FM}}{1 + Kn} \quad (1.66)$$

This simple relationship insures that both limits are satisfactorily obtained and permits a continuous calculation of heating throughout the transition region.

1.6 SLIP FLOW REGIME

Up to this point, only free molecule flow and the transition region into the continuum regime have been discussed. There is yet another small regime within the transition region called the "slip flow" regime. This region has not been found to be very important in re-entry engineering; however, for completeness, it should be identified.

At the wall, a boundary layer forms with a gradient of magnitude

$$\frac{\partial u}{\partial z} \cong \frac{U_{\infty}}{\delta} \quad (1.67)$$

where U_{∞} is the freestream velocity at infinity and δ an effective height. This gradient can be examined in a manner similar to the free molecular flow analysis for evaluating viscosity.

RE-ENTRY FLIGHT REGIMES

21

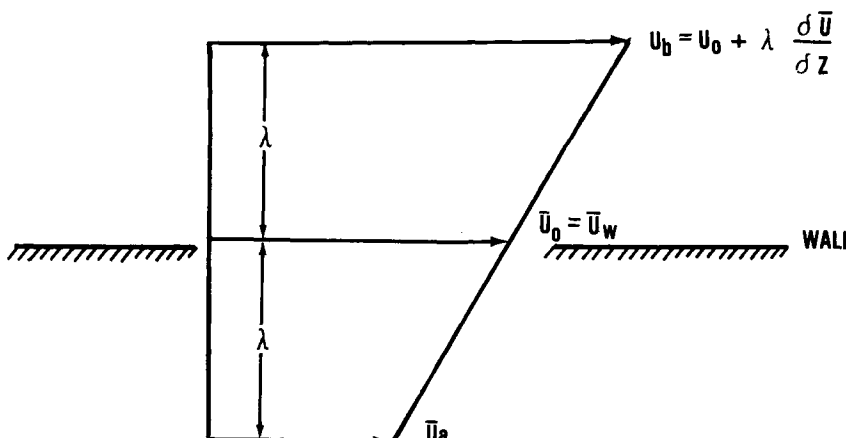


Fig. 1.14 Velocity gradient located a mean free path above and below U_0 .

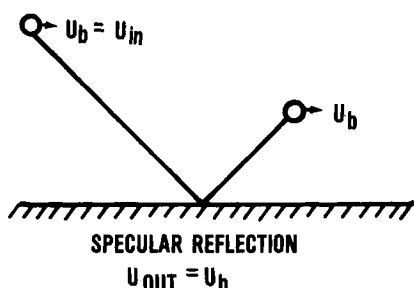


Fig. 1.15 Specular reflection at the wall.

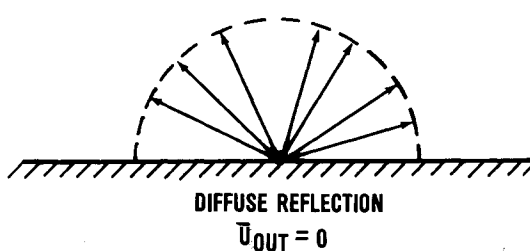


Fig. 1.16 Diffuse reflection occurring after the molecule strikes the wall.

Consider the wall at the location of the velocity U_0 as shown in Fig. 1.14. A molecule coming from a mean free path distance above the wall will have a velocity of U_b since no collisions occur until it strikes the wall. At the wall, two extremes in the reflection velocity are possible, i.e., specular or diffuse, as shown in Figs. 1.15 and 1.16.

Experiments indicate diffuse reflection generally occurs consistent with a "perfectly rough" wall hypothesis. The velocity value at the wall is, there-

fore, the average of the incoming and outgoing velocities, i.e.,

$$\bar{U}_w = \frac{U_{in} + U_{out}}{2} = \frac{\bar{U}_w + \lambda(\partial u / \partial z) + 0}{2} \quad (1.68)$$

Hence

$$\bar{U}_w = \lambda \frac{\partial u}{\partial z} \approx \lambda \frac{U_e}{\delta}$$

or

$$\frac{\bar{U}_w}{U_e} = \frac{\lambda}{\delta} = Kn \quad (1.69)$$

Thus, it is apparent that there is always some slip at the wall, even for the continuum regime. However, for $Kn \ll 1$, we conveniently set $U_w = 0$ for boundary-layer theory. For $0.01 < Kn < 1$, a "slip" velocity of $\bar{U}_w/U_\infty = \lambda/\delta$ can be applied as a correction to the boundary-layer method. The domain where this is appropriate is entitled the *slip flow regime*.

References

¹Allen, H. and Eggers, A., "A Study of the Motion and Aerodynamic Heating of Missiles Entering the Earth's Atmosphere at High Supersonic Speeds," NACA TN 4047, Oct. 1957.

²Gazley, C., "Deceleration and Heating of a Body Entering a Planetary Atmosphere from Space," Rand Corp., Rept. P-955, Feb. 1957.

³U.S. Standard Atmosphere (1962), Government Printing Office, Washington, DC, 1962.

⁴Hirshfelder, J., Curtiss, C., and Bird, R., *Molecular Theory of Gases and Liquids*, Wiley, New York, 1954.

⁵Kennard, E., *Kinetic Theory of Gases*, McGraw-Hill, New York, 1938.

⁶Patterson, G., "Molecular Approach to High Altitude High Speed Flight," University of Toronto, Toronto, Rept. TN-57-311, 1957.

Problems

1.1 Solve $P(h)$ for an adiabatic atmosphere, i.e., $p \sim \rho^\gamma$. What is the temperature "lapse" rate, dT/dh , for this case?

1.2 Compute the radiation equilibrium heat-transfer rates for the materials in Table 1.1. Use an emittance of 0.8.

1.3 Compute the heat-transfer rate in free molecule flow to a flat plate traveling at orbital speed between altitudes from 250,000–400,000 ft.

2

**FLIGHT
MECHANICS****2.1 TRAJECTORY ANALYSIS**

To determine the heat transfer to and the aerodynamic loads on a re-entry vehicle, the trajectory must be ascertained first.¹ In this chapter, the equations for the trajectories of both lifting and ballistic re-entries will be derived.

Governing Equations

The main governing equation in flight mechanics is Newton's second law

$$\mathbf{F} = m\mathbf{a} \quad (2.1)$$

The major decision to be made here is the selection of an appropriate coordinate system. It turns out that the most convenient system to employ is one using wind axes coordinates. This is a rotating coordinate system with respect to Earth-fixed axes. See Fig. 2.1. Therefore, the following relationships are required²:

$$\mathbf{a} = \left(\frac{dV}{dt} \right)_{\text{fixed}} = (\dot{\mathbf{V}} + \boldsymbol{\omega} \times \mathbf{V})_{\text{rotating coordinates}} \quad (2.2)$$

$$\mathbf{k} = \mathbf{k}' \quad (2.3a)$$

$$\boldsymbol{\omega} = \mathbf{k}'(\dot{\theta} - \dot{\gamma}) \quad (2.3b)$$

Using primes for the rotating coordinate system,

$$\mathbf{V} = |V| \mathbf{i}'$$

$$\boldsymbol{\omega} \times \mathbf{V} = \begin{vmatrix} \mathbf{i}' & \mathbf{j}' & \mathbf{k}' \\ 0 & 0 & |\boldsymbol{\omega}| \\ |V| & 0 & 0 \end{vmatrix} = j' \boldsymbol{\omega} V \quad (2.4)$$

RE-ENTRY AERODYNAMICS

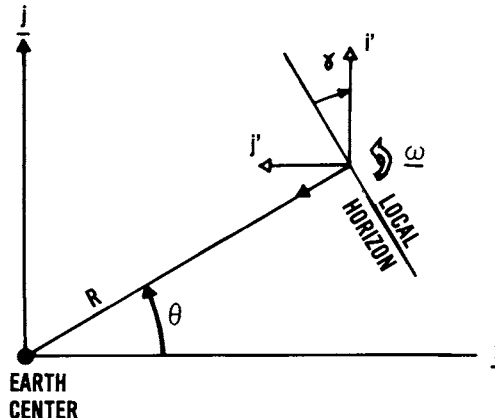


Fig. 2.1 Rotating coordinate system.

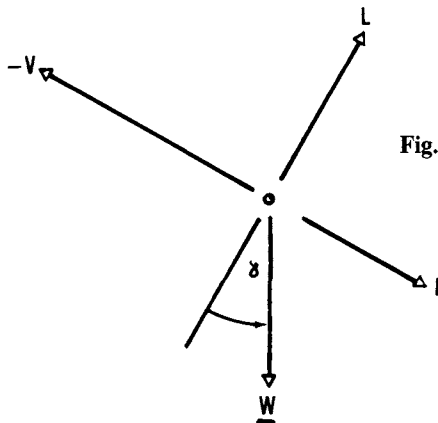


Fig. 2.2 Forces acting on a re-entering body.

$$\begin{aligned} \mathbf{F} &= -j'L - i'D + j'W \cos \gamma - i'W \sin \gamma \\ &= m\mathbf{a} = m\dot{V}\mathbf{i}' + m\omega V\mathbf{j}' \end{aligned} \quad (2.5)$$

Equating scalar components of forces in Fig. 2.2 in the direction of L and D ,

$$-L + W \cos \gamma = m\omega V \quad (2.6)$$

$$-D - W \sin \gamma = m\dot{V} \quad (2.7)$$

It should be noted that

$$\dot{R} = V \sin \gamma \quad (2.8)$$

$$R\dot{\theta} = V \cos \gamma \quad (2.9)$$

These auxiliary relationships will be useful in locating the vehicle with respect to the Earth axes.

Replacing ω with

$$\dot{\theta} - \dot{\gamma} = \frac{V \cos \gamma}{R} - \dot{\gamma} \quad (2.10)$$

and substituting

$$m = W/g \quad (2.11)$$

the following trajectory equations can be generated:

$$\frac{V\dot{\gamma}}{g} = \frac{L}{W} - \left(1 - \frac{V^2}{gR}\right) \cos \gamma \quad (2.12)$$

$$-\dot{V}/g = (D/W) + \sin \gamma \quad (2.13)$$

$$\dot{R} = \dot{h} = V \sin \gamma \quad (2.14)$$

$$R\dot{\theta} = V \cos \gamma \quad (2.15)$$

$$L = C_L S_{\frac{1}{2}} \rho V^2 \quad (2.16)$$

$$D = C_D S_{\frac{1}{2}} \rho V^2 \quad (2.17)$$

$$\rho = \rho_{sl} e^{-\alpha h} \quad (2.18)$$

Given W/S , C_L , C_D , and initial conditions for γ_i , V_i , h_i , and θ_i , the trajectory path may be determined. Various approximations to the above equations can be used to determine simple closed-form solutions and to obtain insight into important features of re-entry. However, numerical integration of the exact equations can be obtained without the simplifying assumptions.

Orbital Mechanics

In orbit, both L and D vanish because ρ becomes extremely small. Therefore, Eqs. (2.12–2.15) can be simplified to

$$\frac{-V\dot{\gamma}}{\cos \gamma} = \frac{g_0 R_0^2}{R^2} - \frac{V^2}{R} \quad (2.19)$$

$$-\dot{V} = \frac{g_0 R_0^2}{R^2} \sin \gamma \quad (2.20)$$

$$\dot{R} = V \sin \gamma \quad (2.21)$$

$$R\dot{\theta} = V \cos \gamma \quad (2.22)$$

where the inverse square law relationship

$$g = g_0 R_0^2 / R^2 \quad (2.23)$$

has been used.

By differentiating, we can eliminate V and γ and replace the R and θ variables, as

$$\ddot{R} = -g + \frac{V^2 \cos^2 \gamma}{R} = \frac{-g_0 R_0^2}{R^2} + R \dot{\theta}^2 \quad (2.24)$$

$$\dot{R} \dot{\theta} + R \ddot{\theta} = \frac{-(V \cos \gamma)}{R} (V \sin \gamma) = -\dot{R} \dot{\theta} \quad (2.25)$$

or

$$\ddot{R} - \dot{\theta}^2 R = -g \quad (2.26)$$

$$R \ddot{\theta} + 2 \dot{\theta} \dot{R} = 0 \quad (2.27)$$

These are the classical equations for a central force field. Integration of these equations is accomplished as follows:

$$\frac{d}{dt}(R^2 \dot{\theta}) = R(R \ddot{\theta} + 2 \dot{R} \dot{\theta}) = 0 \quad (2.28)$$

Integrating Eq. (2.28) results in $R^2 \dot{\theta} = p = \text{constant}$ angular momentum. Inserting this result in Eq. (2.26) produces,

$$\ddot{R} + g = \dot{\theta}^2 R = p^2 / R^3 \quad (2.29)$$

Integration of Eq. (2.29) may be obtained by transforming the variables. Let

$$u = \frac{1}{R}; \frac{du}{d\theta} = -\frac{dR}{R^2 d\theta} \quad (2.30)$$

$$\frac{dR}{dt} = \dot{\theta} \frac{dR}{d\theta} = \frac{p}{R^2} \frac{dR}{d\theta} = -p \frac{du}{d\theta} \quad (2.31)$$

$$\ddot{R} = \dot{\theta}^2 R - g = u^3 p^2 - u^2 g_0 R_0^2 = -u^2 p^2 \frac{d^2 u}{d\theta^2} \quad (2.32)$$

$$\frac{d^2 u}{d\theta^2} + \left(u - \frac{g_0 R_0^2}{p^2} \right) = 0$$

(2.33)

FLIGHT MECHANICS

27

Integration produces

$$u = \frac{1}{R} = \frac{g_0 R_0^2}{p^2} + A \cos(\theta - \theta_1) \quad (2.34)$$

Defining the coordinate system for the minimum R to occur at $\theta = 0$ deg means that $\theta_1 = 0$. Differentiating with respect to time to evaluate A results in

$$\dot{u} = -A \sin \theta \dot{\theta} = -\dot{R}/R^2 \quad (2.35)$$

Hence,

$$A = \frac{\dot{R}}{R^2 \sin \theta \dot{\theta}} = \frac{V \sin \gamma}{R \sin \theta V \cos \gamma} = \left[\frac{\tan \gamma}{R \sin \theta} \right]_0 \quad (2.36)$$

Therefore,

$$\frac{1}{R} = \frac{g_0 R_0^2}{p^2} + \frac{\tan \gamma_0}{R_0 \sin \theta_0} \cos \theta \quad (2.37)$$

where

$$p = R_0 V_0 \cos \gamma_0 \quad (2.38)$$

To recognize the shape of this curve, we will transform to a Cartesian coordinate system from the polar system. Redefine the constants in Eq. (2.37) as follows:

$$a(1 - \varepsilon^2)/R = 1 + \varepsilon \cos \theta \quad (2.39)$$

where

$$\varepsilon = \frac{V_0^2}{g_0 R_0} \frac{\sin \gamma_0}{\sin \theta_0} \cos \gamma_0 \quad (2.40)$$

$$a(1 - \varepsilon^2) = \frac{V_0^2}{g_0} \cos^2 \gamma_0 \quad (2.41)$$

Transform from r, θ to x, y but translate the x origin by $a\varepsilon$. Figure 2.3 shows the relation between x, y and the R, θ axis. The reason for this transformation will become apparent later. Thus,

$$x = R \cos \theta + a\varepsilon \quad (2.42)$$

$$y = R \sin \theta \quad (2.43)$$

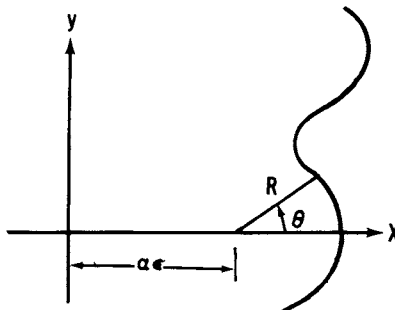


Fig. 2.3 Relation between xy and $R\theta$ axes (x origin translated by $\alpha\epsilon$).

Hence,

$$R^2 = y^2 + (x - a\epsilon)^2 \quad (2.44)$$

The transformed equation becomes

$$R^2 = [a(1 - \epsilon^2) - \epsilon R \cos \theta]^2 = [a(1 - \epsilon^2) - \epsilon(x - a\epsilon)]^2 \quad (2.45)$$

$$y^2 + x^2 - 2a\epsilon x + a^2\epsilon^2 = a^2 - 2a\epsilon + \epsilon^2x^2 \quad (2.46)$$

or

$$\frac{x^2}{a^2} + \frac{y^2}{b^2} = 1 \quad (2.47)$$

where $\epsilon^2 = 1 - (b^2/a^2)$.

This trajectory is recognized as the equation for an ellipse as originally derived by Newton (circa 1680) to confirm Kepler's laws.

The relationship for the energy can be determined as follows:

$$\frac{1}{R_0} = \frac{g_0 R_0^2}{p^2} + \frac{\tan \gamma_0}{R_0 \sin \theta_0} \cos \theta_0 \quad (2.48)$$

$$p^2 = R_0^2 V_0^2 \cos^2 \gamma_0 = \frac{g_0 R_0^3}{1 - (\tan \gamma_0 / \tan \theta_0)} \quad (2.49)$$

$$\frac{V_0^2}{g_0 R_0} = \frac{\sec^2 \gamma_0}{1 - (\tan \gamma_0 / \tan \theta_0)} \quad (2.50)$$

For given values of R_0 and θ_0 , $V_0 = V_0(\gamma_0)$. This implies that an infinite number of trajectories are possible to interconnect two points on the globe. This series of ellipses requires different energy levels to accomplish the same mission. Of interest to the designer is the case of the minimum energy

necessary to maneuver in space. A minimum energy trajectory can be obtained by differentiating the expression in Eq. (2.50) as

$$\frac{\partial V_0^2}{gR_0 \partial \gamma_0} = 0 = \frac{2 \sec^2 \gamma_0 \tan \gamma_0}{1 - \tan \gamma_0 \cot \theta_0} + \frac{\sec^4 \gamma_0 \cot \theta_0}{(1 - \tan \gamma_0 \cot \theta_0)^2} \quad (2.51)$$

or

$$2 \tan \gamma_0 (1 - \tan \gamma_0 \cot \theta_0) + \cot \theta_0 (1 + \tan^2 \gamma_0) = 0 \quad (2.52)$$

or

$$\tan^2 \gamma_0 - 2 \tan \theta_0 \tan \gamma_0 - 1 = 0 \quad (2.53)$$

or

$$\tan(2\gamma_0) = \cot(\theta_0) = -\tan\left(\frac{\pi}{2} - \theta_0\right) \quad (2.54)$$

Hence,

$$\gamma_0 = \frac{\theta_0}{2} - \frac{\pi}{4} \quad (2.55)$$

or

$$\tan \gamma_0 = \tan \theta_0 \pm \sec \theta_0 \quad (2.56)$$

or

$$-\tan \gamma_0 = \frac{1 - \sin \theta_0}{\cos \theta_0} : \text{optimum}$$

(2.57)

Note that for circular orbits, $\gamma_0 = 0$, $\epsilon = 0$, and $V_0^2 = g_0 R_0 \equiv V_c^2$.

The minimum energy expression is

$$(V_0^2)_{\min} = 4g_0 R_0 \left[1 + \tan \frac{\theta_0}{2} \right]^{-2} \tan \frac{\theta_0}{2} \quad (2.58)$$

Lifting Re-entry

Within the confines of the thin atmosphere, the following assumptions are applicable for lifting re-entry (i.e., the Space Shuttle):

$$g = g_0 \qquad \qquad W/SC_L = \text{const}$$

$$\gamma = 0, \dot{\gamma} = 0 \qquad L/D = \text{const}$$

$$V_c^2 = gR$$

Thus, Eqs. (2.12) and (2.13) become

$$\frac{L}{W} = \left[1 - \frac{V^2}{V_c^2} \right] = \left[\frac{SC_L}{2W} \right] \rho V^2 \quad (2.59)$$

$$\frac{D}{W} = \frac{D}{L} \left[\frac{L}{W} \right] = - \frac{\dot{V}}{g} \quad (2.60)$$

Equation (2.59) is algebraic and contains the desired relationship between altitude and velocity for equilibrium glide. Integration of Eq. (2.60) produces the time history of the flight,

$$-\frac{\dot{V}}{g} = \frac{D}{L} \left[1 - \frac{V^2}{V_c^2} \right] \quad (2.61)$$

or

$$\frac{-dV/V_c}{1 - (V^2/V_c^2)} = \frac{Dg}{LV_c} dt \quad (2.62)$$

Integration produces

$$\frac{V}{V_c} = \tanh \left[-\frac{Dg}{LV_c} t \right] \quad (2.63)$$

where $t = 0$ at $V/V_c = 0$, so that negative time is required in interpreting the results.

With these equations, useful relations for the history of the number of g 's experienced and the heating rate ($\dot{q} = K\rho^m V^3$) can be obtained,

$$-\frac{\dot{V}}{g} = \frac{D}{L} \left[1 - \left[\frac{V^2}{V_c^2} \right] \right] = \frac{D}{L} \left[1 - \tanh^2 \left[\frac{-Dgt}{LV_c} \right] \right] \quad (2.64)$$

$$\dot{q} = K\rho^m V^3 = K \left[\frac{2W}{SC_L} \right]^m \left[1 - \left[\frac{V^2}{V_c^2} \right] \right]^m V^{3-2m} = \dot{q}(V) \quad (2.65)$$

Maximum g occurs when $V/V_c \rightarrow 0$. Hence,

$$[\dot{V}/g]_{\max} = D/L \quad (2.66)$$

Maximum heating occurs when $\partial \dot{q} / \partial V = 0$,

$$\frac{\partial \dot{q}}{\partial V} = 0 = \frac{-2m(V/V_c^2)}{1 - (V^2/V_c^2)} + \frac{3-2m}{V} \quad (2.67)$$

or

$$\left[\frac{V}{V_c} \right]_{\dot{q}_{\max}} = \sqrt{1 - \frac{2m}{3}} \quad (2.68)$$

Ballistic Re-entry

A ballistic missile is another re-entry vehicle of considerable interest to the U.S. Air Force. The following assumptions are made for this type of trajectory:

$$L = 0$$

$$W \sin \gamma / D \ll 1, \text{ neglect gravity forces}$$

$$\gamma = \gamma_0 = \text{const, i.e., steep re-entry}$$

Hence, Eqs. (2.13) and (2.14) become

$$-\dot{V}/g = D/W \quad (2.69)$$

$$\dot{h} = V \sin \gamma_0 \quad (2.70)$$

Divide

$$-\frac{dV}{dh} = \frac{gC_D S}{2W \sin \gamma_0} \rho V \quad (2.71)$$

Insert the following expression for density:

$$\rho/\rho_{sl} = e^{-\alpha h} \quad (2.72)$$

Eliminate h ,

$$\frac{d\rho}{\rho} = -\alpha dh \quad (2.73)$$

Thus,

$$\frac{dV}{V} = -\frac{d\rho}{\beta} \quad (2.74)$$

where $\beta = -2W\alpha \sin \gamma_0/gC_D S = \text{ballistic coefficient}$.

Integration produces

$$\frac{V}{V_0} = e^{-\rho/\beta} \text{ since } \rho \rightarrow 0 \text{ at } V = V_0 \quad (2.75)$$

The time history may now be determined,

$$\dot{h} = V \sin \gamma_0 = \frac{dh}{dt} = V_0 e^{-\rho/\beta} \sin \gamma_0 \quad (2.76)$$

Recall that

$$\frac{d\rho}{\rho} = -\alpha dh \quad (2.77)$$

Therefore,

$$-\alpha V_0 \sin \gamma_0 dt = e^{\rho/\beta} \frac{d\rho}{\rho} \quad (2.78)$$

Integration produces

$$-\alpha V_0 \sin \gamma_0 t = \ell n \frac{\rho}{\rho_0} + \frac{\rho}{\beta} + \frac{(\rho/\beta)^2}{2 \cdot 2!} + \frac{(\rho/\beta)^3}{3 \cdot 3!} + \dots \quad (2.79)$$

Again, useful design numbers can be obtained with these closed-form equations in deriving maximum deceleration and heating values,

$$-\frac{\dot{V}}{g} = \frac{D}{W} = \frac{C_D S}{2W} \rho V^2 = -\frac{\beta C_D S}{2W} V^2 \ell n \frac{V}{V_0} \quad (2.80)$$

$$\dot{q} = K \rho^m V^3 = K \left[-\beta \ell n \frac{V}{V_0} \right]^m V^3 \quad (2.81)$$

Maximum values are obtained by differentiation,

$$\frac{2W}{\beta g C_D S} \frac{\partial \dot{V}}{\partial V} = 2V \ell n \frac{V}{V_0} + \frac{V^2}{V} = 0 \quad (2.82)$$

Hence,

$$\ell n(V/V_0) = \frac{1}{2} \quad (2.83)$$

or

$$[V/V_0]_{\dot{V}_{\max}} = e^{-\frac{1}{2}} \quad (2.84)$$

$$\left| -\frac{\dot{V}}{g} \right|_{\max} = \frac{\beta C_D S V_0^2}{4eW} = -\frac{V_0^2 \alpha \sin \gamma_0}{2eg} \quad (2.85)$$

Peak heating occurs when $\partial \dot{q} / \partial V = 0$,

$$\dot{q} \frac{\partial \dot{q}}{\partial V} = 0 = \frac{m(1/V)}{\ell n(V/V_0)} + \frac{3}{V} \quad (2.86)$$

or

$$\ell_n(V/V_0) = -m/3 \quad (2.87)$$

$$[V/V_0]_{\dot{q}_{\max}} = e^{-m/3} \quad (2.88)$$

Orbital Decay Re-entry

In the orbital decay mode of re-entry, the vehicle loses energy (while in a circular orbit) as a result of drag and spirals to the Earth.³

The governing equations assuming $\gamma \ll 1$ and $L = 0$ are

$$\dot{V}/g = -D/W \quad (2.89)$$

where $D/W = [(C_D A \rho_{sl})/2W] \sigma V^2$.

$$-V\dot{\gamma}/g = 1 - (V^2/V_c^2), \quad \sigma = e^{-\alpha h} \quad (2.90)$$

$$\dot{h} = V\gamma \quad (2.91)$$

Time may be eliminated by dividing each equation by \dot{V} ,

$$-\frac{V d\gamma}{dV} = \frac{1 - V^2/V_c^2}{-D/W} \quad (2.92)$$

$$-\frac{V dh}{dV} = \frac{V^2\gamma}{-gD/W} = -\frac{V d\sigma}{\alpha\sigma dV} \quad (2.93)$$

or

$$\gamma = \left[\frac{C_D A g \rho_{sl}}{2\alpha W} \right] \frac{V d\sigma}{dV} = K \frac{V d\sigma}{dV} \quad (2.94)$$

Hence, γ can be eliminated by differentiation with respect to V ,

$$K \frac{V d}{dV} \left[\frac{V d\sigma}{dV} \right] = \frac{1 - (V^2/V_c^2)}{+K(\alpha/g)\sigma V^2} \quad (2.95)$$

This is now a second-order, nonlinear equation that can be numerically integrated. Transformation of variables will help simplify the equation. Let

$$V/V_c = e^{-x} \quad (2.96)$$

$$KV_c \sqrt{\frac{\alpha}{g}} \sigma = y \quad (2.97)$$

Since

$$dV/V = -dx \quad (2.98)$$

$$y \frac{d^2y}{dx^2} = e^{2x} - 1 \quad (2.99)$$

The initial conditions are $V_i = V_c$, $\sigma_i = 0$, and $\gamma_i = 0$. This corresponds to $x = 0$, $y = 0$, and $dy/dx = 0$. Since

$$\frac{d^2y}{dx^2} = \frac{e^{2x} - 1}{y} \rightarrow 0$$

becomes indeterminant, a series solution is used at the start when x is small. Assume a series of form,

$$y = x^{3/2}(a + bx + cx^2 + \dots) \quad (2.100)$$

$$y' = \frac{3}{2}ax^{\frac{1}{2}} + \frac{5}{2}bx^{\frac{3}{2}} + \frac{7}{2}cx^{\frac{5}{2}} \quad (2.101)$$

$$y'' = \frac{3}{4}ax^{-\frac{1}{2}} + \frac{15}{4}bx^{\frac{1}{2}} + \frac{35}{4}cx^{\frac{3}{2}} \quad (2.102)$$

Thus,

$$\begin{aligned} yy'' &= \frac{3}{4}a^2x + \frac{9}{2}abx^2 + \frac{(38ac + 15b^2)}{4}x^3 \\ &= e^{2x} - 1 = 1 + 2x + \frac{(2x)^2}{2!} + \frac{(2x)^3}{3!} + \dots - 1 \end{aligned} \quad (2.103)$$

Equating like terms of the series will permit the evaluation of the coefficients for the power series in y ,

$$a^2 = 8/3, ab = 4/9, 38ac + 15b^2 = 16/3 \quad (2.104)$$

Solving these three equations produces

$$a = \sqrt{8/3}, b/a = 1/6, c/a = 1/24 \quad (2.105)$$

Hence,

$$y = \sqrt{\frac{8}{3}}x^{3/2}\left(1 + \frac{x}{6} + \frac{x^2}{24} + \dots\right) \quad (2.106)$$

This series is accurate at the initial phase of the trajectory. Examining its utility to find maximum \dot{q} and \dot{V} ,

$$\dot{q} \sim \sqrt{\frac{\sigma}{R}} V^3 \sim \sqrt{y} e^{-3x} \quad (2.107)$$

$$\dot{V} \sim \sigma V^2 \sim ye^{-2x} \quad (2.108)$$

Differentiation will produce relationships for the maximum value during re-entry,

$$\frac{d\dot{q}}{dx} = 0 = \frac{e^{-3x}}{2\sqrt{y}} y' - 3\sqrt{y} e^{-3x} \quad (2.109)$$

or

$$[y'/y]_{\dot{q}_{\max}} = 6 \quad (2.110)$$

Likewise,

$$\frac{d\dot{V}}{dx} = 0 = y'e^{-2x} - 2ye^{-2x} \quad (2.111)$$

$$[y'/y]_{\dot{V}_{\max}} = 2 \quad (2.112)$$

Returning to the series solution,

$$\frac{y'}{y} = \frac{\sqrt{\frac{8}{3}} \frac{3}{2} x^{\frac{1}{2}} \left(1 + \frac{5}{18}x + \frac{7}{72}x^2\right)}{\sqrt{\frac{8}{3}} x^{\frac{3}{2}} \left(1 + \frac{x}{6} + \frac{x^2}{24}\right)} = N; \quad \begin{cases} N = 6, \dot{q}_{\max} \\ N = 2, \dot{V}_{\max} \end{cases} \quad (2.113)$$

or

$$x = \frac{3}{2N} \left(1 + \frac{x}{9}\right) \cong \frac{3}{2N} \left(1 + \frac{1}{6N}\right) \quad (2.114)$$

Therefore,

$$V/V_c = e^{-x} = 3^{-(3/2N)[1 + (1/6N)]} \quad (2.115)$$

Table 2.1 can now be used to evaluate the maximum value experienced during re-entry,

$$\dot{q}_{\max} = 1.068 \sqrt{\frac{\sigma}{R}} \left[\frac{V}{1000} \right]^3 = 1.068 \sqrt{\frac{y}{KV_c R \sqrt{\alpha/g}}} \left[\frac{V_c}{1000} \right]^3 e^{-3x} \quad (2.116)$$

Table 2.1 Values Experienced during Re-entry

Condition	N	x_{opt}	$e^{-x_{\text{opt}}} = V/V_c$	$V/V_c \text{exact}$	$V, \text{ft/s}$	y_{opt}
\dot{q}_{\max}	6	0.2569	0.773	0.775	20,100	0.2223
\dot{V}_{\max}	2	0.8125	0.440	0.430	11,000	1.3908

Hence,

$$\dot{q}_{\max} = 24.9 \sqrt{W/C_D A R}, \text{ Btu}/\text{ft}^2 \cdot \text{s} \quad (2.117)$$

$$\left| \frac{\dot{V}}{g} \right|_{\max} = \frac{D}{W} = K \frac{\alpha}{g} \sigma V^2 = \sqrt{\frac{\alpha}{g}} V_c y e^{-2x} \cong 8 \quad (2.118)$$

Thus, orbital decay *always* produces $8g$ deceleration, independent of $W/C_D A$.

Numerical Integration

Although the closed-form solutions are excellent for providing rapid estimations of the design parameters, numerical integrations will be required when refinements are necessary for final design. Today, on modern digital computers, it is possible to obtain trajectory information in only a few seconds of computer time as follows:

$$\dot{V} \equiv \frac{dY_1}{dt} = -g \left[\frac{D}{L} \frac{L}{W} + \sin \gamma \right] = \dot{V}(Y_1, Y_2, Y_3) \quad (2.119)$$

$$\dot{\gamma} \equiv \frac{dY_2}{dt} = \frac{g}{V} \left[\frac{L}{W} - \left[1 - \frac{V^2}{V_c^2} \right] \cos \gamma \right] = \dot{\gamma}(Y_1, Y_2, Y_3) \quad (2.120)$$

$$\dot{h} \equiv \frac{dY_3}{dt} = V \sin \gamma = \dot{h}(Y_1, Y_2) \quad (2.121)$$

where

$$\frac{L}{W} = \left[\frac{SC_L}{2W} \rho_{sl} \right] e^{-\alpha h} V^2 \quad (2.122)$$

A simple Euler's method may be used to numerically integrate this set,

$$Y_1(t + \Delta t) = Y_1(t) + \dot{V} \Delta t \quad (2.123)$$

$$Y_2(t + \Delta t) = Y_2(t) + \dot{\gamma} \Delta t \quad (2.124)$$

$$Y_3(t + \Delta t) = Y_3(t) + \dot{h} \Delta t \quad (2.125)$$

Initial conditions for V_0 , γ_0 , and h_0 are required to commence the integration. The rates are updated after each numerical time step. Integration ceases when $h = 0$.

Hypersonic Phugoid

For shallow lifting re-entries ($\gamma \rightarrow$ small) large, low-frequency oscillations occur in what may be called a hypersonic phugoid mode. Small-perturba-

tion analysis of the trajectory equations can demonstrate this phenomenon. The appropriate equations are

$$\dot{h} = V\gamma \quad (2.126)$$

$$\frac{V\dot{\gamma}}{g} \cong \frac{L}{W} - \left[1 - \frac{V^2}{V_c^2} \right] \quad (2.127)$$

Assume small perturbations,

$$h = h_1 + \Delta h \quad (2.128)$$

$$\gamma = 0 + \Delta\gamma \quad (2.129)$$

Inserting these relationships into the governing equations and neglecting the higher-order terms results in

$$\Delta\dot{h} = V_1 \Delta\gamma \quad (2.130)$$

$$\frac{V_1}{g} \Delta\dot{\gamma} = \frac{\Delta L}{W} + \left[\frac{L_1}{W} - \left[1 - \frac{V_1^2}{V_c^2} \right] \right] = \frac{\Delta\ddot{h}}{g} \quad (2.131)$$

where

$$\frac{L}{W} = \frac{C_L S}{2W} \rho_{sl} V_1^2 e^{-\alpha(h_1 + \Delta h)} \quad (2.132)$$

$$\frac{L}{W} = \frac{L_1}{W} e^{-\alpha\Delta h} = \frac{L_1}{W} (1 - \alpha \Delta h) = \frac{L_1}{W} + \frac{\Delta L}{W} \quad (2.133)$$

$$\frac{\Delta\ddot{h}}{g} = \frac{\Delta L}{W} = -\alpha \frac{L_1}{W} \Delta h = -\alpha \left[1 - \frac{V^2}{V_c^2} \right] \Delta h \quad (2.134)$$

$$\Delta\ddot{h} + \omega^2 \Delta h = 0; \quad \omega^2 = \alpha g \frac{L_1}{W} = \alpha g \left[1 - \frac{V_1^2}{V_c^2} \right] \quad (2.135)$$

$$P = \frac{1}{f} = \frac{2\pi}{\omega} = \frac{2\pi}{\sqrt{\alpha g \left[1 - \left(V_1^2 / V_c^2 \right) \right]}} \quad (2.136)$$

$$P = \frac{170 \text{ s}}{\sqrt{1 - (V_1^2 / V_c^2)}} = \frac{2.84 \text{ min}}{\sqrt{1 - (V_1^2 / V_c^2)}} \quad (2.137)$$

$$\alpha^{-1} = 23,700 \text{ ft}, \quad V_c = 26,000 \text{ ft/s}$$

See Table 2.2.

Table 2.2 Phugoid Period Evaluated for Different Values of Velocity

<i>V</i> ₁	<i>P</i> , min
25,000	10.3
20,000	4.44
15,000	3.48
10,000	3.08
5,000	2.89

Numerical integrations of the governing equations exhibit this phugoid initiated by out-of-equilibrium initial conditions.

2.2 RANGE MODULATION

A major advantage inherent in a lifting re-entry vehicle is the ability to attain an alternate landing site off the orbital track. The extent of this range modulation is controlled by the *L/D* and bank angle ϕ_w of the vehicle. The maximum lateral range is of primary interest and is dictated by the maximum usable *L/D* of the vehicle. In this section, the trajectory equations will be restructured to include the effects of yaw due to banked flight. The governing equations in wind axes are

$$m\dot{V} = -D - W \sin \gamma \quad (2.138)$$

$$mVr_w = -C + W \left[1 - \frac{V^2}{V_c^2} \right] \cos \gamma \sin \phi_w \quad (2.139)$$

$$mVq_w = L - W \left[1 - \frac{V^2}{V_c^2} \right] \cos \gamma \cos \phi_w \quad (2.140)$$

$$\dot{x} = V \cos \gamma \cos \psi_w \quad (2.141)$$

$$\dot{y} = V \cos \gamma \sin \psi_w \quad (2.142)$$

where

$$r_w = \text{yaw rate} \quad \phi_w = \text{bank angle}$$

$$q_w = \text{pitch rate} \quad \psi_w = \text{yaw angle}$$

$$p_w = \text{roll rate}$$

The following rate equations for the Euler angles will also be required:

$$\dot{\phi}_w = p_w + (q_w \sin \phi_w + r_w \cos \phi_w) \tan \gamma \quad (2.143)$$

$$\dot{\gamma} = q_w \cos \phi_w - r_w \sin \phi_w \quad (2.144)$$

$$\dot{\psi}_w = (q_w \sin \phi_w + r_w \cos \phi_w) \sec \gamma \quad (2.145)$$

Rearranging the governing equations in terms of these rate equations produces

$$m\dot{V} = -D - W \sin \gamma \quad (2.146)$$

$$mV\dot{\psi}_w = (L \sin \phi_w - C \cos \phi_w) \sec \gamma \quad (2.147)$$

$$mV\dot{\gamma} = L \cos \phi_w + C \sin \phi_w - W [1 - (V^2/V_c^2)] \cos \gamma \quad (2.148)$$

The applicable conditions during lifting re-entry are

$$\gamma = 0 \quad C = (C_{c\beta})\beta = 0$$

$$\dot{\gamma} = 0 \quad \dot{\phi}_w = 0$$

$$\beta = 0, \text{ required due to the heating limit} \quad \phi_w = \text{large angle}$$

The resulting equations are

$$\dot{V}/g = -D/W \quad (2.149)$$

$$(L/W)\cos \phi_w = 1 - (V^2/V_c^2) \quad (2.150)$$

$$V\dot{\psi}_w/g = (L/W)\sin \phi_w \quad (2.151)$$

$$\dot{x} = V \cos \psi_w \quad (2.152)$$

$$\dot{y} = V \sin \psi_w \quad (2.153)$$

It is possible to obtain a closed-form solution to the equations by analytic integration. If this were not possible, numerical integration would have to be used. First,

$$\frac{dV}{g dt} = -\frac{D}{W} = -\frac{D}{L} \left[1 - \frac{V^2}{V_c^2} \right] \sec \phi_w \quad (2.154)$$

For constant L/D and ϕ_w , this equation integrates to ascertain the time of flight,

$$-\frac{gt}{V_c} = \frac{L}{D} \cos \phi_w \tanh^{-1} \frac{V}{V_c} \quad (2.155)$$

The magnitude of $(L/D)\cos \phi_w$ directly controls the duration of re-entry and, thus, the time the vehicle is exposed to the heating. The Space Shuttle banks at ± 60 deg to reduce the integrated heating by a factor of two.

The equation for yaw angle is determined next by dividing $\dot{\psi}_w$ by V ,

$$\frac{d\psi_w}{dV} = \frac{\dot{\psi}_w}{V} = \frac{(gL/VW)\sin \phi_w}{-g(D/W)} = -\frac{L}{VD} \sin \phi_w \quad (2.156)$$

which integrates to

$$\psi_w = -(L/D)\sin \phi_w \ell n(V/V_c) \quad (2.157)$$

We can now determine both the longitudinal and lateral range values by

$$\Delta x = \int_0^t V \cos \psi_w dt \quad (2.158)$$

or changing variables from t to V ,

$$\frac{g \Delta x}{V_c^2} = - \int_{V_c}^0 \frac{L}{D} \cos \phi_w \left[\frac{V/V_c}{1 - (V^2/V_c^2)} \right] \cos \left[-\frac{L}{D} \sin \phi_w \ell n \frac{V}{V_c} \right] \frac{dV}{V_c} \quad (2.159)$$

This integral collapses to the following by letting $\eta = \ell n(V^2/V_c^2)$ and $a = \frac{1}{2}L/D \sin \phi_w$:

$$\frac{g \Delta x}{V_c^2} = \frac{L}{2D} \cos \phi_w \int_0^\infty \frac{\cos a\eta}{e^\eta - 1} d\eta \quad (2.160)$$

Similarly,

$$\frac{g \Delta y}{V_c^2} = \frac{L}{2D} \cos \phi_w \int_0^\infty \frac{\sin a\eta}{e^\eta - 1} d\eta \quad (2.161)$$

These two integrals may be evaluated by the infinite series,

$$\frac{1}{e^\eta - 1} = \sum_{n=1}^{\infty} e^{-n\eta} \text{ since } \sum_{n=0}^{\infty} x^n = \frac{1}{1-x} \quad (2.162)$$

which is a binomial expansion. The two integrals required are

$$\int_0^\infty \frac{\cos a\eta}{e^\eta - 1} d\eta = \int_0^\infty \cos a\eta \sum_{n=1}^{\infty} e^{-n\eta} d\eta = \sum_{n=1}^{\infty} \frac{n}{a^2 + n^2} \quad (2.163)$$

and

$$\int_0^\infty \frac{\sin a\eta}{e^\eta - 1} d\eta = \int_0^\infty \sin a\eta \sum_{n=1}^{\infty} e^{-n\eta} d\eta = \sum_{n=1}^{\infty} \frac{a}{a^2 + n^2} \quad (2.164)$$

where $a = \frac{1}{2}(L/D)\sin\phi_w$. Note that these series still require numerical evaluation.

A case of interest is the maximum value for both longitudinal and lateral range. The maximum longitudinal range for $\phi_w = 0$ is

$$\left[\frac{g\Delta x}{V_c^2} \right]_{\max} = -\frac{1}{2} \frac{L}{D} \ell n \left[1 - \frac{V_i^2}{V_c^2} \right] \quad (2.165)$$

The maximum lateral range occurs at ϕ optimum as deduced from the following approximation to the numerical series solution:

$$\cot^2 \phi_{\text{opt}} \approx 1 + 0.106(L/D)^2 \quad (2.166)$$

The corresponding range is

$$\left[\frac{g\Delta y}{V_c^2} \right]_{\max} \approx \frac{(L/D)^2}{5.2\sqrt{1 + 0.106(L/D)^2}} \quad (2.167)$$

An estimate can be made of the maximum L/D value required for a vehicle to completely cover the globe with its landing footprint,

$$\frac{g\Delta y}{V_c^2} = \frac{\Delta y}{R_e} = \frac{\pi}{2} \left(\begin{array}{l} \text{maximum required} \\ \text{to cover the globe} \end{array} \right)$$

Hence,

$$\frac{(L/D)^2}{5.2\sqrt{1 + 0.106(L/D)^2}} = \frac{\pi}{2} \quad (2.168)$$

This situation occurs for an L/D of about 3.5. This hypersonic L/D value is the highest value required. Unfortunately, a value of 3.5 is extremely difficult to attain at hypersonic speed due to the nose bluntness and frictional effects.

2.3 STABILITY ANALYSIS

Vehicle Stability

There is no difference in the approach taken to analyze the stability of a re-entry vehicle as compared to the stability analysis of a low-speed vehicle.⁴ However, the relative importance of the various aerodynamic forces required for the analysis is very different. In this section, a brief review of the stability analysis will be outlined.

The governing equations describing vehicle dynamics are

$$\mathbf{F} = m\mathbf{a} \quad (2.169)$$

$$\mathbf{T} = d\mathbf{H}/dt = \dot{\mathbf{H}} + \boldsymbol{\omega} \times \mathbf{H} \quad (2.170)$$

where

$$\mathbf{H} = \underline{\mathbf{I}} \cdot \boldsymbol{\omega} \quad (2.171)$$

In this stability analysis, a wind axes system is used to describe the forces in Eq. (2.169). [These were shown previously as Eqs. (2.138–2.140).] Thus, $\mathbf{F} = m\mathbf{a}$ in wind axes becomes

$$-D - W \sin \gamma = m\dot{V} \quad (2.172)$$

$$-C + W \left[1 - \frac{V^2}{V_c^2} \right] \cos \gamma \sin \phi_w = mVr_w \quad (2.173)$$

$$-L + W \left[1 - \frac{V^2}{V_c^2} \right] \cos \gamma \cos \phi_w = -mVq_w \quad (2.174)$$

$$\dot{h} = V \sin \gamma \quad (2.175)$$

To analyze the torque on the vehicle, it is more convenient to use a body axes system. Because of this discrepancy, we must be able to transform from one coordinate system to the other. It is generally convenient to select a body axes aligned with the principal inertial axes to simplify the description of inertial terms. Therefore,

$$\underline{\mathbf{I}} = \begin{vmatrix} I_x & 0 & 0 \\ 0 & I_y & 0 \\ 0 & 0 & I_z \end{vmatrix} \quad (2.176)$$

Let

$$\boldsymbol{\omega} = pi + qj + rk \quad (2.177)$$

Therefore,

$$\mathbf{T} = \dot{\mathbf{H}} + \boldsymbol{\omega} \times \mathbf{H} = [I_x \dot{p} + (I_z - I_y) qr] \mathbf{i} \quad (2.178)$$

$$+ [I_y \dot{q} + (I_x - I_z) pr] \mathbf{j} \quad (2.179)$$

$$+ [I_z \dot{r} + (I_y - I_x) pq] \mathbf{k} \quad (2.180)$$

The external torque on a re-entry vehicle (with no thrust) about the center of gravity is composed of only aerodynamic moments, as

$$\mathbf{T} = Li + Mj + Nk \quad (2.181)$$

where

$$L = C_l q * Sb \quad (2.182)$$

$$M = C_m q * Sc \quad (2.183)$$

$$N = C_n q * Sb \quad (2.184)$$

in which $q * = \frac{1}{2} \rho V^2$ is the dynamic pressure.

Equating the aerodynamic torque to the inertial moments produces three relationships for p , q , and r , as

$$I_x \dot{p} + (I_z - I_y) qr = C_l q * Sb \quad (2.185)$$

$$I_y \dot{q} + (I_x - I_z) pr = C_m q * Sc \quad (2.186)$$

$$I_z \dot{r} + (I_y - I_x) pq = C_n q * Sb \quad (2.187)$$

To proceed further, the aerodynamic moment coefficients must be described. These are defined in terms of wind axes variables; therefore, a transformation between the different axes systems is needed. For a Euler angle sequence of ψ , θ , and ϕ ,

$$p_w = \dot{\phi}_w - \dot{\psi}_w \sin \theta_w \quad (2.188)$$

$$q_w = \dot{\theta}_w \cos \phi_w + \dot{\psi}_w \cos \theta_w \sin \phi_w \quad (2.189)$$

$$r_w = \dot{\psi}_w \cos \theta_w \cos \phi_w - \dot{\theta}_w \sin \phi_w \quad (2.190)$$

The same equations without subscript w refers to body axes. The aerodynamic angles are

$$\tan \alpha = w/u \text{ and } \sin \beta = v/V \quad (2.191)$$

Relationships for the aerodynamic angle derivatives are also required, i.e.,

$$\dot{\alpha} = q - q_w \sec \beta - (p \cos \alpha - r \sin \alpha) \tan \beta \quad (2.192)$$

$$\dot{\beta} = r_w + p \sin \alpha - r \cos \alpha \quad (2.193)$$

$$p_w = (p \cos \alpha + r \sin \alpha) \cos \beta + (q - \dot{\alpha}) \sin \beta \quad (2.194)$$

Also,

$$\dot{x} = V \cos \theta_w \cos \psi_w \quad (2.195)$$

$$\dot{y} = V \cos \theta_w \sin \psi_w \quad (2.196)$$

$$\dot{z} = -V \sin \theta_w \quad (2.197)$$

We will examine the small perturbations of these equations. The reference steady-state situation will be $\gamma \equiv \theta_w$, $\phi = 0$, $\psi = 0$, and $\beta = 0$. But both α and θ can be large. This is a necessary condition for hypersonic re-entry for lifting vehicles, i.e., the Space Shuttle entered at $\alpha = 40$ deg and $\gamma = 0$ on its first flight.

The following approximations, then, greatly simplify the interrelationship between the aerodynamic angles and body reference angles:

$$p_w = \dot{\phi}_w \quad p = \dot{\phi} - \dot{\psi} \sin \theta \quad (2.198)$$

$$q_w = \dot{\theta}_w = \dot{\gamma} \quad q = \dot{\theta} \quad (2.199)$$

$$r_w = \dot{\psi}_w \quad r = \dot{\psi} \cos \theta \quad (2.200)$$

Also, $\dot{\alpha} = q - q_w = \dot{\theta} - \dot{\gamma}$, which integrates to $\theta = \gamma + \alpha$. Thus,

$$\dot{\beta} = r_w + p \sin \alpha - r \cos \alpha \quad (2.201)$$

$$p_w = p \cos \alpha + r \sin \alpha \quad (2.202)$$

These integrate for ($\gamma = 0$) to $\beta = \psi_w - \psi + \phi \sin \alpha$; $\phi_w = \phi \cos \alpha$.

We are now in position to describe the aerodynamic forces and moments in terms of the above angles, i.e., $C_m = C_m(\alpha, \beta, p, q, r)$, etc.

Let us first examine the pitching moment created by a horizontal tail rotating at $\dot{\theta}$ about the center of gravity of the spacecraft (Fig. 2.4),

$$\dot{\theta} = q$$

In this situation, the rotation of the tail induces an angle of attack equal to

$$\tan \alpha_e = \dot{\theta} l / V \quad (2.203)$$

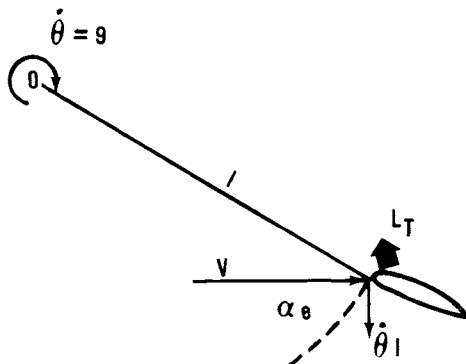


Fig. 2.4 Pitching moment created by a horizontal tail rotating about the center of gravity of an aerospace craft.

The induced lift is

$$L_T = (q * S_T C_{L\alpha})(\dot{\theta}l/V) \quad (2.204)$$

and the moment is

$$M_T = -lL_t \quad (2.205)$$

The moment coefficient due to the contribution of this effect is

$$C_m = \frac{M_T}{q * S_c} = -\frac{S_T}{S} \frac{l}{c} C_{L\alpha} \frac{\dot{\theta}l}{V} = C_{mq} \left(\frac{\dot{\theta}l}{V} \right) \quad (2.206)$$

Consider a case where $\dot{\theta} = 1$ rad/s and $l = 20$ ft. At $V = 200$ ft/s, $\alpha_e = 6$ deg, while at $V = 20,000$ ft/s, $\alpha_e = 0.06$ deg. The general conclusion drawn from this situation is that hypersonic forces due to rotation are negligible. Hence, $C_{mq} = 0$ and also $C_{mp} = 0$, $C_{mr} = 0$.

All rotary derivatives at hypersonic speeds are small. Only in unusual circumstances are they included. Therefore, $C_m = C_m(\alpha, \beta)$, etc. This greatly simplifies the stability analysis; however, the consequence of this condition is extremely important. Since the rotary derivatives produce the damping of the vehicle, undamped or neutral oscillations should be anticipated. The following is a method for describing the aerodynamic coefficients at hypersonic speed to conduct a stability analysis:

$$C_L = (C_{L\alpha})\alpha \quad C_c = -(C_{y\beta})\beta \quad (2.207)$$

$$C_D = C_{D0} + (C_{D\alpha})\alpha \quad C_l = (C_{l\beta})\beta \quad (2.208)$$

$$C_m = (C_{m\alpha})\alpha \quad C_n = (C_{n\beta})\beta \quad (2.209)$$

The governing equations are shown in Table 2.3.

The stability modes summarized in Table 2.4 are similar to those observed at low speeds; however, the numerical values can be quite different. The fact that negligible damping exists totally changes the design criteria. Normally, the aircraft designer attempts to establish modes with a frequency of 0.5 cycle/s and a damping ratio of about 0.7. This will establish satisfactory handling qualities as confirmed by the pilot's Cooper scale rating system. At hypersonic speeds, this is not possible (except artificially through the stability augmentation system); therefore, the handling quality criteria must be changed. Since zero damping implies periodic motion with constant amplitude, the pilot must damp out oscillations by "out-of-phase" control modulation. To accomplish this, the oscillation must possess a period long enough to permit sufficient time for pilot phase control ($P > 10$ s). Therefore, for zero damping, near-zero frequency is required. This condition is not comfortable to fly, but has been deemed acceptable through flight simulator training. Therefore, the stability constraints are, for frequencies with small positive numbers,

$$\omega_\alpha \rightarrow +0 \text{ and } \omega_\beta \rightarrow +0$$

Table 2.3 Governing Flight Dynamic Equations

Longitudinal Equations	Lateral Equations
$-\frac{\dot{V}}{g} = \frac{D}{W} + \gamma$	$I_x \dot{p} = L$
$I_y \dot{q} = M$	$\frac{V}{g} r_w = \left(1 - \frac{V^2}{V_c^2}\right) \phi_w - \frac{C}{W}$
$-\frac{V}{g} q_w = 1 - \frac{V^2}{V_c^2} - \frac{L}{W}$	$I_z \dot{r} = N$
where $q = \dot{\theta}, \quad q_w = \dot{\gamma}$	where $\dot{\beta} = r_w + p \sin \alpha - r \cos \alpha$ $\dot{\phi}_w = p_w = p \sin \alpha + r \sin \alpha$
Integrated $\theta = \alpha + \gamma, \quad \dot{h} = V\gamma$ $q * = \frac{1}{2} \rho_{sl} e^{-\hat{a}h} V^2$ $M = (q * ScC_{ma})\alpha$ $D = q * Sc_D$ $L = q * Sc_L$	Integrated $\phi_w = \phi \cos \alpha, \quad \beta = \psi_w - \psi + \phi \sin \alpha$ $L = (q * SbC_{l\beta})\beta$ $C = -(q * SC_{Y\beta})\beta$ $N = (q * SbC_{n\beta})\beta$
Variables: V, h, θ	β, r_w, ϕ_w

Table 2.4 Summary of Stability Modes

Mode	Name	Equation
<u>Longitudinal</u>		
$\ddot{\theta} + \omega_\alpha^2 \theta = 0$	Short period	$\theta = \hat{\theta} e^{i\omega_\alpha t}$
$\Delta \ddot{h} + \omega_h^2 \Delta h = 0$	Phugoid	$\Delta h = \hat{h} e^{i\omega_h t}$
$\dot{V} = -gD/W$	Dissipation	$V = V_c - \int (g\dot{D}/W) dt$
Stability criteria		
$\omega_\alpha^2 = -\frac{q * ScCm_\alpha}{I_y} > 0$		$\omega_h^2 = \hat{\alpha}g(1 - \frac{V^2}{V_c^2}) > 0$
<u>Lateral</u>		
$\ddot{\beta} + \omega_\beta^2 \beta = \dot{r}_w \rightarrow 0$	Dutch roll	$\beta = \hat{\beta} e^{i\omega_\beta t}$
$\ddot{\phi}_w + \omega_\phi^2 \beta = 0$	Roll convergence	$\phi_w = \hat{\phi} e^{-\left[\omega_w \frac{\omega_\phi^2}{\omega_\beta^2}\right]t}$
$r_w - \omega_v \phi_w + \omega_Y \beta = 0$	Spiral mode	$r_w = \hat{r} e^0 = \text{const}$
Stability criteria		
$\omega_\beta^2 = q * Sb \left[\frac{C_{n\beta} \cos \alpha}{I_z} - \frac{C_{l\beta} \sin \alpha}{I_x} \right] > 0$		
$\omega_\phi^2 = -q * Sb \left[\frac{C_{n\beta} \sin \alpha}{I_z} + \frac{C_{l\beta} \cos \alpha}{I_x} \right] > 0$		
$\omega_Y = \frac{g}{V} \frac{q * S}{W} C_{Y\beta} > 0$		$\omega_v = \frac{g}{V} \left(1 - \frac{V^2}{V_c^2} \right) > 0$

Gyroscopic Stabilization

For missile applications, stability can be achieved at hypersonic speeds (where little damping is present) by rolling about the x axis. Consider zero aerodynamic torque about the body, where $T = 0$, and small perturbations for p , q , and r ,

$$p = \Omega + p'(t) \quad (2.210)$$

$$q = q'(t) \quad (2.211)$$

$$r = r'(t) \quad (2.212)$$

Hence,

$$I_x \dot{p}' = 0 \quad (2.213)$$

$$I_y \dot{q}' - (I_z - I_x) \Omega r' = 0 \quad (2.214)$$

$$I_z \dot{r}' + (I_y - I_x) \Omega q' = 0 \quad (2.215)$$

Assume

$$I_y = I_z \gg I_x \text{ and } \frac{I_z - I_x}{I_y} \equiv K < 1 \quad (2.216)$$

Hence,

$$\dot{q}' - K\Omega r' = 0 \quad (2.217)$$

$$\dot{r}' + K\Omega q' = 0 \quad (2.218)$$

or

$$\ddot{q}' + K^2\Omega^2 q' = 0 \quad (2.219)$$

$$q' = q_0 \cos K\Omega t = \dot{\theta} \cos \phi + \dot{\psi} \sin \phi \quad (2.220)$$

and

$$r' = -q_0 \sin K\Omega t = \dot{\psi} \cos \phi - \dot{\theta} \sin \phi \quad (2.221)$$

$$p' = \Omega = \dot{\phi} \quad (2.222)$$

The equations can be integrated to produce the following relationships for the Euler angles:

$$\dot{\phi} = \Omega \quad \phi = \Omega t \quad (2.223)$$

$$\dot{\theta} = q_0 \cos(1 - K)\phi \quad \theta = \frac{q_0}{(1 - K)\Omega} \sin(1 - K)\Omega t \quad (2.224)$$

$$\dot{\psi} = q_0 \sin(1 - K)\phi \quad \psi = -\frac{q_0}{(1 - K)\Omega} \cos(1 - K)\Omega t \quad (2.225)$$

Note that

$$\dot{\theta}^2 + \dot{\psi}^2 = \frac{q_0^2}{(1 - K)^2 \Omega^2} = \text{const} \quad (2.226)$$

Although coning motion of the nose occurs, no departure results, indicating that a simple limit cycle occurs. This is the fundamental principle of gyroscopic stabilization and is used in both artillery and missile applications.

References

¹Loh, W., *Reentry and Planetary Entry Physics and Technology*, Springer-Verlag, New York, 1968.

² Constant, F., *Theoretical Physics*, Addison-Wesley, Reading, MA, 1954.

³ Chapman, D., "An Approximate Analytical Method for Studying Entry Into Planetary Atmospheres," NACA TN 4276, May 1958.

⁴ Etkin, B., *Dynamics of Atmospheric Flight*, Wiley, New York, 1972.

Problems

2.1 Consider the moon as a satellite of the Earth with a period of 28 days. Compute the moon's circular velocity and radius from the Earth's center.

2.2 Calculate the required distance above the Earth for a synchronous orbit satellite that will appear stationary to an observer on the Earth's equator.

2.3 For a lifting body with a hypersonic L/D of 2.0, compute the time of re-entry from a near-Earth circular orbit after a retrofire of 500 ft/s.

2.4 For a W/SC_L of 100 lb/ft², determine the velocity and altitude for which peak laminar heating occurs on a lifting re-entry vehicle.

2.5 For an orbital decay re-entry vehicle with a $W/SC_D = 100$ lb/ft², determine the altitude for peak laminar heating and maximum deceleration.

2.6 Perform the numerical integration using Euler's method for an orbital decay re-entry with a $W/SC_D = 100$ lb/ft². Check the results of Problem 2.5.

2.7 Compute the period of the hypersonic phugoid for the Space Shuttle configuration.

2.8 For the configuration of Problem 2.3, compute the lateral and longitudinal range for a constant bank angle of 30 deg.

2.9 For the Space Shuttle configuration, compute the hypersonic "short-period" and "Dutch roll" frequencies.

2.10 For an axisymmetric missile with the following characteristics, determine the coning motion frequency:

$$I_x = 3 \times 10^3 \text{ slug} \cdot \text{ft}^2 \quad I_z = 1.2 \times 10^4 \text{ slug} \cdot \text{ft}^2$$

$$I_y = 1.2 \times 10^4 \text{ slug} \cdot \text{ft}^2 \quad \Omega = 10,000 \text{ rpm}$$

This page intentionally left blank

3

HYPersonic AERODYNAMICS

3.1 GOVERNING EQUATIONS

Various levels of sophistication can be employed to attack a problem in aerodynamics. The approach taken depends upon the accuracy required, time and funds available, etc. Table 3.1 lists the prediction methods and their restrictions. In this chapter, the governing equations of fluid mechanics (Navier-Stokes equations) will be derived; however, prior to this derivation, some vector analysis relationships will be summarized for convenience.¹

Table 3.1 Aerodynamic Prediction Methods

Level	Type	Limitation	Complexity	Computer Time
0	Empirical	Qualitative	Algebraic	Seconds
I	Linear	Small $\alpha M = 1$	Algebraic	Minutes
II	Inviscid	No separation	Differentials	Hour
III	Navier-Stokes	No restriction	Partial differential	Hours

Vector Analysis

Vector: $\mathbf{V} = iu + jv + kw$

Elemental area: $d\mathbf{A} = i dA_x + j dA_y + k dA_z$

Dot product:

$$\mathbf{V} \cdot d\mathbf{A} = u dA_x + v dA_y + w dA_z$$

Divergence of
vector:

$$\nabla \cdot \mathbf{V} = \frac{\partial u}{\partial x} + \frac{\partial v}{\partial y} + \frac{\partial w}{\partial z}$$

Dyadic:

$$\underline{\mathbf{P}} = \begin{vmatrix} \sigma_{11} & \tau_{12} & \tau_{13} \\ \tau_{21} & \sigma_{22} & \tau_{23} \\ \tau_{31} & \tau_{32} & \sigma_{33} \end{vmatrix} = \begin{array}{l} i\bar{u}\sigma_{11} + j\bar{v}\tau_{12} + k\bar{w}\tau_{13} \\ + j\bar{i}\tau_{21} + j\bar{j}\sigma_{22} + j\bar{k}\tau_{23} \\ + k\bar{i}\tau_{31} + k\bar{j}\tau_{32} + k\bar{k}\sigma_{33} \end{array}$$

(Note: for the directions of stress components, see Fig. 3.1.)

Dot product of
dyadic:

$$\begin{aligned} \mathbf{V} \cdot \underline{\mathbf{P}} &= i(u\sigma_{11} + v\tau_{21} + w\tau_{31}) \\ &\quad + j(u\tau_{12} + v\sigma_{22} + w\tau_{32}) \\ &\quad + k(u\tau_{13} + v\tau_{23} + w\sigma_{33}) \end{aligned}$$

Divergence of
dyadic:

$$\begin{aligned} \nabla \cdot \underline{\mathbf{P}} &= i \left(\frac{\partial \sigma_{11}}{\partial x} + \frac{\partial \tau_{21}}{\partial y} + \frac{\partial \tau_{31}}{\partial z} \right) \\ &\quad + j \left(\frac{\partial \tau_{12}}{\partial x} + \frac{\partial \sigma_{22}}{\partial y} + \frac{\partial \tau_{32}}{\partial z} \right) \\ &\quad + k \left(\frac{\partial \tau_{13}}{\partial x} + \frac{\partial \tau_{23}}{\partial y} + \frac{\partial \sigma_{33}}{\partial z} \right) \end{aligned}$$

Substantial
derivative:

$$\begin{aligned} \frac{D\mathbf{V}}{Dt} &= \frac{\partial \mathbf{V}}{\partial t} + (\mathbf{V} \cdot \nabla) \mathbf{V} \\ &= \frac{\partial \mathbf{V}}{\partial t} + \nabla \frac{\mathbf{V}^2}{2} - \mathbf{V} \times (\nabla \times \mathbf{V}) \end{aligned}$$

Green's theorem:

$$\iint \mathbf{V} \cdot d\mathbf{A} = \iiint (\nabla \cdot \mathbf{V}) dV$$

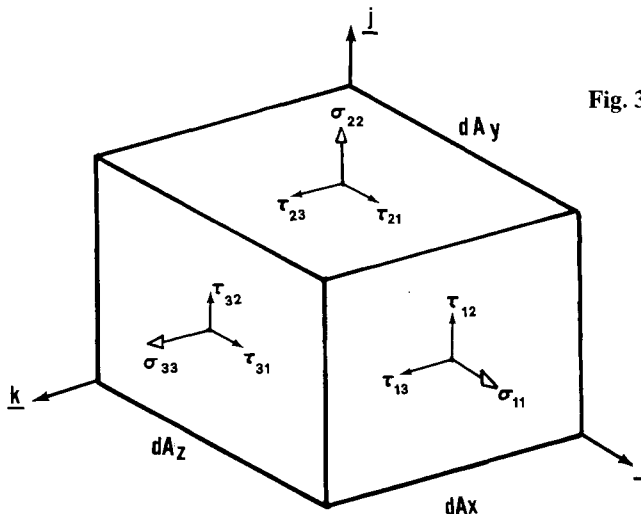


Fig. 3.1 Stress components.

Derivation of Navier-Stokes Equations

The governing equations of fluid mechanics are derived from statements of the conservation of mass, momentum, and energy for an arbitrary control volume, as shown in Fig. 3.2.

Continuity equation. The conservation of mass can be stated as

Net outflow of mass through surface = decrease of mass in control volume

$$\oint \rho V \cdot dA = -\frac{\partial m}{\partial t} = -\frac{\partial}{\partial t} \iiint \rho dV \quad (3.1)$$

But Green's theorem states

$$\oint \rho V \cdot dA = \iiint (\nabla \cdot \rho V) dV \quad (3.2)$$

Hence, after substitution

$$\iiint \left[\frac{\partial \rho}{\partial t} + \nabla \cdot \rho V \right] dV = 0 \quad (3.3)$$

Since the control volume V is completely arbitrary, the integrand of the integral must vanish, i.e.,

$$\frac{\partial \rho}{\partial t} + \nabla \cdot \rho V = 0 \quad (3.4)$$

which is the continuity equation.

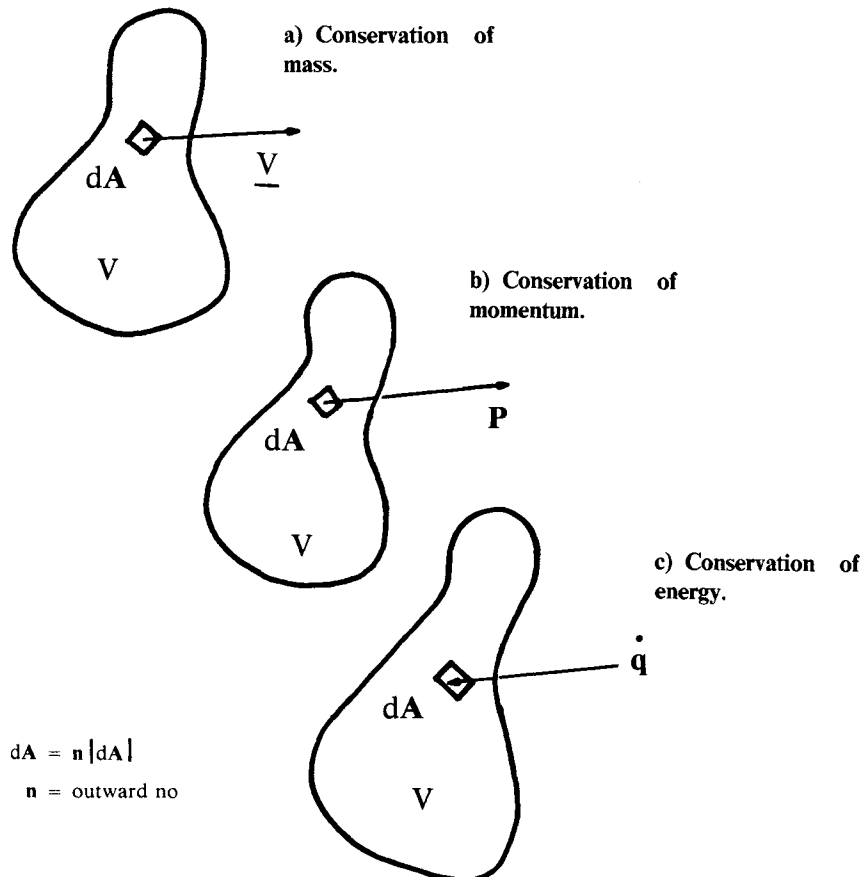


Fig. 3.2 Control volume for the Navier-Stokes equations ($dA = n|dA|$, n = outward normal).

Momentum equation. The conservation of momentum can be stated as

$$\text{Sum of external forces} = \text{rate of change of momentum}$$

$$\Sigma \mathbf{F} = \iiint \rho \frac{D\mathbf{V}}{Dt} dV \quad (3.5)$$

$$\Sigma \mathbf{F} = \text{sum of stresses} \times \text{area}$$

in unit vector directions

$$= \iint_{\underline{\underline{A}}} \mathbf{P} \cdot d\mathbf{A} \quad (3.6)$$

where \mathbf{P} is the stress dyadic, stress tensor, or stress matrix.

HYPersonic AERODYNAMICS

55

A dyadic is treated as a “double vector” and is manipulated as such. It is symmetric and composed of three normal stresses and six shear stresses,

$$\underline{\underline{P}} = (-p + \lambda \nabla \cdot \underline{\underline{V}}) \underline{\underline{I}} + \mu (\nabla \underline{\underline{V}} + \underline{\underline{V}} \nabla) \quad (3.7)$$

Green’s theorem is used as follows:

$$\Sigma \underline{\underline{F}} = \oint \underline{\underline{P}} \cdot d\underline{A} = \iiint (\nabla \cdot \underline{\underline{P}}) dV \quad (3.8)$$

Hence,

$$\iiint \left[\rho \frac{D\underline{\underline{V}}}{Dt} - \nabla \cdot \underline{\underline{P}} \right] dV = 0 \quad (3.9)$$

As before, the condition that the integrand must vanish requires that

$$\rho \frac{D\underline{\underline{V}}}{Dt} = \nabla \cdot \underline{\underline{P}} \quad (3.10)$$

which is the momentum equation.

Energy equation. The conservation of energy can be stated as

$$\text{Rate of heat added} + \text{rate of work done} = \text{rate of change in internal energy}$$

$$\frac{dQ}{dt} + \frac{dW}{dt} = \frac{dE}{dt} \quad (3.11)$$

$$\oint \dot{\underline{\underline{q}}} \cdot d\underline{A} + \Sigma \underline{\underline{F}} \cdot \underline{\underline{V}} = \iiint \rho \frac{De}{Dt} dV \quad (3.12)$$

or

$$\iint [\dot{\underline{\underline{q}}} + \underline{\underline{P}} \cdot \underline{\underline{V}}] dA = \iiint \rho \frac{De}{Dt} dV \quad (3.13)$$

where

$$e = C_v T + V^2/2 \quad (3.14)$$

and

$$\dot{\underline{\underline{q}}} = k \nabla T \quad (3.15)$$

Green's theorem produces

$$\iiint \nabla \cdot [\underline{\underline{P}} \cdot \underline{V} + \dot{\underline{q}}] dV = \iiint \rho \frac{De}{Dt} dV \quad (3.16)$$

Similarly, for the integrand to vanish,

$$\rho \frac{De}{Dt} = \nabla \cdot [\underline{\underline{P}} \cdot \underline{V} + \dot{\underline{q}}] \quad (3.17)$$

which is the energy equation.

Divergence Form of Equations

Multiplying e times the continuity equation (3.4) and adding to the energy equation (3.17) produces the following:

$$\begin{aligned} e \left(\frac{\partial \rho}{\partial t} + \nabla \cdot \rho \underline{V} \right) + \rho \frac{De}{Dt} &= e \frac{\partial \rho}{\partial t} + \rho \frac{\partial e}{\partial t} + e \nabla \cdot \rho \underline{V} + \rho \underline{V} \cdot \nabla e \\ &= \frac{\partial \rho e}{\partial t} + \nabla \cdot \rho \underline{V} e = \nabla \cdot (\underline{\underline{P}} \cdot \underline{V} + \dot{\underline{q}}) \end{aligned}$$

or

$$\frac{\partial}{\partial t} (\rho e) + \nabla \cdot (\rho \underline{V} e - \underline{\underline{P}} \cdot \underline{V} - \dot{\underline{q}}) = 0 \quad (3.18)$$

Similarly, adding \underline{V} times the continuity to the momentum equation produces the divergence form of the momentum equation,

$$\frac{\partial}{\partial t} (\rho \underline{V}) + \nabla \cdot [\rho \underline{V} \underline{V} - \underline{\underline{P}}] = 0 \quad (3.19)$$

Note that the conservation of mass, momentum, and energy can now be written in identical form using the divergence vector in Cartesian coordinates,

$$\frac{\partial U}{\partial t} + \frac{\partial E}{\partial x} + \frac{\partial F}{\partial y} + \frac{\partial G}{\partial z} = 0 \quad (3.20)$$

where

$$U = \begin{vmatrix} \rho \\ \rho u \\ \rho v \\ \rho w \\ \rho e \end{vmatrix} \quad (3.21)$$

HYPERSONIC AERODYNAMICS

57

$$E = \begin{vmatrix} \rho u \\ \rho u^2 - \sigma_{11} \\ \rho uv - \tau_{12} \\ \rho uw - \tau_{13} \\ \rho ue - u\sigma_{11} - v\tau_{12} - w\tau_{13} - kT_x \end{vmatrix} \quad (3.22)$$

in which

$$\sigma_{11} = -p + \lambda \nabla \cdot V + 2\mu u_x \quad (3.23)$$

$$\tau_{12} = \mu(u_y + v_x) \quad (3.24)$$

$$\tau_{13} = \mu(u_z + w_x) \quad (3.25)$$

The continuity, momentum, and energy equations (two scalar, one vector) contain four unknowns, i.e., V , ρ , p , and T . The equation of state is needed to solve the system completely. For the present case, an ideal gas can be assumed for which the equation of state is

$$p = \rho RT \quad (3.26)$$

This is the fourth equation required. Values for the transport and thermodynamic properties (μ , k , C_v , R) are also required as input. These equations, along with the appropriate boundary conditions, are capable of representing nearly any aerodynamic problem in the aviation field.

3.2 AERODYNAMIC PREDICTION METHODS

In this section, lower forms or approximations of the Navier-Stokes equations will be derived, based on Table 3.1.

Level III: Navier-Stokes.

$$\frac{\partial U}{\partial t} + \frac{\partial E}{\partial x} + \frac{\partial F}{\partial y} + \frac{\partial G}{\partial z} = 0 \quad (3.20)$$

Level IIIA: Parabolized Navier-Stokes. Here $\partial U / \partial t = 0$ and Eq. (3.20) reduces to

$$\frac{\partial E}{\partial x} = -\frac{\partial F}{\partial y} - \frac{\partial G}{\partial z} \quad (3.27)$$

where

$$E = \begin{vmatrix} \rho u \\ \rho u^2 + p \\ \rho uv \\ \rho uw \\ \rho ue \end{vmatrix} \quad (3.28)$$

It should be noted that viscous terms occur only in F and G .

Level IIIB: Two-Dimensional Boundary Layer. For this case, $\partial U / \partial t = 0$, $\partial G / \partial z = 0$, and

$$\underline{\underline{P}} = \begin{vmatrix} -p & \mu u_y \\ \mu u_y & -p \end{vmatrix} \quad (3.29)$$

or

$$(\rho u)_x + (\rho v)_y = 0 \quad (3.30)$$

$$(\rho u^2 + p)_x + (\rho uv - \mu u_y)_y = 0 \quad (3.31)$$

$$p_y = 0 \quad (3.32)$$

$$(\rho u H)_x + (\rho v H - u \tau - k T_y)_y = 0 \quad (3.33)$$

Level IIA: Inviscid (Euler).

$$\mu = 0, \quad k = 0$$

$$\underline{\underline{P}} = -p \underline{\underline{I}} \quad (3.34)$$

$$\frac{\partial U}{\partial t} = 0 \quad (3.35)$$

$$\nabla \cdot \rho \underline{\underline{V}} = 0 \quad (3.36)$$

$$\nabla \cdot (\rho \underline{\underline{V}} \underline{\underline{V}} + p \underline{\underline{I}}) = 0 \quad (3.37)$$

$$\nabla \cdot (\rho \underline{\underline{V}} H) = 0 \quad (3.38)$$

where $H = e + p/\rho$.

By combining the last equation with the first, one finds that $H = \text{const}$. Hence, one differential equation reduces to an algebraic equation, thereby reducing the computer time to solve the system.

Alternate forms of the inviscid momentum and energy equations are often used, such as

$$\frac{D \underline{\underline{V}}}{Dt} = - \frac{\nabla p}{\rho} = \frac{\partial \underline{\underline{V}}}{\partial t} + \nabla \frac{V^2}{2} - \underline{\underline{V}} \times \boldsymbol{\omega} \quad (3.39)$$

and

$$\frac{\gamma p}{\rho} = a^2 = a_0^2 - \frac{\gamma - 1}{2} V^2 \quad (3.40)$$

HYPERSONIC AERODYNAMICS

59

Level IIB: Inviscid, Irrotational (Full Potential). A great simplification arises when the vorticity of the flow is zero, $\omega = 0$. This implies that the viscosity vanishes (which has already been assumed) and that no shocks exist. In practice, this means that $M_n < 1.5$ (for which a 7% total pressure drop occurs) and $p_2/p_1(M_n = 1.5) < 2.46$ or that only weak shocks are permitted. When this occurs a velocity potential can be introduced,

$$\mathbf{V} = \nabla \phi \quad (3.41)$$

Automatically,

$$\boldsymbol{\omega} = \nabla \times \mathbf{V} = \nabla \times \nabla \phi = 0 \quad (3.42)$$

since the curl of the gradient vanishes identically. The governing equations become

$$\nabla \cdot \rho \nabla \phi = 0 \quad (3.43)$$

$$\frac{\gamma}{2} \rho \nabla (\nabla \phi)^2 + \nabla (\rho a^2) = 0 \quad (3.44)$$

and

$$a^2 = a_0^2 - \frac{\gamma - 1}{2} (\nabla \phi)^2 \quad (3.45)$$

These equations produce the full potential equation,

$$a^2 \nabla^2 \phi = \nabla \phi \cdot (\nabla \phi \cdot \nabla \nabla \phi) \quad (3.46)$$

Expanding these in Cartesian coordinates results in

$$a^2 (\phi_{xx} + \phi_{yy} + \phi_{zz}) = u^2 \phi_{xx} + v^2 \phi_{yy} + w^2 \phi_{zz} + 2uv\phi_{xy} + 2uw\phi_{xz} + 2vw\phi_{yz} \quad (3.47)$$

where $u = \phi_x$, $v = \phi_y$, and $w = \phi_z$.

Level I: Linearized Equation. Level 1 is further restricted by simplifying the nonlinear partial differential potential equation to make it linear, a form for which analytic methods of solution have been developed.

Assume a small perturbation

$$u = U_\infty + u'(x, y, z) \quad (3.48)$$

$$v = v'(x, y, z) \quad (3.49)$$

$$w = w'(x, y, z) \quad (3.50)$$

Table 3.2 Summary of Aerodynamic Prediction Methods

Level	Type	No. of Terms	No. of Boundary Conditions	Restriction
III	Navier-Stokes	77	27	None
	A) Parabolized		23	$\frac{\partial^2}{\partial x^2} = 0$
	B) Boundary layer		9	$v/u \ll 1$
II	Inviscid			
	A) Euler	15	12	$\mu = 0$
I	Full potential	9	6	Weak shocks
	Linear	3	6	$u = U_\infty + u'$

or

$$\phi = xU_\infty + \phi' \quad (3.51)$$

Hence,

$$(1 - M_\infty^2)\phi'_{xx} + \phi'_{yy} + \phi'_{zz} = 0 \quad (3.52)$$

Table 3.2 presents a summary of the prediction methods. The number of boundary conditions required is shown in Table 3.3.

3.3 HYPERSONIC AERODYNAMIC CHARACTERISTICS

The Navier-Stokes equations provide an all-inclusive procedure for computing re-entry vehicle force and moment coefficients at hypersonic speeds.

HYPERSONIC AERODYNAMICS

Table 3.3 Required Number of Boundary Conditions

Level	Type	Variables	Boundary Condition			Total
			x	y	z	
III	Navier-Stokes	<i>u</i>	2	2	2	
		<i>v</i>	2	2	2	
		<i>w</i>	2	2	2	
		<i>p</i>	1	1	1	
		<i>T</i>	2	2	2	27
IIIA	Parabolized Navier-Stokes	<i>u</i>	1	2	2	
		<i>v</i>	1	2	2	
		<i>w</i>	1	2	2	
		<i>p</i>	1	1	1	
		<i>T</i>	1	2	2	23
IIIB	Two-dimensional boundary layer	<i>u</i>	1	2		
		<i>v</i>	0	1		
		<i>p</i>	1	1		
		<i>T</i>	1	2		9
IIA	Inviscid Euler	<i>u</i>	1	1	1	
		<i>v</i>	1	1	1	
		<i>p</i>	1	1	1	
		<i>T</i>	1	1	1	12
IIB	Full potential	ϕ	2	2	2	6
I	Linear	ϕ	2	2	2	6

However, simpler approximate methods are frequently required in preliminary design. Simple techniques are developed in this section for rapidly determining the aerodynamic pressures and resultant six-component force and moment characteristics for hypersonic glide vehicles. The methods are applicable between 10 and 50 deg angle of attack, since this covers the $(L/D)_{\max}$ range of interest (from 4 to 1). For extremely low or extremely high angles of attack, prediction of the aerodynamic characteristics becomes more complex and need not be investigated here. The techniques discussed here are further limited to the continuum flow regime in that the aerodynamic characteristics are of primary interest (for stability and performance) only when the dynamic pressure is significant. At low dynamic pressures ($q < 10 \text{ lb/ft}^2$), reaction controls are required for stability and control of space vehicles. At orbital speed, a dynamic pressure of 10 lb/ft^2 occurs at an altitude of about 265,000 ft for which the mean free path is

about 0.01 ft. The Knudsen number based upon a 10 ft chord would be 10^{-3} , indicating that a continuum flow model may be used.

Expressions for the pressure distribution over simple shapes (spheres, cylinders, and planar surfaces) are first derived. A generalized configuration is defined composed of the preceding simple elements, and an analytical expression for the aerodynamic coefficients resulting from integration of the surface pressures is presented. Finally, a summary of the six-component aerodynamic characteristics is tabulated for convenience in programming on high-speed computers.

Pressure Distribution Theory

For rapid prediction of aerodynamic forces and pressures on hypersonic aerodynamic vehicles, simple, basic theory is desirable. Perhaps the most popular theory for this type of analysis is the Newtonian impact theory and its various modifications.²

The Newtonian flow concept assumes that the freestream gas, upon striking a surface, loses its component of momentum normal to that surface and then moves along the surface with its tangential component of momentum unchanged (inelastic collision). From this assumption, the pressure coefficient is defined by

$$C_p = 2 \sin^2 \delta \quad (3.53)$$

where δ is the local flow inclination with the freestream (angle measured between the velocity vector and the surface) and

$$C_p = (p - p_\infty) / q_\infty \quad (3.54)$$

In Ref. 3, the oblique shock relations are modified for the hypersonic case in which the shock wave angle approaches the body slope and an identical result is obtained, which illustrates the basic validity of the Newtonian flow theory for hypersonic conditions.

In Ref. 4, the modified Newtonian theory is presented as

$$C_p = C_{p_s} \sin^2 \delta \quad (3.55)$$

where C_{p_s} is the stagnation pressure coefficient.

A further modification is called the generalized Newtonian theory,

$$\frac{C_p}{C_{p_{\max}}} = \frac{\sin^2 \delta}{\sin^2 \delta_{\max}} \quad (3.56)$$

This form of the Newtonian theory is useful for pointed shapes such as tangent ogives.

In both of the preceding modifications, the basic form of the equation

$$C_p = k \sin^2\delta \quad (3.57)$$

is retained. The k factor reflects the change in pressure coefficient because of such factors as initial nose slope, Mach number, and change in gas composition, while the $\sin^2\delta$ term accounts for the surface orientation and geometry. Newtonian flow theory in its basic form is applicable only to hypersonic flow over highly inclined surfaces⁵; however, extension of the theory is possible if the present form is retained and the k factor adjusted.

The chief advantage in retaining the expression of the pressure coefficient in the form of Eq. (3.57) is found in the determination of force coefficients in that the required integrations are made relatively simple. A further advantage exists in that the force coefficient is directly proportional to the k factor. Therefore, the variation in the k factor over a range of flight conditions directly defines the variation of the force coefficients.

Blunt Surfaces in Impact Flow

Variation of the k factor for the stagnation region of a surface is illustrated in Fig. 3.3. In this figure, the variation of k for a real gas is shown for a range of Mach numbers and altitudes. Also shown is the variation of k for an ideal gas determined from the following relationship:

$$C_{p_s} = \left(\frac{P_{t_2}}{P_{t_1}} - \frac{P_1}{P_{t_1}} \right) \left(\frac{q}{P_t} \right)^{-1} \quad (3.58)$$

For a given type of flow and a given Mach number, Fig. 3.3 can be used to determine the C_{p_s} of modified Newtonian theory. Note that real-gas k

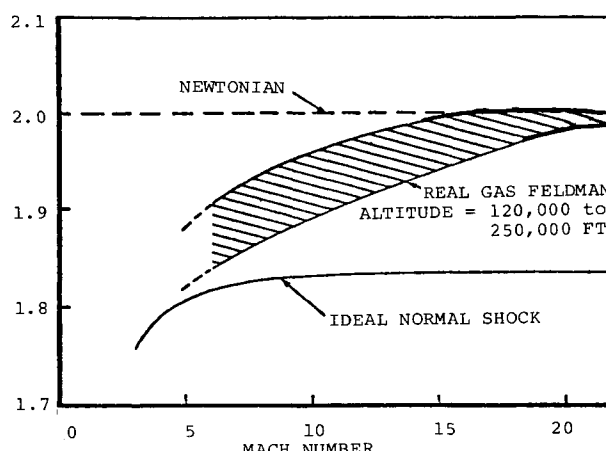


Fig. 3.3 Variation of stagnation pressure coefficient with Mach number.

factor values are seen to be rather insensitive to altitude in the range chosen.

The applicability of modified Newtonian theory on hemispheres and hemicylinders is illustrated in Fig. 3.4. This figure shows that Eq. (3.57), where k is determined from Fig. 3.3, is adequate for evaluating pressures and forces on these surfaces.

In the analysis of swept leading edges, crossflow theory is used. This reduces the complex three-dimensional problem to a simpler one in two dimensions. Using crossflow theory, Eq. (3.57) becomes

$$C_{ps} = k \cos^2 \Lambda_e \quad (3.59)$$

where Λ_e is the effective sweep angle of the leading edge.

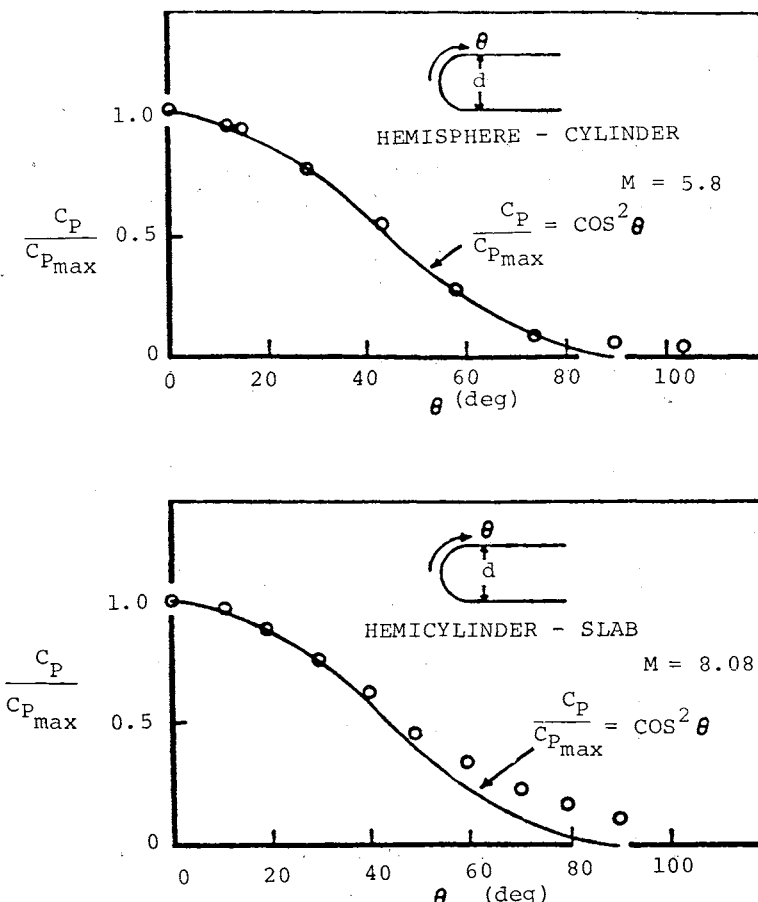


Fig. 3.4 Applicability of Newtonian theory to hemispheres and hemicylinders.

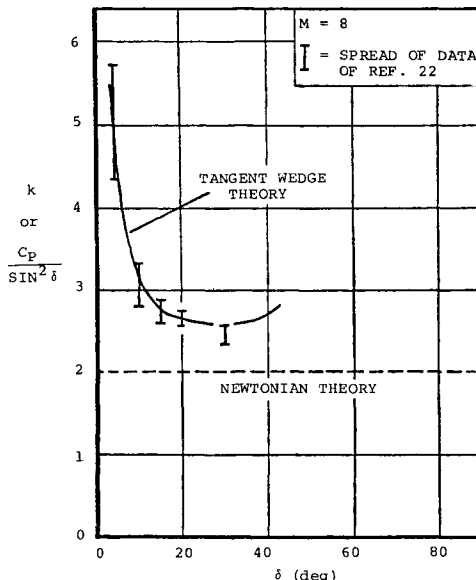


Fig. 3.5 Lower-surface pressure coefficients.

Flat Surfaces in Impact Flow

Where the modified Newtonian theory is significantly in error and the surface under consideration is large, some correction must be applied. An example of such a situation is the large lower surface of a blunt, swept delta wing. Figure 3.5 shows the change in pressure coefficients on a blunt wedge due to a change in the angle of attack. For angles of attack between 5 and 15 deg, the "tangent wedge" theory appears representative of the mean of the data. For angles of attack above 15 deg, the flow appears to change in nature and approaches Newtonian values until at 90 deg the flow stagnates at C_{p_s} .

As no single simple theory will predict the change in the nature of the flow across the angle-of-attack spectrum, several empirical correlation schemes have been attempted. The most successful of the schemes considered is the one shown in Fig. 3.6. The faired straight line through the data has the equation

$$k = 1.95 + 0.21 \cot \delta \quad (3.60)$$

For surface inclinations below 10 deg, the representation in Figs. 3.5 and 3.6 rapidly loses significance because, at $\delta = 0$ for any Mach number, k approaches infinity, which requires a change in the expression for C_p . Interaction and induced pressure effects also become dominant at low angles of attack, which requires a change in the analytical procedure. For these reasons, values of α much below 10 deg will not be considered.

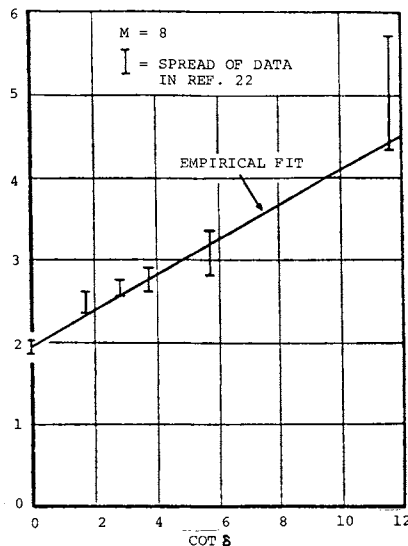


Fig. 3.6 Empirical correlation of lower-surface pressure coefficients.

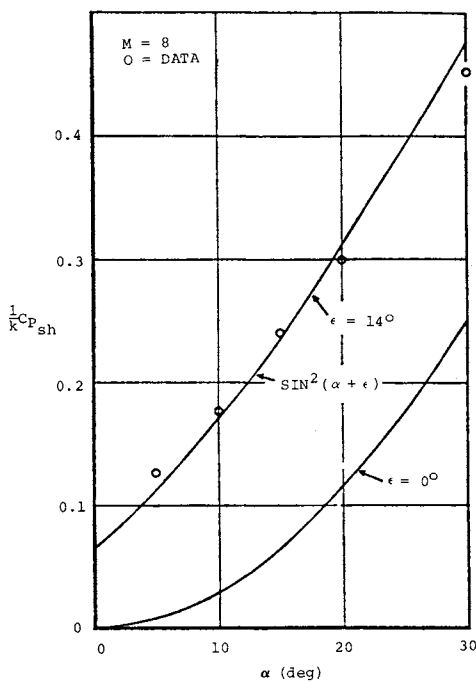


Fig. 3.7 Induced pressure correlation of blunt leading edges.

More comprehensive analyses must be applied only when the vehicle in question is considered to fly at low angles of attack. As presently anticipated, only gliders having L/D 's greater than 4 will fly at angles of attack less than 10 deg. These vehicles will require refined analysis at low angles of attack.

Induced Pressures

A blunted wedge at angle of the attack produces a curved shock wave near the leading edge. Farther away from the leading edge, the shock wave asymptotically approaches that of a sharp wedge. Because of this shock curvature, induced pressures commence at the leading-edge shoulder and diminish as the shock curvature reduces. Techniques are available that provide numerical solutions of the flowfield from which pressure distributions may be ascertained. However, since numerical results are not available in quantity, empirical correlation of the induced pressures is attempted.

From experimental pressure distributions, a linear variation in ΔC_p from zero at the centerline to $\Delta C_{p_{sh}}$ at the shoulder adequately accounts for the induced pressure distribution effects on delta wings with relatively small leading-edge radii. From the leading-edge pressure distribution of Ref. 2, the shoulder pressure may be ascertained by shifting the flow angle for the Newtonian pressure coefficient by a small value ϵ , so that

$$C_{p_{sh}} = k \sin^2(\alpha + \epsilon) \quad (3.61)$$

The induced pressure coefficients at the leading-edge shoulder are presented in Fig. 3.7 for various α values. From this figure, it is apparent that the form of Eq. (3.61) adequately accounts for induced pressure if a value of ϵ of 14 deg is included, while the unmodified Newtonian ($\epsilon = 0$) is quite inadequate. For swept leading edges,

$$C_{p_{sh}} = k \cos^2 \Lambda_e \sin^2(\alpha_e + \epsilon) \quad (3.62)$$

where Λ_e and α_e are defined by Eqs. (3.83) and (3.84). When the identity is used

$$\cos^2 \Lambda_e \sin^2 \alpha_e = \sin^2 \alpha \cos^2 \beta \quad (3.63)$$

Equation (3.63) may be expanded for small values of β and ϵ as follows:

$$C_{p_{sh}} = k \sin^2 \alpha (1 + 2\epsilon \cot \alpha_e) \quad (3.64)$$

The difference in shoulder pressure values is required in the determination of the rolling moment due to the yaw of delta wings. This pressure difference can be obtained by using Eq. (3.64) for the right and left shoulders as follows:

$$\Delta_{R-L} C_{p_{sh}} = 2k\epsilon \sin^2 \alpha (\cot \alpha_{e_R} - \cot \alpha_{e_L}). \quad (3.65)$$

For the geometry of interest in this study,

$$\Delta_{R-L} \cot \alpha_e \approx 4\beta$$

Therefore,

$$\Delta_{R-L} C_{p_{sh}} = k_i \beta \sin^2 \alpha \quad (3.66)$$

where

$$k_i = 8k\varepsilon = 3.8 \text{ per radian} \quad (3.67)$$

Surface Skin Friction

Several methods have been presented in the literature for the prediction of laminar skin friction on flat plates in supersonic and hypersonic flows. These methods are usually complex and laborious to apply and often require evaluation of the flowfield behind the compression shock wave. One of the more successful methods is the reference enthalpy method. This method has been used to predict skin friction over a flat plate for a wide range of flight conditions. Since the data are given in terms of flight parameters instead of flow parameters at the edge of the boundary layer, this reference is ideal. For further simplification of the prediction of laminar skin friction, an empirical curve was fitted to the data presented in Ref. 2. This single line is represented by

$$C_{f_{\text{lamin}}} \sqrt{R_{e_\infty}} = 0.45 \cos \alpha + 4.65 \frac{V_\infty}{10,000} \sin \alpha \cos^{2.2} \alpha \quad (3.68)$$

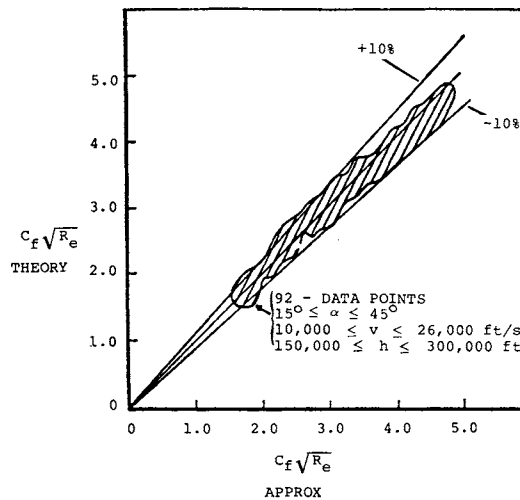


Fig. 3.8 Comparison of empirically determined laminar skin-friction equations.

HYPERSONIC AERODYNAMICS

69

where α is the surface angle of attack and

$$C_f = \frac{\tau_w}{\frac{1}{2} \rho_\infty V_\infty^2}, \quad \tau_w = \text{local shear stress} \quad (3.69)$$

This equation deviates no more than 20% from the data presented by Schmidt² for low-altitude, high-angle-of-attack flight and is more accurate (approximately by $\pm 10\%$) for the rest of the altitude and angle-of-attack range. This accuracy is sufficient for preliminary design as long as the vehicle is in continuum flow where shear stresses do not dominate. A comparison of Eq. (3.68) with the method of Schmidt is shown in Fig. 3.8. This equation is seen to be applicable for the majority of the re-entry flight corridor.

As is the case with laminar skin friction, many techniques are defined in the open literature for the prediction of turbulent skin friction on flat plates in supersonic and hypersonic flows. Unfortunately, these methods are even more complex than those for laminar flow and rely on empirical relations derived from data obtained in wind-tunnel or flight tests. Analysis is often further complicated by the need to evaluate the flowfield properties outside the boundary layer. Schmidt has used the reference-enthalpy technique to construct a comprehensive series of graphs for the prediction of turbulent skin friction on a flat plate for a wide range of flight parameters. As in the laminar study by Schmidt, the data are given in terms of flight parameters, not local flow parameters, and are, therefore, quite useful in preliminary

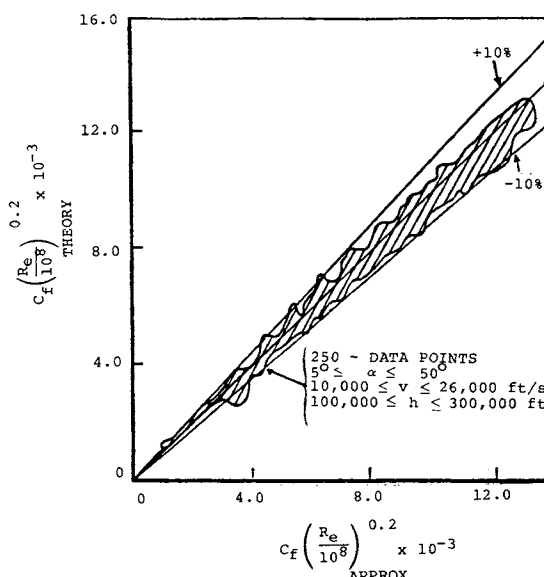


Fig. 3.9 Comparison of empirically determined turbulent skin-friction equations.

design. An empirical curve fit of Schmidt's data resulted in the following equation:

$$C_{f_{\text{turb}}} (R_{e_\infty})^{0.2} = 0.048(\sin 4.5\alpha) + 0.70 \frac{V_\infty}{10,000} \cos^{2.25}\alpha \sin^{1.5}\alpha \quad (3.70)$$

The degree to which this equation covers the analysis of Schmidt is seen in Fig. 3.9. This close comparison proves that the equation is sufficiently accurate for preliminary design purposes.

Determination of Aerodynamic Characteristics

The purpose of this section is to apply the previously developed theoretical and empirical relations to the various basic components of a generalized hypersonic lifting re-entry vehicle and, considering the relative location of the components, to describe the aerodynamic characteristics of the configuration. Dependence of the aerodynamic characteristics on surface geometry and orientation is reflected in the Newtonian format,

$$C_p = k \sin^2\delta \quad (3.57)$$

as developed in the previous section. Determination of δ and integration of C_p for the required aerodynamic characteristics of surfaces with geometries not easily expressed analytically often can be done precisely only by numerical methods. This complexity is to be avoided whenever possible. For this reason, only simple geometric shapes will be analyzed here. Quite accurate analyses of complex geometric shapes can be made by proper selection and combination of the simple shapes covered herein.

As important as the definition of the components is their location relative to the center of gravity of the vehicle in question. Therefore, the geometry and the coordinate system of the generalized configuration to be analyzed must be established. Efficient, lifting, hypersonic vehicles possess a flat bottom surface with a highly swept planform to maximize C_L and L/D . The nose and leading edges must be blunt (i.e., circular, elliptical, etc.) to withstand the heating environment. Vertical fins are required to provide directional stability and are most practical and effective outboard and in the most rearward position. The body is located on the upper surface unexposed to the high heating. Figure 3.10 is a three-view sketch of the generalized configuration to be considered, showing the general dimensions of the overall configuration, various components, and location of the center of gravity. (A similar approach may be used for other geometries.²)

With a generalized configuration defined, the aerodynamic characteristics can be analyzed in terms of the general dimensions of the configuration. Defining these general dimensions for a specific configuration permits rapid determination of the aerodynamic characteristics of that configuration.

The aerodynamic coefficients derived herein, and the associated sign convention, are defined in the Nomenclature. The symbol and sign convention used by NASA has been used unless otherwise noted.

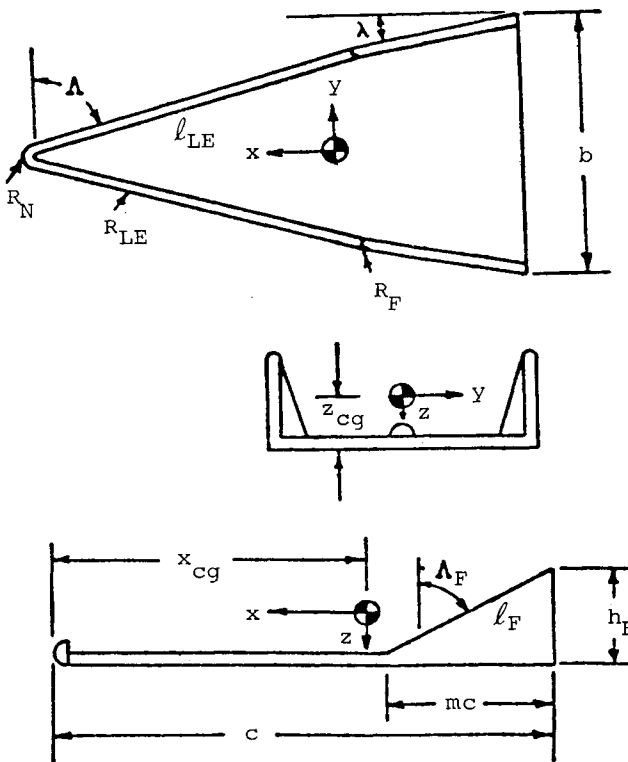


Fig. 3.10 Generalized configuration geometry.

Derivation of the coefficients for the different components, in general, followed three basic steps:

- 1) Determination of a simple representative shape.
- 2) Integration of the theoretical pressure coefficients over that simple shape and evaluation of the basic force coefficients.
- 3) Determination of appropriate moment coefficients through consideration of the displacement distances of the component from the vehicle center of gravity.

Six component characteristics were defined for each configuration component. The lengthy details of the integrations required to derive the aerodynamic force coefficients were omitted and only the results presented.²

Summary of Derived Components

The derived coefficients are summarized in Table 3.4 for convenient reference. Only the basic equations are given. The terms such as k factor, α , Λ_e , α_e , etc., in the equations must be made to apply to the configuration component that is evaluated. The lateral and directional coefficients were determined to be linear with β for small angles and, hence, only the derivatives are presented. Numerical values of the derivatives are in radians.

**Table 3.4 Summary of Derived Coefficients
(all derivatives and all angles in radians)**

Nose equations

$$C_N = \frac{\pi R_N^2 k_N}{4S} \sin \alpha (1 + \cos \alpha) \quad (3.71)$$

$$C_A = \frac{\pi R_N^2 k_N}{4S} \frac{(1 + \cos \alpha)^2}{2} \quad (3.72)$$

$$C_m = C_N \frac{x_N}{c} - C_A \frac{z_N}{c} \quad (3.73)$$

$$C_{\gamma_B} = -\frac{C_A}{\cos \alpha} \quad (3.74)$$

$$C_{\ell_B} = \frac{C_A}{\cos \alpha} \frac{z_N}{b} \quad (3.75)$$

$$C_{n_B} = -\frac{C_A}{\cos \alpha} \frac{x_N}{b} \quad (3.76)$$

Leading-edge equations (for a pair of leading-edge elements; use ℓ_{LE} for one leading edge)

$$C_N = \left(\frac{4R_{LE}\ell_{LE}}{3S} \right) k_{LE} \sin \alpha (\cos \Lambda_e + \cos \Lambda \cos \alpha) \quad (3.77)$$

$$C_A = \left(\frac{4R_{LE}\ell_{LE}}{3S} \right) \frac{k_{LE}}{2} \cos \Lambda (\cos \Lambda_e + \cos \Lambda \cos \alpha)^2 \quad (3.78)$$

$$C_m = C_N \frac{x_{LE}}{c} - C_A \frac{z_{LE}}{c} \quad (3.79)$$

$$C_{\gamma_B} = -\left(\frac{4R_{LE}\ell_{LE}}{3S} \right) k_{LE} \sin^2 \Lambda \cos \Lambda_e (1 + \cos \alpha_e)^2 \quad (3.80)$$

$$C_{\ell_B} = \left(\frac{4R_{LE}\ell_{LE}}{3S} \right) k_{LE} \sin \Lambda (1 + \cos \alpha_e) \times \left[\frac{z_{LE}}{b} \sin \Lambda \cos \Lambda_e (1 + \cos \alpha_e) - \frac{y_{LE}}{b} \sin \alpha \right] \quad (3.81)$$

$$C_{n_B} = \left(\frac{4R_{LE}\ell_{LE}}{3S} \right) k_{LE} \sin \Lambda \cos \Lambda_e (1 + \cos \alpha_e)^2 \times \left(\frac{-x_{LE}}{b} \sin \Lambda + \frac{y_{LE}}{b} \cos \Lambda \right) \quad (3.82)$$

$$(\sin \Lambda_e)_L^R = \sin \Lambda \cos \alpha \cos \beta \mp \cos \Lambda \sin \beta \quad (3.83)$$

$$(\cot \alpha_e)_L^R = \cos \Lambda \cot \alpha \pm \frac{\sin \Lambda}{\sin \alpha} \tan \beta \quad (3.84)$$

Lower-surface equations

$$C_N = k_\alpha \left(\frac{S_L}{S} \right) \sin^2 \alpha \quad (3.85)$$

$$C_A = G \left(\frac{S_w}{S} \right) \frac{0.45 \cos \alpha + 4.65(V_\infty/10,000) \sin \alpha \cos^{2.2} \alpha}{(V_\infty c/v_\infty)^{0.5}} \quad (\text{for laminar flow}) \quad (3.86)$$

(Table continued on next page.)

Table 3.4 (cont.) Summary of Derived Coefficients

$$C_A = G \left(\frac{S_w}{S} \right) \frac{0.048 \sin(4.5\alpha) + 0.70(V_\infty/10,000) \cos^{2.25}\alpha \sin^{1.5}\alpha}{(V_\infty c/v_\infty)^{0.2}} \quad (\text{for turbulent flow}) \quad (3.87)$$

$$C_m = C_N \frac{x_L}{c} - C_A \frac{z_L}{c} \quad (3.88)$$

$$C_{\gamma_\beta} = -\frac{C_A}{\cos \alpha} \quad (3.89)$$

$$C_{\ell_\beta} = \frac{C_A}{\cos \alpha} \frac{z_L}{b} - k_i \sin^2 \alpha \left(\frac{S_L}{S} \right) \frac{2y_{LE}}{9b}, \quad k_i = 3.8 \quad (3.90)$$

$$C_{n_\beta} = -\frac{C_A}{\cos \alpha} \frac{x_L}{b} \quad (3.91)$$

where

$$G = \frac{2}{n(1+n)} \left[\frac{1-m^{1+n}}{1-m^2} \right]$$

$n = 0.5$ laminar, 0.8 turbulent

$m = \text{planform taper ratio}$

Vertical fin equations (for a pair of fins)

$$C_N = -\frac{8R_F \ell_F k_{LE}}{3S} \cos^2(\Lambda_F + \alpha) \sin \Lambda_F \quad (3.92)$$

$$C_A = 2k_F \frac{S_F}{S} (\lambda^3 \cos^2 \alpha) + \frac{8R_F \ell_F k_{LE}}{3S} \cos^2(\Lambda_F + \alpha) \cos \Lambda_F \quad (3.93)$$

$$C_m = -2k_F \frac{S_F}{S} (\lambda^3 \cos^2 \alpha) \left(\frac{z_F}{c} \right) - \frac{8R_F \ell_F k_{LE}}{3S} \cos^2(\Lambda_F + \alpha) \times \left[\frac{x_{F,LE}}{c} \sin \Lambda_F + \frac{z_{F,LE}}{c} \cos \Lambda_F \right] \quad (3.94)$$

$$C_{\gamma_\beta} = -4k_F \frac{S_F}{S} (\lambda \cos \alpha) \quad (3.95)$$

$$C_{\ell_\beta} = -4k_F \frac{S_F}{S} (\lambda \cos \alpha) \left(-\frac{z_F}{b} \right) \quad (3.96)$$

$$C_{n_\beta} = 4k_F \frac{S_F}{S} (\lambda \cos \alpha) \left(-\frac{x_F}{b} + \lambda \frac{y_F}{b} \right) \quad (3.97)$$

S_F for one fin, ℓ_F for one fin.

Equations for transfer of moment reference center

$$\Delta C_m = -C_N \frac{\Delta x}{c} + C_A \frac{\Delta z}{c} \quad (3.98)$$

$$\Delta C_{\ell_\beta} = C_{\gamma_\beta} \frac{\Delta z}{b} \quad (3.99)$$

$$\Delta C_{n_\beta} = -C_{\gamma_\beta} \frac{\Delta x}{b} \quad (3.100)$$

Transformation equations from body to wind axes

$$C_L = C_N \cos \alpha - C_A \sin \alpha \quad (3.101)$$

$$C_D = C_N \sin \alpha + C_A \cos \alpha \quad (3.102)$$

3.4 HYPERSONIC VS SUBSONIC AERODYNAMICS

Our instincts have been developed from childhood in subsonic aerodynamics. Observing bird flight, flying kites and model airplanes, and traveling in aircraft have enabled us to develop a "feel" for this regime.

In this section, an attempt at developing a "feel" for hypersonics will be made. First, contrast the difference between the random energy (due to the molecular motion) of a gas and the ordered energy due to the mass flow rate,

$$\text{Random energy} = \frac{1}{2}ma^2$$

(since $\bar{v} \approx a$, the mean molecular speed)

$$\text{Ordered energy} = \frac{1}{2}mV^2$$

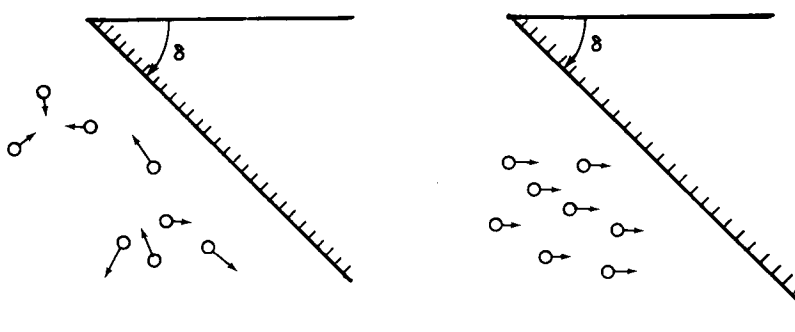
The ratio becomes

$$\frac{\text{Ordered energy}}{\text{Random energy}} = \frac{\frac{1}{2}mV^2}{\frac{1}{2}ma^2} = \frac{V^2}{a^2} = M^2 \quad (3.103)$$

In subsonic flow, $a^2 \gg V^2$, so that the random energy dominates; at hypersonic speed, $V^2 \gg a^2$, ordered energy prevails. Figure 3.11 graphically shows why impact theory is a good but simple model for hypersonic flow.

Newtonian aerodynamics, in which all molecules are traveling in the same direction, produces a simple relationship for pressure,

$$PA = \dot{m}V_n = \rho AV_n^2 \quad (3.104)$$



a) Molecular velocity (number extremes).

b) Comparison at Mach.

Fig. 3.11 Impact theory for subsonic and hypersonic cases.

$$V_n = V_1 \sin \delta \quad (3.105)$$

Hence,

$$\frac{P}{\rho_1 V_1^2} = \frac{C_p}{2} = \sin^2 \delta \quad (3.106)$$

This simple relationship is valid for both two and three dimensions. No such simplicity is possible in subsonic flow (or transonic, which is worse). Note: Newton derived this simple pressure relationship for incompressible flow in 1680. It obviously failed in that regime, but 300 years later we found a use for it.

The sum of these two energies is accomplished in the equation for total enthalpy,⁵

$$H = h + (V^2/2) = C_p T_0 \quad (3.107)$$

But

$$h = C_p T = a^2 / (\gamma - 1) \quad (3.108)$$

Hence,

$$\frac{a_0^2}{\gamma - 1} = \frac{a^2}{\gamma - 1} + \frac{V^2}{2} \quad (3.109)$$

or

$$\frac{a^2}{a_0^2} + \frac{\gamma - 1}{2} \frac{V^2}{a_0^2} = 1 \quad (3.110)$$

This is the equation for an ellipse as plotted in Fig. 3.12. A limited region of this ellipse contains hypersonic flow. In this region, the term $a/a_0 \ll 1$ and can be eliminated from the energy equation.

The Mach number, therefore, ceases to be a significant parameter of the problem. Only V_∞ and ρ_∞ are useful descriptors of the freestream. Both T_∞ and P_∞ are small terms and have little consequence on the numerical outcome. For example, at the stagnation point,

$$P_2 = \rho_1 V_1^2 \quad (3.111)$$

$$T_2 = V_1^2 / 2C_p \quad (3.112)$$

$$\rho_2 = \frac{P_2}{R T_2} = \frac{\rho_1 V_1^2}{(R/2C_p)V_1^2} = \frac{2\gamma}{\gamma - 1} \rho_1 \quad (3.113)$$

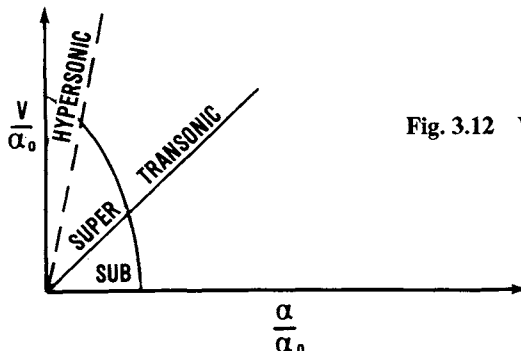


Fig. 3.12 Velocity ellipse: plot of Eq. (3.110).

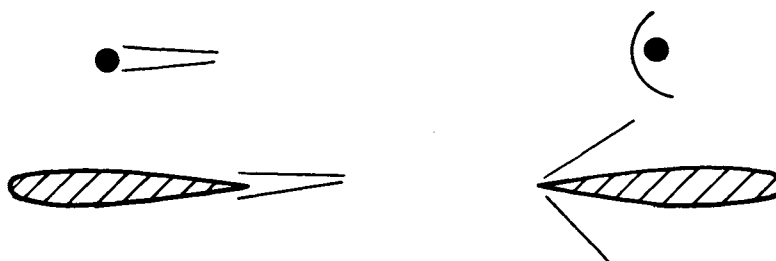
Based upon this simple model, we can deduce information concerning hypersonic aerodynamic characteristics and contrast it with subsonics.

Aerodynamic Drag

In subsonic flow, the size of the wake determines the amount of drag. Emphasis in low-speed design is placed on fairing rearward to reduce drag. A single wire can produce as much drag as a large fairing. Recognition of this fact became apparent after World War I, when the replacement of many-wire structural supports by single faired members resulted in improved aerodynamic performance.

At hypersonic speeds, the base region is in a vacuum and geometric details in the base have little influence on the drag. The stagnation point has the greatest pressure, which decreases rapidly as the slope decreases (i.e., $C_p = 2 \sin^2\delta$). The size of the stagnation region, therefore, determines the drag. A small cylinder possesses the same drag as a large wedge.

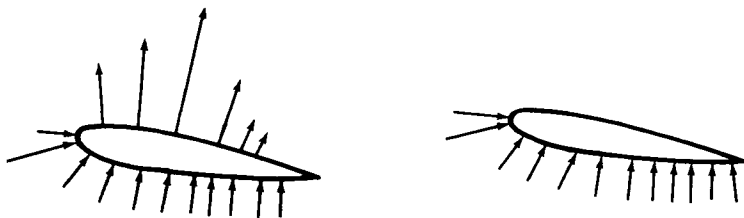
Contrasting hypersonic drag characteristics with subsonic: one fairs rearward in subsonics and forward in hypersonics to minimize drag (see Fig. 3.13).



a) Subsonic ($M \ll 1$): equal drag configurations, *rearward* fairing, size of wake determines the drag.

b) Hypersonic ($M \gg 1$): equal drag configurations, *forward* fairing, size of stagnation region determines the drag.

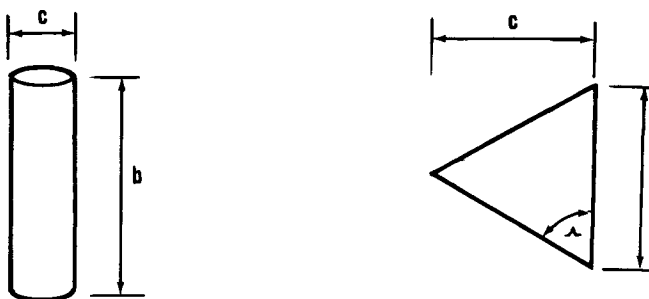
Fig. 3.13 Comparison of aerodynamic drag.



a) Subsonic ($M \ll 1$): upper surface produces the lift.

b) Hypersonic ($M \gg 1$): lower surface produces the lift.

Fig. 3.14 Aerodynamic lift.



a) Subsonic ($M \ll 1$): $\mathcal{A} = b^2 / bc = b/c \gg 1$.

b) Hypersonic ($M \gg 1$): $\mathcal{A} = b^2 / (1/2 bc) = 2b/c = 4 \cot \Lambda$.

Fig. 3.15 Comparison of planforms.

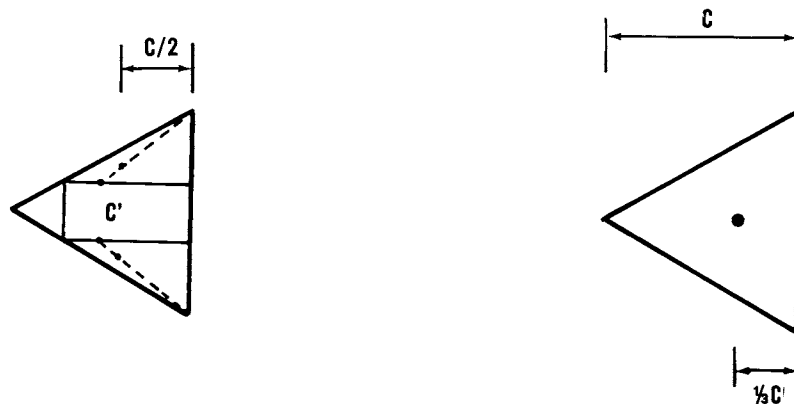
Aerodynamic Lift

To generate lift at subsonic speed, a cambered airfoil is placed at a small angle of attack, but with care so as not to separate the flow on the upper surface. Large suction forces on the upper side dictate the magnitude of the lift. (See Fig. 3.14.)

At hypersonic speed, little lift is developed from the upper surface so that separation is of little consequence. Only the pressure forces on the lower surface generate lift. Therefore, it is possible to divide the design features in a compatible manner by designing the lower surface for hypersonic flight and the upper surface for subsonic.

Planform Features

We know that, at subsonic speeds, a high-aspect-ratio, unswept wing minimizes induced drag (or end effects) and maximizes L/D . At high speeds, large sweep minimizes the leading-edge drag, dictating a low aspect



(a) Subsonic ($M \ll 1$): upper surface,
center of pressure at $c'/2$.
(b) Hypersonic ($M \gg 1$): lower sur-
face, center of pressure at $\frac{1}{3}c$.

Fig. 3.16 Comparison of centers of pressure.

ratio for efficient L/D . Hence, a major incompatibility occurs, requiring a compromise or a sophisticated variable sweep design.

Another feature of the planform selection is the center of pressure shift that occurs when decelerating from supersonic to subsonic speeds. Qualitatively, at high speed, the aerodynamic center is at the area centroid for a flat surface (since $C_p = 2 \sin^2 \delta = \text{const}$ when $\delta = \text{const}$). At subsonic speeds, the aerodynamic center shifts to the quarter chord, consistent with potential flow theory. A delta wing with a top-mounted fuselage can be designed to minimize this shift (i.e., the Space Shuttle).

A comparison of planforms is shown in Figs. 3.15 and 3.16.

Directional Stability

Consider the hypersonic weather vane shown in Fig. 3.17. The yawing moment is

$$N = \Delta C_p q S c \quad (3.114)$$

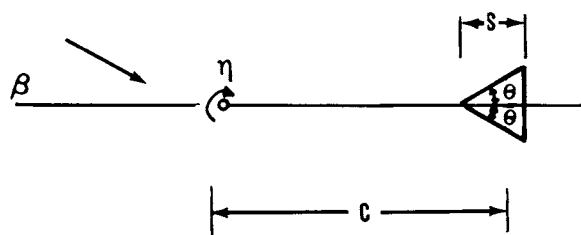


Fig. 3.17 Hypersonic weather vane.

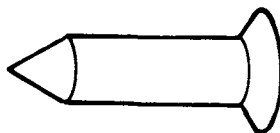


Fig. 3.18 Re-entry missiles thicken the trailing-edge thickness to increase the directional stability.

$$\Delta C_p = 2 \sin^2(\theta + \beta) - 2 \sin^2(\theta - \beta) \cong 8\theta\beta \quad (3.115)$$

$$C_n = N/qSc = 8\theta\beta \quad (3.116)$$

Hence,

$$\frac{\partial C_n}{\partial \beta} = C_{n_\beta} = 8\theta \quad (3.117)$$

One means of increasing directional stability is to widen the trailing-edge thickness θ . The X-15 was one of the first systems to exploit this feature. Re-entry missiles also utilize this characteristic along with gyroscopic stability through spinning (see Fig. 3.18).

Thermal Barrier

The total temperature at hypersonic speed is

$$H = h + \frac{V^2}{2} = C_p T_0 = C_p T_\infty + \frac{V_\infty^2}{2} \quad (3.118)$$

$$T_\infty = -69^\circ\text{F} = 460 - 69 = 391^\circ\text{R}$$

$$C_p = 6006 \text{ ft}^2/\text{s}^2 \cdot {}^\circ\text{R}$$

$$T_0 = T + V_\infty^2/2C_p$$

See Fig. 3.19 and Table 3.5 for values of T_0 at various flight velocities.

Table 3.5 Total Temperatures

$V_\infty, \text{ft/s}$	$T_0, {}^\circ\text{F}$
1,000	14
2,000	264
3,000	680— <i>AI</i>
5,000	2,012— <i>Ti</i>
10,000	8,256— <i>C</i>
20,000	33,231

$\left. \begin{matrix} 680 & - \\ 2,012 & - \\ 8,256 & - \end{matrix} \right\} \text{ Thermal barrier}$

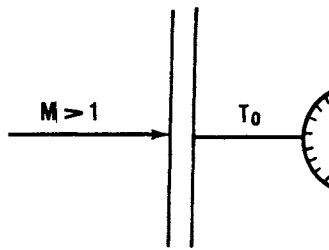


Fig. 3.19 Total temperature for the hypersonic case.

References

¹Hankey, W., "Introduction to Computational Aerodynamics," AFWAL TR-82-3031, June 1981.

²Hankey, W., "Optimization of Lifting Reentry Vehicles," ASD TDR 62-1102, March 1963.

³Hayes, W. and Probstein, R., *Hypersonic Flow Theory*, Academic Press, New York, 1959.

⁴Lees, L., "Recovery Dynamics-Heat Transfer at Hypersonic Speed in a Planetary Atmosphere," *Space Technology*, Wiley, New York, 1959.

⁵Shapiro, A., *The Dynamics and Thermodynamics of Compressible Fluid Flow*, Ronald Press, New York, 1953.

Problems

3.1 Compute and plot the pressure distribution around a cylindrical leading edge for a 75 deg swept delta wing at 30 deg angle of attack. What is the effective sweep angle and effective angle of attack for the stagnation point?

3.2 Determine the size of a top-mounted fuselage on a flat-bottom delta wing re-entry configuration to insure the location of the center of pressure is at the same position for both hypersonic and subsonic speeds.

3.3 Compute the hypersonic values of C_L , C_D , and C_M for the following conditions:

$$\alpha = 45 \text{ deg} \quad \text{Altitude} = 200,000 \text{ ft}$$

$$\Lambda = 75 \text{ deg} \quad M = 20$$

$$R_N = 1 \text{ ft} \quad \text{Flat-bottom delta wing}$$

$$R_{LE} = 0.5 \text{ ft} \quad C = 40 \text{ ft}$$

$$x_{cg} = \frac{2}{3} \text{ chord}$$

4 **RE-ENTRY HEATING**

4.1 SIMPLIFIED ANALYSIS

In any engineering problem, one requires an approximate method for obtaining rapid estimates.¹ These estimates are used to evaluate the seriousness of the problem and identify the most critical condition. If the situation is warranted, more sophisticated methods can be employed and possibly followed up by model tests to confirm the analysis. In this section, approximate heating methods are developed. In later sections, more exact methods will be derived.

Reynolds' Analogy

The most powerful method for obtaining simple heating estimates is to use Reynolds' analogy. This theory takes advantage of the similarity between shear stress and the heating rate. The analogy is exact for only one flow condition (i.e., zero pressure gradient, $Pr = 1$); however, useful trends can be obtained for other cases. Also, constants can be adjusted to improve the accuracy by comparison with experiment.

The equation for shear stress is

$$\tau_w = \left(\mu \frac{\partial u}{\partial y} \right)_w \equiv \frac{1}{2} \rho_e V_e^2 C_f \quad (4.1)$$

where

$$C_f = C_f(Re) \quad (4.2)$$

is the friction coefficient depending on the Reynolds number Re . The heating rate has a similar equation representing the transport of energy as opposed to the transport of momentum in the shear stress equation,

$$\dot{q}_w = \left[k \frac{\partial T}{\partial y} \right]_w \equiv St \rho_e V_e (H_{aw} - H_w) \quad (4.3)$$

Dividing Eq. (4.1) by Eq. (4.3) results in

$$\frac{\tau_w}{\dot{q}_w} = \frac{\frac{1}{2}\rho_e V_e^2 C_f}{St\rho_e V_e (H_{aw} - H_w)} = \frac{\mu \frac{\partial u}{\partial y}}{k \frac{\partial T}{\partial y}} \approx \frac{\mu \frac{V_e}{\delta}}{C_p \left[\frac{H_{aw} - H_w}{\delta} \right]} \quad (4.4)$$

Hence,

$$\frac{C_f}{2} = \frac{\mu C_p}{k} St \quad (4.5)$$

Since the Prandtl number Pr is approximately equal to unity, i.e.,

$$Pr = \mu C_p / k \approx 1 \quad (4.6)$$

then

$$St = C_f / 2 \quad (4.7)$$

which is referred to as the Reynolds analogy.

Much information is available on skin friction that can be exploited to obtain heating rate estimates. See Fig. 4.1. Empirical correlations for skin-friction coefficients have been developed over the past century,

$$C_f / 2 = A / Re^n \quad (4.8)$$

where, for laminar flow, $A = 0.332$ and $n = 0.5$; for turbulent flow, $A = 0.0296$ and $n = 0.2$. Transition occurs at approximately $Re = 10^6$; however, if the design can permit the conservatism, one uses the higher of the two values to obtain the heating rate estimate.

Inserting Eq. (4.8) into the heat-transfer equation produces

$$\dot{q} = St \rho_e V_e (H_{aw} - H_w) = \frac{A}{[\rho_e V_e x / \mu_e]^n} [\rho_e V_e x / \mu_e]^n \rho_e V_e (H_{aw} - H_w) \quad (4.9)$$

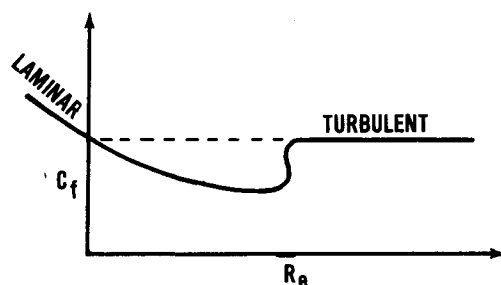


Fig. 4.1 Heating rate at the stagnation region.

or

$$\dot{q} = A (\rho_e V_e)^{1-n} [\mu_e/x]^n (H_{aw} - H_w) \quad (4.10)$$

Stagnation Region

The heating rate at the stagnation region² will be explored first, since this is known to be critical. Hypersonic approximations will be used to obtain values for $\rho_e V_e$, μ_e , and H_e . The stagnation point is shown in Fig. 4.2. The flow crosses a normal shock wave and stagnates. The stagnation conditions can be obtained from Newtonian impact theory,

$$P_s \cong \rho_\infty V_\infty^2 \quad (4.11)$$

$$H_s \cong \frac{V_\infty^2}{2} \quad (4.12)$$

$$\rho_s \cong \frac{\gamma P_s}{(\gamma - 1) H_s} = \frac{2\gamma}{\gamma - 1} \rho_\infty \quad (4.13)$$

The flow model used away from the stagnation point assumes that the streamline external to the boundary layer is isentropic. This is certainly true for any streamline external to the viscous region. Although large entropy gradients occur normal to the streamlines (since the flow passes through a curved shock wave), entropy is constant along streamlines in inviscid steady flow.

The following isentropic relations are used:

$$\rho_e / \rho_s = (P_e / P_s)^{1/\gamma} \quad (4.14)$$

$$h_e / H_s = (P_e / P_s)^{(\gamma-1)/\gamma} \quad (4.15)$$

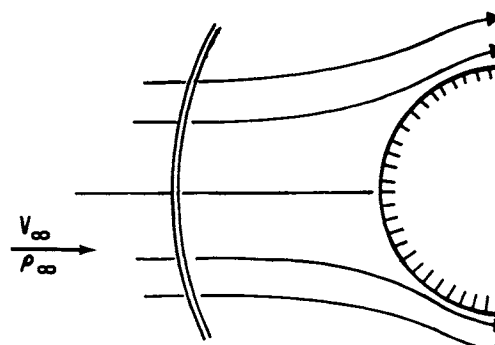


Fig. 4.2 Skin friction vs Reynolds number in regions of laminar and turbulent flows.

$$V_e^2/2 = H_s [1 - (h_e/H_s)] \quad (4.16)$$

or

$$V_e/V_\infty = [1 - (P_e/P_s)^{(\gamma-1)/\gamma}]^{1/2} \quad (4.17)$$

All properties along the streamline can be related to the pressure ratio and stagnation property values. This is analogous to the flow through a wind tunnel in which all local values can be related to *one* local quantity plus the stagnation section values.

A relationship called Sutherland's law is required for viscosity,

$$\mu = \mu_0 T^{3/2} / (T + S) \quad (4.18)$$

where $S = 198.6^\circ R \ll T_s$ and $\mu_0 = 2.27 \times 10^{-8} \text{ lb} \cdot \text{s}/\text{ft}^2 \sqrt{^\circ R}$. Hypersonically,

$$\mu \approx \mu_0 T^{1/2} = (\mu_0/C_p^{1/2}) h_e^{1/2} \equiv C_\mu h_e^{1/2} \quad (4.19)$$

where $C_\mu = \mu_0/\sqrt{C_p}$.

We can now insert these values into the heating rate equation and find a relationship for the stagnation point heat transfer. In addition, we assume $H_{aw} = H_s \gg H_w$. Hence,

$$\rho_e = \left(\frac{2\gamma}{\gamma-1} \rho_\infty \right) \left(\frac{P_e}{P_s} \right)^{1/\gamma} \quad (4.20)$$

$$V_e = V_\infty \left[1 - \left(\frac{P_e}{P_s} \right)^{(\gamma-1)/\gamma} \right]^{1/2} \quad (4.21)$$

$$\mu_e = \frac{C_\mu}{\sqrt{2}} V_\infty \left(\frac{P_e}{P_s} \right)^{(\gamma-1)/2\gamma} \quad (4.22)$$

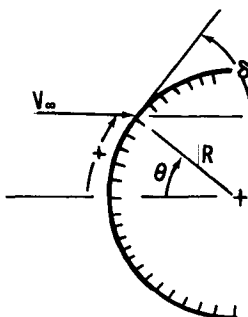


Fig. 4.3 Circular cross section showing stagnation point heat transfer.

$$H_{aw} - H_w = V_\infty^2/2 \quad (4.23)$$

$$\dot{q} = K \frac{\rho_\infty^{1-n} V_\infty^3}{R^n} F(x) \quad (4.24)$$

where

$$K = \frac{A [2\gamma/(\gamma-1)]^{1-n} C \mu^n}{J 2^{1+n/2}} \quad (4.25)$$

$$F(x) = \left(\frac{R}{x} \right)^n \left(\frac{P_e}{P_s} \right)^{(2-3n+n\gamma)/2\gamma} \left[1 - \left(\frac{P_e}{P_s} \right)^{(\gamma-1)/\gamma} \right]^{(1-n)/2} \quad (4.26)$$

R = nose radius, ft

ρ_∞ = density, slug/ft³

V_∞ = velocity, ft/s

J = 778 ft · lb/Btu

\dot{q} = Btu/ft² · s

Given the pressure distribution, the heat transfer in the stagnation region can now be determined. A circular cross section of the region is shown in Fig. 4.3. The following Newtonian flow relationships can be used to obtain the pressure:

$$\delta + \theta = 90 \text{ deg} \quad (4.27)$$

$$C_p = 2 \sin^2 \delta \quad (4.28)$$

Hence,

$$C_p = 2 \cos^2 \theta \quad (4.29)$$

or

$$P_e/P_s = \cos^2 \theta \quad (4.30)$$

$$x/R = \theta \quad (4.31)$$

Therefore,

$$F(x) = (\cos \theta)^{(2-3n+n\gamma)/\gamma} \frac{[1 - \cos^{2(\gamma-1)/\gamma} \theta]^{(1-n)/2}}{\theta^n} \quad (4.32)$$

This distribution, along with the simple relationships derived previously, can provide excellent simple prediction methods (note that K has been modified based upon experimental data), such as

$$\dot{q}_{\max, \text{lam}} = 21 \sqrt{\frac{\rho_\infty}{R}} \left(\frac{V_\infty}{1000} \right)^3 \left(1 - \frac{H_w}{H_s} \right) \quad (4.33)$$

$$\dot{q}_{\max, \text{turb}} = \frac{4}{x^{0.2}} \left(\frac{\rho_\infty}{\rho_{sl}} \right)^{0.8} \left(\frac{V_\infty}{1000} \right)^3 \left(1 - \frac{H_w}{H_s} \right) \quad (4.34)$$

where \dot{q} is in units of Btu/ft²s, ρ of slug/ft³, R and x of ft, and V_∞ of ft/s.

4.2 COMPONENT HEATING

Wing Leading-Edge Heating

After the nose stagnation region has been analyzed, the next most critical condition to be considered is the wing leading edge. The stagnation point heating rate on a cylinder normal to the flow may be related to the heating of a sphere by a coordinate transformation. As will be shown in a later section, this turns out to result in a very simple relationship,

$$\dot{q}_{\text{cylinder}} = \dot{q}_{\text{sphere}} / (2)^n \quad (4.35)$$

The wing leading edge is seldom normal to the flow, however, and geometric considerations for wing sweep and angle of attack must be applied.

It is well known that sweeping the leading edge of the wing of a hypervelocity vehicle will reduce the convective heat input to the wing. The correction for sweep is usually obtained by relating the heating for a swept leading edge to an unswept one. Recall that stagnation heating was derived to be

$$\dot{q} = A (\rho_s u_s)^{1-n} \left(\frac{\mu_s}{x} \right)^n (H_e - H_w) \quad (4.36)$$

Performing a ratio of the heating between a swept and a unswept cylinder produces

$$\frac{\dot{q}(\Lambda)}{\dot{q}(\Lambda = 0)} = \left[\frac{\rho_\Lambda u_\Lambda}{\rho_{ref} u_{ref}} \right]^{1-n} \left[\frac{\mu_\Lambda}{\mu_{ref}} \right]^n \quad (4.37)$$

The stagnation line conditions on a swept cylinder are (see Fig. 4.4),

$$P_s = \rho_\infty V_n^2 = \rho_\infty V^2 \cos^2 \Lambda_e \quad (4.38)$$

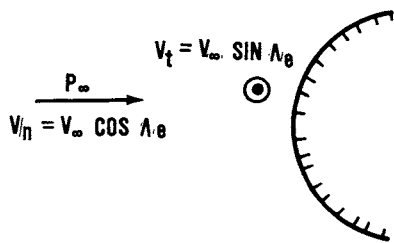


Fig. 4.4 Conditions of the stagnation point line on a swept cylinder.

$$C_p T_s = H_s - \frac{V_t^2}{2} = \frac{V_\infty^2}{2} - \frac{V_\infty^2}{2} \sin^2 \Lambda_e = \frac{V_\infty^2}{2} \cos^2 \Lambda_e \quad (4.39)$$

$$\rho_s = \frac{P_s}{R T_s} = \frac{2\gamma}{\gamma - 1} \rho_\infty \quad (4.40)$$

Thus,

$$\rho_\Lambda / \rho_{\text{ref}} = 1 \quad (4.41)$$

$$u_\Lambda / u_{\text{ref}} = \cos \Lambda_e \quad (4.42)$$

$$\mu_\Lambda / \mu_{\text{ref}} = \sqrt{T_\Lambda / T_{\text{ref}}} = \sqrt{\cos^2 \Lambda_e} \quad (4.43)$$

Substituting these values into the heating ratio results in

$$\frac{\dot{q}_\Lambda}{\dot{q}(\Lambda = 0)} = \cos^{1-n} \Lambda_e \cos^n \Lambda_e = \Lambda_e \quad (4.44)$$

This simple relationship was derived for zero angle of attack. When a delta wing is pitched to an angle of attack, the effective sweep is decreased and the effective local angle of attack on the leading edge is greatly increased, as

$$\Lambda_e = \sin^{-1}(\sin \Lambda \cos \alpha) = \text{effective sweep angle} \quad (4.45)$$

$$\alpha_e = \tan^{-1}\left(\frac{\tan \alpha}{\cos \Lambda}\right) = \text{effective angle of attack} \quad (4.46)$$

The effective angles are derived from the geometry. In deriving geometric relationships, vector analysis is a useful technique. Consider a standard stability coordinate system, i, j, k . (See Fig. 4.5.) The velocity unit vector (for $\beta = 0$) is

$$\mathbf{v} = i \cos \alpha + k \sin \alpha$$

A unit vector tangent to the leading edge is

$$\mathbf{t} = i \sin \Lambda - j \cos \Lambda \quad (4.47)$$

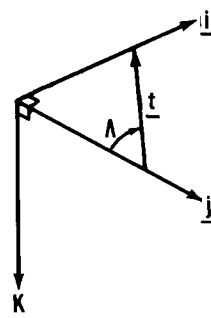


Fig. 4.5 Standard stability coordinate system.

The velocity vector is then decomposed into two components,

$$\mathbf{v}V_\infty = \mathbf{t}V_t + \mathbf{n}V_n \equiv V_\infty(t \sin \Lambda_e + n \cos \Lambda_e) \quad (4.48)$$

since

$$\mathbf{v} \cdot \mathbf{t} = \cos \alpha \sin \Lambda \quad (4.49)$$

Hence,

$$\sin \Lambda_e = \cos \alpha \sin \Lambda \quad (4.50)$$

The unit vector \mathbf{n} normal to the leading edge can be determined from \mathbf{t} and \mathbf{v} , as

$$\mathbf{n} = \frac{\mathbf{t} \times \mathbf{v} \times \mathbf{t}}{|\mathbf{t} \times \mathbf{v} \times \mathbf{t}|} = \frac{i \cos \alpha \cos^2 \Lambda + j \cos \alpha \cos \Lambda \sin \Lambda + k \sin \alpha}{\cos \Lambda_e} \quad (4.51)$$

Therefore,

$$\mathbf{n} \cdot \mathbf{k} = \sin \alpha_e = \sin \alpha / \cos \Lambda_e \quad (4.52)$$

From this relationship (Fig. 4.6) and $\sin \Lambda_e = \cos \alpha \sin \Lambda$, we wish to find $\alpha_e(\alpha, \Lambda)$.

Find:

$$\tan^2 \alpha_e = \frac{1}{\cos^2 \alpha_e - 1} = \frac{1}{(\cos^2 \Lambda_e / \sin^2 \alpha) - 1} \quad (4.53)$$

$$= \frac{\sin^2 \alpha}{1 - \cos^2 \alpha \sin^2 \Lambda - \sin^2 \alpha} = \frac{\tan^2 \alpha}{\cos^2 \Lambda} \quad (4.54)$$

Therefore,

$$\tan \alpha_e = \tan \alpha / \cos \Lambda \quad (4.55)$$

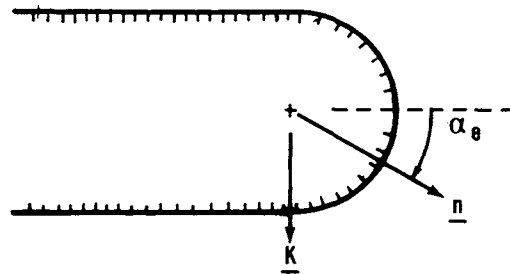


Fig. 4.6 Relation with unit vector n normal to the leading edge.

The geometry of a generalized lifting re-entry wing section is shown in Fig. 4.7 for which α_e and Λ_e are plotted as functions of α and Λ in Figs. 4.8 and 4.9.

Lower-Surface Heating

The lower surface of a lifting re-entry vehicle can be approximated as a flat plate at the angle of attack. Pressure gradients on a flat-bottom delta wing surface are small, permitting the use of simplified theory. Two empirical relationships obtained through many years of testing can be used to advantage.

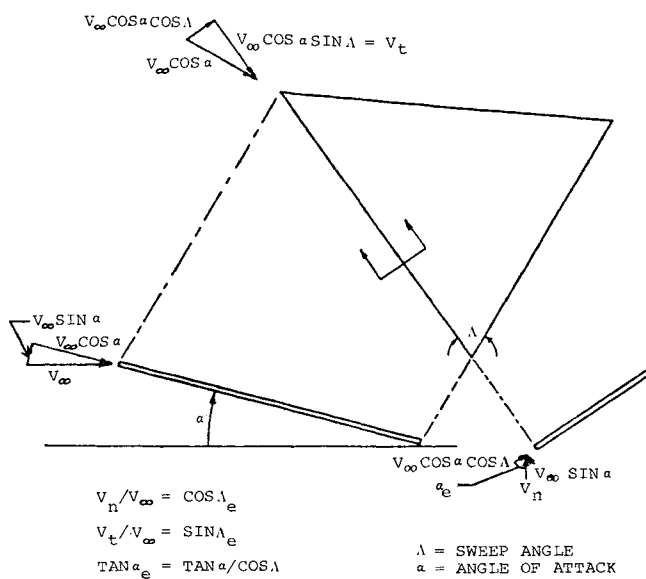


Fig. 4.7 Geometry of generalized lifting re-entry wing section.

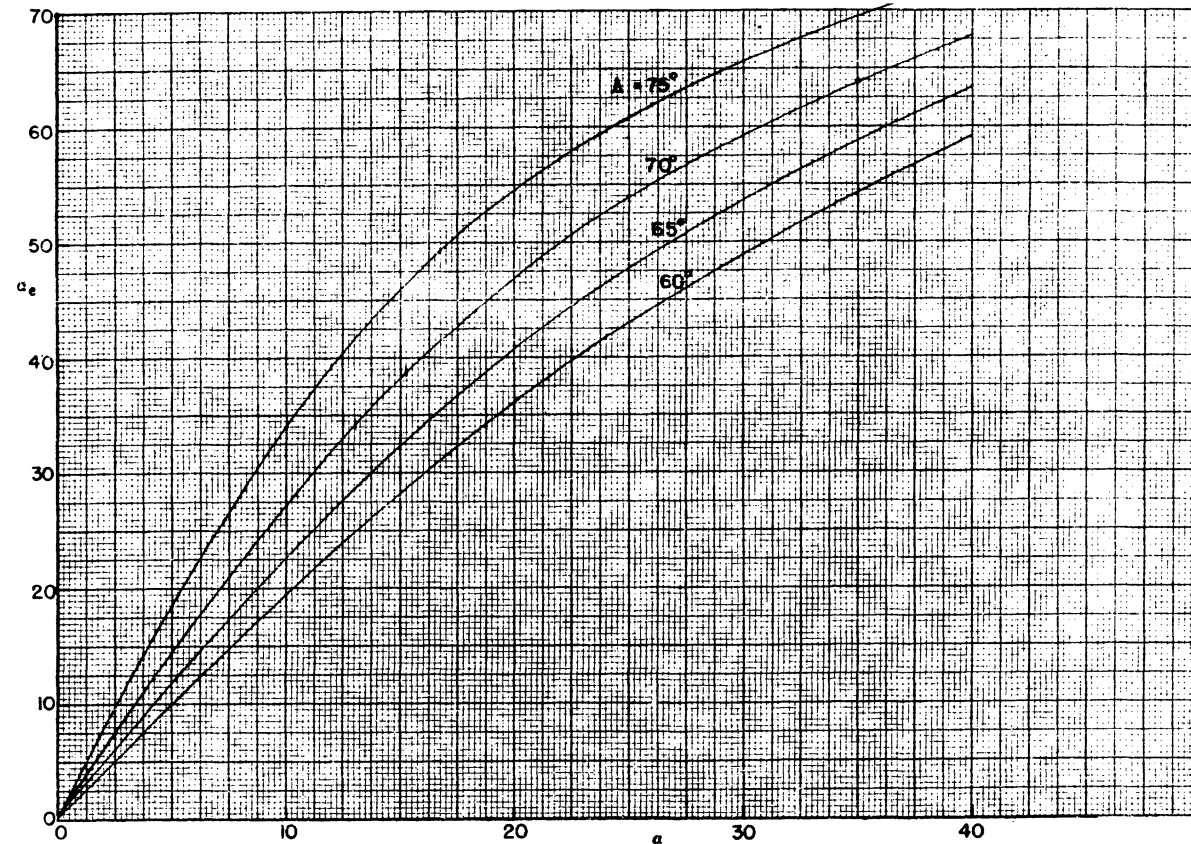


Fig. 4.8 Properties of generalized wing sections as a function of the angle of attack: effective angle of attack.

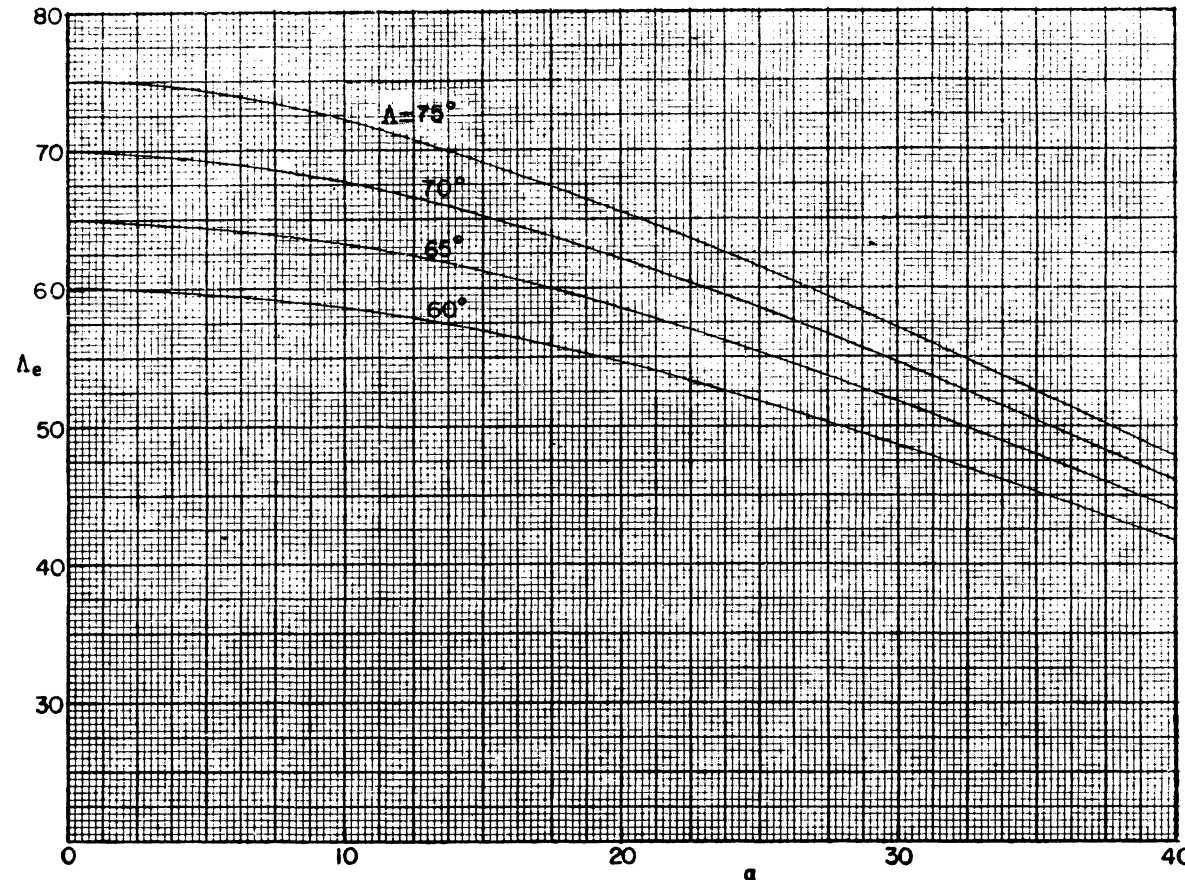


Fig. 4.9 Properties of generalized wing sections as a function of the angle of attack: effective angle of sweep.

The first relationship is the *adiabatic wall* temperature (including Prandtl number effects) for both laminar and turbulent flow,

$$r = \text{recovery factor} = \frac{T_{aw} - T_e}{T_s - T_e} < 1 \quad (4.56)$$

For hypersonic speeds, enthalpy is used in place of temperature in order to account for real-gas effects,

$$r = \frac{h_{aw} - h_e}{h_s - h_e} \quad (4.57)$$

where r is $P_r^{\frac{1}{2}} = 0.846$ for laminar flow and $P_r^{\frac{1}{3}} = 0.894$ for turbulent flow.

Since a great deal of empirical data on flat plates is available for incompressible flow, another important feature is the method used to convert from compressible to incompressible flow. The *reference enthalpy* h^* method is used for this purpose.

Large temperature variations occur across the boundary layer during re-entry. By selecting an appropriate average temperature (or enthalpy) the results for constant temperature (incompressible) can be used. The evaluation of the appropriate average temperature is attributed to Eckert,

$$h^* - h_e = 0.5(h_w - h_e) + 0.22(h_{aw} - h_e) \quad (4.58)$$

By using an incompressible equation for the heat transfer and evaluating all properties at an enthalpy of h^* , good results can be obtained, as

$$\dot{q} = A(\rho^* u_e)^{1-n} (\mu^*/x)^n (h_{aw} - h_w) \quad (4.59)$$

where

$$\rho^* = C_p P_e / R h^* \quad (4.60)$$

$$\mu^* = C \mu \sqrt{h^*} \quad (4.61)$$

$$P_e \cong \rho_\infty V_\infty^2 \sin^2 \alpha \quad (4.62)$$

$$u_e/V_\infty \cong \cos \alpha \quad (4.63)$$

$$h^* = h_e + 0.5(h_w - h_e) + 0.22(h_{aw} - h_e) \quad (4.64)$$

$$\begin{aligned} \frac{\dot{q}(\alpha)}{\dot{q}_{\text{ref}}} &= \left(\frac{\rho^* u_e}{\rho_{\text{ref}}^* u_{\text{ref}}} \right)^{1-n} \left(\frac{h^*}{h_{\text{ref}}} \right)^{n/2} \\ &= \left(\frac{P}{P_{\text{ref}}} \right)^{1-n} \left(\frac{h^*}{h_{\text{ref}}} \right)^{(3/2)n-1} \left(\frac{u_e}{u_{\text{ref}}} \right)^{1-n} \\ &= (\sin^2 \alpha \cos \alpha)^{1-n} \end{aligned} \quad (4.65)$$

since

$$(h^*/h_{\text{ref}})^{(3/2)n-1} \sim 1.$$

This relationship is inserted into the heating equation to produce the lower surface heating relationship,

$$\dot{q}_{\text{flat}} = \frac{K}{x^n} \left(\frac{V_\infty}{1000} \right)^3 \left(1 - \frac{h_w}{h_s} \right) (\rho_\infty \sin^2 \alpha \cos \alpha)^{1-n} \quad (4.66)$$

where $n = 0.5$ and $K = 12.1$ for laminar flow and $n = 0.2$ and $K = 4220$ for turbulent flow.

The units in these equations are $\dot{q} = \text{Btu}/\text{ft}^2 \cdot \text{s}$, $x = \text{ft}$, $V_\infty = \text{ft}/\text{s}$, and $\rho_\infty = \text{slug}/\text{ft}^3$.

4.3 BOUNDARY-LAYER EQUATIONS

Derivation of the Compressible Boundary-Layer Equations

The reduction of the Navier-Stokes equations to the region near a surface boundary produces a simpler set of equations.³ This reduction is accomplished by an order of magnitude analysis and was first accomplished by Prandtl in 1908. The procedure will be repeated here. We start with steady, two-dimensional Navier-Stokes equations,

$$\nabla \cdot \rho V = 0 \quad (4.67)$$

$$\nabla \cdot (\rho V V - \underline{\mathbf{P}}) = 0 \quad (4.68)$$

$$\nabla \cdot (\rho V e - V \cdot \underline{\mathbf{P}} - \dot{q}) = 0 \quad (4.69)$$

The magnitude of terms we will first interpret are in the stress tensor,

$$\underline{\mathbf{P}} = \begin{vmatrix} \sigma_{11} & \tau_{12} \\ \tau_{21} & \sigma_{22} \end{vmatrix}$$

where

$$\sigma_{11} = -p + \lambda \nabla \cdot V + 2\mu u_x \quad (4.70)$$

$$\tau_{21} = \tau_{12} = \mu(u_y + v_x) \quad (4.71)$$

Near the surface, $v/u \ll 1$ and $\partial Q/\partial y \gg \partial Q/\partial x$. In this region, $\underline{\mathbf{P}}$ simplifies. Hence,

$$\underline{\mathbf{P}} \cong \begin{vmatrix} -p & \mu u_y \\ \mu u_y & -p \end{vmatrix}$$

and also, since $v/u \ll 1$,

$$\underline{V} \cdot \underline{P} \cong -i(up) - j(up - u\mu u_y) \quad (4.72)$$

In addition,

$$\dot{\underline{q}} = k\nabla T \cong jk \frac{\partial T}{\partial y} \quad (4.73)$$

The governing equations become

$$E_x + F_y = 0 \quad (4.74)$$

where

$$E = \begin{vmatrix} \rho u \\ \rho u^2 + p \\ \rho uv - \mu u_y \\ \rho ue + up \end{vmatrix}, \quad F = \begin{vmatrix} \rho v \\ \rho uw - \mu u_y \\ \rho v^2 + p \\ \rho ve + vp - \mu uu_y - kT_y \end{vmatrix}$$

The energy equation can be simplified by means of the following identities:

$$H = e + \frac{P}{\rho}, \quad \mu H_y = \mu uu_y + PrkT_y \quad (4.75)$$

or

$$H = C_p T + \frac{u^2}{2} + \frac{v^2}{2}, \text{ since } p = \rho RT \text{ and } Pr = \frac{\mu C_p}{k} \quad (4.76)$$

Thus,

$$[\rho u H]_x + [\rho v H - \mu H_y + (Pr - 1)kT_y]_y = 0 \quad (4.77)$$

The boundary conditions required are shown in Table 4.1.

Note: Only the first derivatives in x exist. The order-of-magnitude analysis has reduced the Navier-Stokes equations from elliptic to parabolic in the x direction. This fact greatly simplifies the solution procedure since it implies that we can march in the x direction under certain additional restrictions (these are supersonic and unseparated flow conditions). This reduced set of equations are called the "parabolized Navier-Stokes" equations. When applicable, they are an extremely efficient numerical set.

Note: Only the viscous terms have been eliminated. The Euler equations are completely contained within the parabolized Navier-Stokes set. The boundary-layer equations arise from a further reduction of this set.

RE-ENTRY HEATING

95

Table 4.1 Boundary Conditions Required for Energy Equation

Variable	No. of Boundary Conditions	
	x	y
<i>u</i>	1	2
<i>v</i>	1	1
<i>p</i>	1	1
<i>T</i>	1	2

Examine the normal momentum equation,

$$(\rho uv - \mu u_y)_x + (\rho v^2 + p)_y = 0 \quad (4.78)$$

Comparing these terms with others in the governing equations shows them to be of lower order near the surface and therefore can be eliminated,

$$(\rho uv - \mu u_y)_x \ll (\rho uv - \mu u_y)_y$$

$$\rho v^2 \ll \rho u^2 \quad (4.79)$$

Hence, the normal momentum reduces to

$$p_y = 0 \quad (4.80)$$

This system no longer contains the Euler equations. Hence, an additional solution procedure is required to obtain information about the inviscid field. The boundary-layer method “uncouples” the viscous and inviscid regions and permits two different simplified procedures. This is both the beauty of the method and the downfall of the approach.

The governing equations for the boundary layer are

$$(\rho u)_x + (\rho v)_y = 0 \quad (4.81)$$

$$(\rho u^2 + p)_x + (\rho uv - \mu u_y)_y = 0 \quad (4.82)$$

$$p_y = 0$$

$$(\rho u H)_x + [\rho v H - \mu H_y + (Pr - 1)k T_y]_y = 0 \quad (4.83)$$

The usual form is to subtract $u[(\rho u)_x + (\rho v)_y]$ from the *x* momentum equation and $H[(\rho u)_x + (\rho v)_y]$ from the energy equation. Also, we will set

RE-ENTRY AERODYNAMICS

$Pr = 1$ to simplify the system; however, this is not required in general,

$$\begin{aligned}
 (\rho u)_x + (\rho v)_y &= 0 \\
 \rho uu_x + \rho vu_y &= (\mu u_y)_y - p_x \quad (4.84) \\
 p_y &= 0 \\
 \rho uH_x + \rho vH_y &= (\mu H_y)_y \quad (4.85)
 \end{aligned}$$

The equation of state closes the system,

$$\frac{p}{\rho} = \frac{\gamma - 1}{\gamma} \left(H - \frac{u^2}{2} \right) \quad (4.86)$$

Pressure may be eliminated by means of the outer boundary condition,

$$\rho_e u_e u_{e_x} = - \frac{dp_e}{dx} = - \frac{dp}{dx} \quad (4.87)$$

Therefore, three equations result,

$$\begin{aligned}
 (\rho u)_x + (\rho v)_y &= 0 \\
 \rho uu_x + \rho vu_y &= (\mu u_y)_y + \rho_e u_e u_{e_x} \\
 \rho uH_x + \rho vH_y &= (\mu H_y)_y \quad (4.88)
 \end{aligned}$$

The boundary conditions are

$$u(0, y) = u_\infty, \quad u(x, 0) = 0, \quad u(x, \infty) = u_e$$

$$v(x, 0) = 0$$

$$H(0, y) = H_e, \quad H(x, 0) = H_w, \quad H(x, \infty) = H_e = \text{const}$$

See Table 4.2.

**Table 4.2 Boundary Conditions Required
for Boundary-Layer Equations**

Variable	No. of Boundary Conditions	
	x	y
u	1	2
v	0	1
H	1	2

This is the system of equations for which theoreticians have spent over 70 years solving. Thanks to their efforts we have extremely useful methods to solve this set. One additional feature must be treated: the inclusion of a generalized curvilinear coordinate system.

Curvilinear Coordinates

In deriving the boundary-layer equations, we assumed a two-dimensional Cartesian coordinate system. This implies that we can consider only the flow over flat plates. In this section, we will generalize the result to an arbitrary curvilinear coordinate system. See Fig. 4.10.

In generalized coordinates, the divergence of a vector is

$$\nabla \cdot \mathbf{F} = \frac{\partial}{\partial u_1}(h_2 h_3 F_1) + \frac{\partial}{\partial u_2}(h_3 h_1 F_2) + \frac{\partial}{\partial u_3}(h_1 h_2 F_3) \quad (4.89)$$

where the arc lengths equal

$$dS_1 = h_1 du_1, dS_2 = h_2 du_2, dS_3 = h_3 du_3$$

For the coordinate system shown in Fig. 4.10,

$$dS_1 = (R + y) d\theta \quad (4.90)$$

$$dS_2 = dy \quad (4.91)$$

$$dS_3 = dx \text{ or } r_0(x) d\phi$$

for either two-dimensional or axisymmetric configurations. Let $dx = R d\theta$. Hence,

$$dS_1 = \left(1 + \frac{y}{R}\right) dx \cong dx \text{ for } \frac{y}{R} \ll 1 \quad (4.93)$$

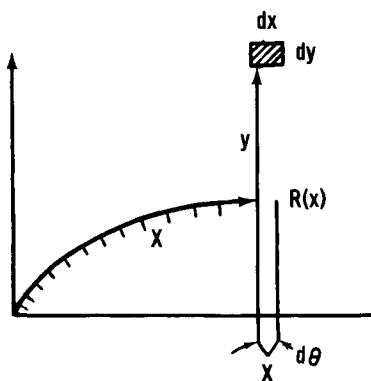


Fig. 4.10 Two-dimensional Cartesian coordinate system.

Therefore,

$$h_1 = 1 \quad du_1 = dx \quad (4.94)$$

$$h_2 = 1 \quad du_2 = dy \quad (4.95)$$

$$h_3 = r_0^K \quad \frac{\partial F}{\partial u_3} = 0 \quad (4.96)$$

where $K = 0$ for a two-dimensional configuration and $K = 1$ for an axisymmetric one. Thus,

$$\nabla \cdot \rho V = \frac{\partial}{\partial x}(r_0^K \rho u) + \frac{\partial}{\partial y}(r_0^K \rho v) = 0 \quad (4.97)$$

All other equations remain unchanged.

Therefore, the simple inclusion of the r_0^K term in continuity permits one to calculate the boundary layer over any two-dimensional or axisymmetric configuration provided $\delta/R \ll 1$.

We are now prepared to investigate the solution of these equations. Three procedures will be examined, i.e., analytic (similarity) solutions, integral methods, and numerical techniques.

Boundary-Layer Analytic Solutions

The governing compressible, two-dimensional, or axisymmetric boundary-layer equations are derived to be the following:

$$(\rho u r_0^K)_x + (\rho v r_0^K)_y = 0 \quad (4.98)$$

$$\rho u u_x + \rho v u_y = (\mu u_y)_y + \rho_e u_e u_{e_x} \quad (4.99)$$

$$\rho u H_x + \rho v H_y = (\mu H_y)_y, \quad Pr = 1 \quad (4.100)$$

where

$$r_0(x) \text{ is given, } H = C_p T + \frac{u^2}{2}, \quad p = \rho R T \quad (4.101)$$

These are a set of partial differential equations representing the conservation of mass, momentum, and energy and containing three variables u , v , and H . The variable ρ can be eliminated by the equation of state,

$$\frac{\rho_e}{\rho} = \frac{p_e}{R T_e} \cdot \frac{R T}{p} = \frac{T}{T_e} = \frac{H - (u^2/2)}{C_p T_e} \quad (4.102)$$

Boundary conditions for this system are

$$v(x, 0) = 0$$

$$u(x, 0) = 0 \quad H(x, 0) = H_w$$

$$u(x, \infty) = u_e(x) = \text{given} \quad H(x, \infty) = H_e = \text{const}$$

$$u(0, y) = u_\infty \quad H(0, y) = H_e$$

Define a stream function to eliminate v ,

$$\rho u r_0^K = \Psi_y \quad (4.103)$$

$$\rho v r_0^K = -\Psi_x \quad (4.104)$$

Continuity becomes $(\Psi_y)_x - (\Psi_x)_y = 0$ and is automatically satisfied.

The two governing equations become

$$\Psi_y u_x - \Psi_x u_y = r_0^K (\mu u_y)_y + r_0^K \rho_e u_e u_{e_x} \quad (4.105)$$

$$\Psi_y H_x - \Psi_x H_y = r_0^K (\mu H_y)_y \quad (4.106)$$

To obtain an analytic solution, separate the variables; i.e., assume $\Psi = X(x)Y(y)$. If successful, one obtains two ordinary differential equations (ODE) that can then be integrated analytically (or numerically). The solution must, of course, be required to satisfy the boundary conditions. In this case, the variables cannot be separated in the form assumed ($\Psi = XY$). However, if we are clever enough, we might be able to find a transformation that will separate the variables, i.e., assume

$$\Psi = g(\xi)f(\eta) \text{ and } g = \sqrt{2\xi}$$

where

$$d\xi = j(x)dx, \quad j = \rho_e \mu_e u_e r_0^{2K}$$

$$d\eta = h(x)\rho dy, \quad h = u_e r_0^K / g$$

This is the Levy-Lees transformation.

The chain rule will change the variables

$$\frac{\partial}{\partial x} = \xi_x \frac{\partial}{\partial \xi} + \eta_x \frac{\partial}{\partial \eta} = j \frac{\partial}{\partial \xi} + \eta_x \frac{\partial}{\partial \eta} \quad (4.107)$$

$$\frac{\partial}{\partial y} = \xi_y \frac{\partial}{\partial \xi} + \eta_y \frac{\partial}{\partial \eta} = h\rho \frac{\partial}{\partial \eta} \quad (4.108)$$

Two operators appear in both equations and must be transformed. First,

$$(\mu Q_y)_y = \eta_y (\mu h \rho Q_\eta)_\eta = \eta_y h \rho_e \mu_e (CQ_\eta)_\eta \quad (4.109)$$

where $C = \rho \mu / \rho_e \mu_e$. Second,

$$\begin{aligned} \Psi_y Q_x - \Psi_x Q_y &= \eta_y \Psi_\eta (jQ_\xi + \eta_x Q_\eta) - (j\Psi_\xi + \eta_x \Psi_\eta) \eta_y Q_\eta \\ &= j\eta_y [\Psi_\eta Q_\xi - \Psi_\xi Q_\eta] \end{aligned} \quad (4.110)$$

With these two transformations, the governing equations become

$$(Cu_\eta)_\eta = g\Psi_\eta u_\xi - g\Psi_\xi u - \frac{\rho_e}{\rho} g^2 u_{e\xi} \quad (4.111)$$

$$(CH_\eta)_\eta = g\Psi_\eta H_\xi - g\Psi_\xi H_\eta \quad (4.112)$$

where

$$\Psi_\eta = g \frac{u}{u_e} \text{ and } \frac{\rho_e}{\rho} = \frac{H - (u^2/2)}{h_e}$$

Redefining the variables

$$u/u_e = f' = f_\eta \text{ and } S = (H/H_e) - 1$$

results in

$$(Cf'')' + g\Psi_\xi f'' = \frac{g^2 u_{e\xi}}{u_e} \left(f'^2 - \frac{\rho_e}{\rho} \right) + g^2 f' f'_\xi \quad (4.113)$$

$$(CS')' + g\Psi_\xi S' = g^2 f' S_\xi \quad (4.114)$$

Note, however, that

$$f'^2 - \frac{\rho_e}{\rho} = f'^2 - \frac{(1+S)H_e - (u_e^2/2)f'^2}{h_e} = -\frac{H_e}{h_e}(S+1) + \frac{u_e^2}{2h_e}f'^2$$

or

$$f'^2 - \frac{\rho_e}{\rho} = \frac{H_e}{h_e} (f'^2 - S - 1) \quad (4.115)$$

Let

$$\beta \equiv g^2 \frac{H_e u_{e\xi}}{h_e u_e} = g^2 \frac{M_{e\xi}}{M_e} = 2\xi \frac{M_{e\xi}}{M_e}$$

Since $\Psi_\eta = gf'$, then

$$g\Psi_\xi = g \frac{\partial}{\partial \xi} \int g f' d\eta \quad (4.116)$$

Note that $g_\xi = 1/g$.

If we assume that both f and S are functions of only η (also $C = 1$), then two ODE's are produced,

$$f''' + ff'' = \beta(f'^2 - S - 1) \quad (4.117)$$

$$S'' + fS' = 0 \quad (4.118)$$

An additional condition is that $\beta = \text{const} = 2\xi M_{e\xi}/M_e$, which integrates to

$$M_e = C\xi^{\beta/2}$$

This is the similarity condition.

The boundary conditions then become

$$f(0) = 0$$

$$f'(0) = 0 \quad S(0) = S_w$$

$$f'(\infty) = 0 \quad S(\infty) = 0$$

These equations are coupled unless $S_w = 0$ or $\beta = 0$. Numerical integrations of these equations have been carried out and tabulated.

Once these solutions have been obtained, we must transform back to the physical plane to obtain shear stress and heat transfer at the wall,

$$\tau_w = \left(\mu \frac{\partial u}{\partial y} \right)_w = h \rho_w \mu_w u_e f''(0) = \rho_e u_e^2 C_{f/2} \quad (4.120)$$

Table 4.3 Examples of Similarity Solutions

$S(0)$	β	$f''(0)$	$-S'(0)/S(0)$	$\frac{S(0)f''(0)}{-S'(0)} = \frac{C_{f/2}}{St}$
0	1	1.232	0.5705	2.16
0	0.50	0.9277	0.5390	1.72
0	0	0.4696	0.4696	1.00
0	-0.1988	0	0.3258	0
-1	1	0.6489	0.5067	1.28
-1	0.5	0.5811	0.4942	1.18
-1	0	0.4696	0.4696	1.0
-1	-0.3264	0	0.2478	0

$$\dot{q}_w = \left(k \frac{\partial T}{\partial y} \right)_w = h \frac{\rho_w}{C_p} k_w H_e S'(0) = St \rho_e u_e (H_e - H_w) \quad (4.121)$$

Dividing these two equations produces an exact Reynolds' analogy,

$$\frac{St}{C_{f/2}} = \frac{-S'(0)}{P_{r_w} S(0) f''(0)} = F[S(0), \beta] \quad (4.122)$$

Note that the proportionality constant is not, in general, unity.

Table 4.3 lists some similarity solutions.⁴ A summary of global quantities is shown in Table 4.4 at the end of this section.

Table 4.4 Summary of Global Quantities

$S(0)$	β	$f''(0)$	$S'(0)$	$\theta_{tr} N$	H_{tr}	$\theta_{tr}^* N$
+ 1.0	20.00	8.32032	-0.79348	-0.21840	-2.95481	-0.49052
	10.00	5.79955	-0.75997	-0.15222	-4.91004	-0.35006
	2.00	2.48768	-0.66146	0.06727	16.98925	0.08138
	1.00	1.73668	-0.61558	0.17610	7.86175	0.27686
	0.50	1.23481	-0.57289	0.27462	05.99271	0.44319
	0.28571	0.96305	-0.54332	0.33835	5.46209	0.54504
	0.00	0.46960	-0.46960	0.46960	5.18220	0.73848
	-0.04	0.37182	-0.45001	0.49606	5.26153	0.77431
	-0.08	0.25435	-0.42283	0.52612	5.45698	0.81336
	-0.12	0.08379	-0.37229	0.56047	6.08750	0.85525
	-0.12950S	0.00000	-0.33892	0.56761	6.72191	0.86349
	-0.12R	-0.12588	-0.25909	0.53650	9.28853	0.83394
	-0.08R	-0.16908	-0.16518	0.42294	16.49727	0.73824
	-0.04R	-0.13782	-0.08546	0.27255	36.64144	0.62446
+ 0.5	20.00	6.80892	-0.37756	-0.06726	-6.11152	-0.16158
	10.00	4.77511	-0.36224	-0.01787	-27.81691	-0.06736
	2.00	2.09961	-0.31772	0.14941	5.52651	0.23490
	1.00	1.49158	-0.29726	0.23443	4.36261	0.37890
	0.50	1.08492	-0.27844	0.31254	3.94270	0.50516
	0.28571	0.86493	-0.26559	0.36357	3.82643	0.58425
	0.00	0.46960	-0.23480	0.46960	3.88665	0.73848
	-0.04	0.39363	-0.22717	0.49105	3.96009	0.76774
	-0.08	0.30568	-0.21731	0.51543	4.08679	0.80002
	-0.12	0.19545	-0.20285	0.54380	4.33825	0.83607
	-0.15735S	0.00000	-0.16709	0.57426	5.35531	0.87230
	-0.12R	-0.15091	-0.10264	0.49021	9.89870	0.79554
	-0.08R	-0.15550	-0.06787	0.38140	16.59624	0.70759
	-0.04R	-0.11958	-0.03423	0.24030	36.44035	0.60162

(Table continued on next page)

RE-ENTRY HEATING

103

Table 4.4 (cont.) Summary of Global Quantities

$S(0)$	β	$f''(0)$	$S'(0)$	$\theta_{tr}N$	H_{tr}	θ_{tr}^*N
$*S'(0)/S(0)$						
0.0	20.00	5.18072	0.70907	0.08276	2.07979	0.13685
	10.00	3.67523	0.68217	0.11523	2.08950	0.19028
	2.00	1.68722	0.60520	0.23078	2.15541	0.37790
	1.00	1.23259	0.57047	0.29234	2.21623	0.47528
	0.50	0.92768	0.53898	0.35027	2.29694	0.56454
	0.28571	0.76274	0.51786	0.38872	2.36781	0.62222
	0.00	0.46960	0.46960	0.46960	2.59110	0.73848
	-0.04	0.41495	0.45849	0.48603	2.65639	0.76110
	-0.08	0.35351	0.44493	0.50468	2.74409	0.78626
	-0.12	0.28176	0.42736	0.52628	2.87177	0.81469
	-0.16	0.19078	0.40165	0.55219	3.09067	0.84759
	-0.19884S	0.00000	0.32581	0.58543	4.02923	0.88698
	-0.16R	-0.12557	0.21907	0.52250	6.75200	0.82714
	-0.12R	-0.14294	0.15917	0.43744	10.05630	0.75489
	-0.08R	-0.13223	0.10428	0.33273	16.46750	0.67249
	-0.04R	-0.09664	0.04955	0.20228	35.94357	0.57434
-0.2	20.00	4.48429	0.13749	0.14177	0.53150	0.24546
	10.00	3.20661	0.13250	0.16753	0.81404	0.28457
	2.00	1.51346	0.11830	0.26287	1.37876	0.43150
	1.00	1.12410	0.11195	0.31526	1.56562	0.51192
	0.50	0.86228	0.10623	0.36526	1.72148	0.58744
	0.28571	0.72053	0.10243	0.39873	1.82484	0.63702
	0.00	0.46960	0.09392	0.46960	2.07288	0.73848
	-0.04	0.42335	0.09202	0.48402	2.13375	0.75842
	-0.12	0.31289	0.08691	0.51924	2.31179	0.80583
	-0.20	0.14282	0.07675	0.57006	2.74728	0.87024
	-0.22115S	0.00000	0.06408	0.59223	3.52183	0.89582
	-0.20R	-0.08638	0.05119	0.56672	4.76208	0.86997
	-0.12R	-0.13321	0.02809	0.41334	10.01894	0.73697
	-0.04R	-0.08553	0.00824	0.18453	35.58789	0.56138
-0.4	20.00	3.75284	0.26531	0.19960	-0.10988	0.34637
	10.00	2.71619	0.25623	0.21879	0.14144	0.37265
	2.00	1.33335	0.23063	0.29448	0.76387	0.48264
	1.00	1.01219	0.21927	0.33794	0.99518	0.54728
	0.50	0.79519	0.20913	0.38015	1.18356	0.60979
	0.28571	0.67745	0.20246	0.40870	1.30154	0.65156
	0.00	0.46960	0.18784	0.46960	1.55466	0.73848
	-0.08	0.38985	0.18096	0.49606	1.67648	0.77502
	-0.16	0.28750	0.17069	0.53125	1.86768	0.82207
	-0.20	0.21842	0.16258	0.55463	2.03097	0.85217
	-0.24756S	0.00000	0.12509	0.60119	3.03940	0.90734
	-0.20R	-0.10045	0.08762	0.54367	4.92383	0.85049
	-0.16R	-0.11968	0.06712	0.47287	6.83187	0.78810
	-0.08R	-0.10427	0.03023	0.28489	16.07477	0.63820

(Table continued on next page)

Table 4.4 (cont.) Summary of Global Quantities

$S(0)$	β	$f''(0)$	$S'(0)$	$\theta_{tr}N$	H_{tr}	θ_{tr}^*N
-0.6	20.00	2.97574	0.38133	0.25540	-0.46744	0.43789
	10.00	2.19796	0.36942	0.26837	-0.28101	0.45327
	2.00	1.14560	0.33608	0.32542	0.26016	0.53090
	1.00	0.89627	0.32140	0.36028	0.48769	0.58117
	0.50	0.72618	0.30839	0.39491	0.67770	0.63150
	0.28571	0.63340	0.29991	0.41862	0.79575	0.66583
	0.00	0.46960	0.28176	0.46960	1.03644	0.73848
	-0.08	0.40748	0.27354	0.49176	1.14238	0.76933
	-0.16	0.32996	0.26198	0.52094	1.29130	0.80903
	-0.24	0.21759	0.24185	0.56385	1.55874	0.86499
	-0.27780S	0.00000	0.18074	0.61307	2.59965	0.92236
	-0.24R	-0.07026	0.14154	0.57706	3.67395	0.88478
	-0.16R	-0.10531	0.08521	0.44419	6.73182	0.76649
	-0.08R	-0.08533	0.03531	0.25548	15.67498	0.61688
-0.8	20.00	2.13484	0.48212	0.30760	-0.70299	0.51729
	10.00	1.64218	0.46931	0.31511	-0.57885	0.52444
	2.00	0.94832	0.43337	0.35535	-0.16563	0.57572
	1.00	0.77554	0.41755	0.38216	0.02944	0.61334
	0.50	0.65496	0.40359	0.40949	0.19889	0.65251
	0.28571	0.58827	0.39457	0.42847	0.30532	0.67979
	0.00	0.46960	0.37568	0.46960	0.51822	0.73848
	-0.12	0.39895	0.36237	0.49824	0.66077	0.77861
	-0.20	0.33641	0.34902	0.52551	0.79921	0.81597
	-0.28	0.24411	0.32597	0.56695	1.03368	0.87063
	-0.30861S	0.00000	0.22601	0.62789	2.24035	0.94060
	-0.28R	-0.03950	0.19405	0.60465	2.80472	0.91518
	-0.20R	-0.08041	0.12373	0.49019	4.82017	0.80846
	-0.12R	-0.07511	0.06003	0.32090	9.28397	0.66947
-1.0	20.00	1.19344	0.56109	0.35255	-0.88074	0.57939
	10.00	1.03080	0.55099	0.35656	-0.81091	0.58266
	2.00	0.73864	0.52063	0.38367	-0.53741	0.61622
	1.00	0.64886	0.50666	0.40330	-0.39112	0.64344
	0.50	0.58114	0.49422	0.42383	-0.25764	0.67270
	0.28571	0.54192	0.48618	0.43824	-0.17187	0.69341
	0.00	0.46960	0.46960	0.46960	0.00000	0.73848
	-0.12	0.42578	0.45835	0.49129	0.11129	0.76937
	-0.20	0.38751	0.44771	0.51153	0.21230	0.79781
	-0.28	0.33523	0.43183	0.54045	0.35612	0.83761
	-0.36	0.24475	0.39990	0.59091	0.62726	0.90392
	-0.36	0.04112	0.28850	0.65762	1.60410	0.97671
	-0.32641S	0.00000	0.24778	0.63897	2.06364	0.95367
	-0.28R	-0.03094	0.19969	0.59075	2.75848	0.90363
	-0.20R	-0.04855	0.12184	0.46170	4.52578	0.78690
	-0.12R	-0.03388	0.04298	0.27458	8.36154	0.63421

Stagnation Point Analytic Solutions

As an example, consider the exact solution for a stagnation point. In the previous section, we derived the heating rate equation,

$$\dot{q}_w = h \frac{\rho_w u_w}{Pr} H_e S'(0) \quad (4.123)$$

where

$$h = \frac{u_e r_0^K}{\sqrt{2\xi}}, \quad \xi = \int_0^x \rho_e \mu_e u_e r_0^{2K} dx \quad (4.124)$$

In the stagnation region, the flow is locally incompressible, $u_e = cx$ from potential theory $u_e \sim \sin \theta$, and $r_0 = x$. Substituting these conditions, the following can be determined:

$$\xi = \rho_s \mu_s \int_0^x c x x^{2K} dx = \frac{\rho_s \mu_s u_e x^{1+2K}}{2(1+K)} \quad (4.125)$$

$$h = \frac{u_e r_0^K}{\sqrt{2\xi}} = \sqrt{\frac{(1+K)}{\rho_s \mu_s}} \frac{u_e}{x} \quad (4.126)$$

$$\beta = \frac{2\xi du_e}{u_e d\xi} = \frac{1}{1+K} \quad (4.127)$$

Hence,

$$\dot{q}_w = \frac{C_w}{Pr} \sqrt{(1+K) \rho_s \mu_s \frac{u_e}{x}} H_e S'(0) \quad (4.128)$$

where

$$C_w = \rho_w \mu_w / \rho_s \mu_s \quad (4.129)$$

Letting $C_w = 1$ and $Pr = 1$ and recalling that $S(0) = H_w/H_e - 1$,

$$\dot{q}_s = \left[\frac{S'(0)}{-S(0)} \right] \sqrt{(1+K) \rho_s \mu_s \frac{du_e}{dx}} (H_e - H_w) \quad (4.130)$$

where $S'(0)/-S(0)$ is a function of β and $S(0)$.

This relationship is identical to the one derived in Sec. 4.1, with the exception of the constant multiplier.

Integral methods. For conditions in which similarity (i.e., $M_e = c\xi^{\beta/2}$) does not exist, alternative methods must be used. Local similarity is an approach in which similarity is assumed at each station as computed from the local pressure gradient, but this method does not properly account for the history of the flow. Another technique is to use integral methods. The

governing equations are integrated in the y direction, using assumed profiles. The result is an approximate ODE in the x direction, which produces the heating distribution along the body.

The integrated governing equations are

$$\int_0^\infty (\rho u)_x dy = - \int_0^\infty (\rho v)_y dy = -\rho_e v_e \quad (4.131)$$

$$\int_0^\infty (\rho uu_x - \rho_e u_e u_{ex}) dy + \int_0^\infty \rho vu_y dy = \int_0^\infty (\mu u_y)_y dy = -\tau_w \quad (4.132)$$

$$\int_0^\infty (\rho u H_x) dy + \int_0^\infty \rho v H_y dy = \int_0^\infty (\mu H_y)_y dy = -\dot{q}_w \quad (4.133)$$

Note:

$$\int_0^\infty \rho v G_y dy = (\rho v G)_0^\infty - \int_0^\infty G(\rho v)_y dy \quad (4.134)$$

$$= \rho_e v_e G_e + \int_0^\infty G(\rho u)_x dy \quad (4.135)$$

$$\begin{aligned} &= - \int_0^\infty G_e(\rho u)_x dy + \int_0^\infty G(\rho u)_x dy \\ &= \int_0^\infty (G - G_e)(\rho u)_x dy \end{aligned} \quad (4.136)$$

Hence, the integral relations become

$$\tau_w = \int_0^\infty (\rho_e u_e u_{ex} - \rho uu_x) dy + \int_0^\infty (u_e - u)(\rho u)_x dy \quad (4.137)$$

$$\dot{q}_w = \int_0^\infty (H_e - H)(\rho u)_x dy - \int_0^\infty \rho u H_x dy \quad (4.138)$$

These can be reformed to become

$$\tau_w = \frac{\partial}{\partial x} \int_0^\infty (u_e - u)\rho u dy + u_{ex} \int_0^\infty (\rho_e u_e - \rho u) dy \quad (4.139)$$

$$\dot{q}_w = \frac{\partial}{\partial x} \int_0^\infty (H_e - H)\rho u dy \quad (4.140)$$

The following integrals are defined for convenience:

$$\delta^* = \int_0^\infty \left(1 - \frac{\rho u}{\rho_e u_e}\right) dy \quad (4.141)$$

$$\theta = \int_0^\infty \left(1 - \frac{u}{u_e}\right) \frac{\rho u}{\rho_e u_e} dy \quad (4.142)$$

$$\theta_H = \int_0^\infty \left(1 - \frac{H}{H_e}\right) \frac{\rho u}{\rho_e u_e} dy \quad (4.143)$$

$$\tau_w = \frac{d}{dx} \left(\rho_e u_e^2 \theta \right) + \rho_e u_e \delta^* \frac{du_e}{dx} = \frac{C_f}{2} \rho_e u_e^2 \quad (4.144)$$

$$\dot{q}_w = \frac{d}{dx} (\rho_e u_e H_e \theta_H) = St \rho_e u_e H_e \quad (4.145)$$

By approximating u/u_e and T/T_e , as polynomials, for example, relationships can be produced for both shear stress and heat transfer,

$$\text{Momentum: } \frac{C_f}{2} = \frac{d\theta}{dx} + (2\theta + \delta^*) \frac{u_{ex}}{u_e} + \theta \frac{\rho_{ex}}{\rho_e} \quad (4.146)$$

$$\text{Energy: } St = \frac{1}{\rho_e u_e} (\rho_e u_e \theta_H)_x \quad (4.147)$$

The goal is to represent the three unknowns in the momentum equation, i.e., C_f , θ , and δ^* , as one unknown. In this way, with both u_e and ρ_e given, an equation with one unknown in x can be integrated. The following simple example will demonstrate the procedure.

Consider incompressible flow with a linear velocity profile such as shown in Fig. 4.11. Hence,

$$u/u_e = y/\delta \quad (4.148)$$

$$\delta^* = \int_0^\delta \left(1 - \frac{u}{u_e}\right) dy = \int_0^\delta \left(1 - \frac{y}{\delta}\right) dy = \left[y - \frac{y^2}{2\delta}\right]_0^\delta = \frac{\delta}{2} \quad (4.149)$$

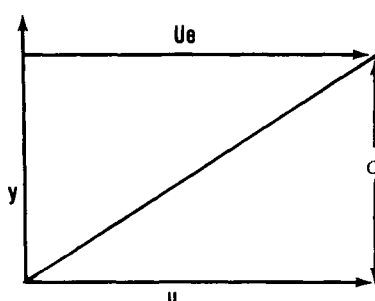


Fig. 4.11 Incompressible flow with a linear velocity profile.

$$\theta = \int_0^\delta \left(1 - \frac{u}{u_e}\right) \frac{u}{u_e} dy = \int_0^\delta \left(1 - \frac{y}{\delta}\right) \frac{y}{\delta} dy = \left[\frac{y^2}{2\delta} - \frac{y^3}{3\delta^2} \right] = \frac{\delta}{6} \quad (4.150)$$

$$\frac{C_f}{2} = \frac{\tau_w}{\rho_e u_e^2} = \frac{[\mu(\partial u/\partial y)]_w}{\rho_e u_e^2} = \frac{\nu(u_e/\delta)}{u_e^2} = \frac{\nu}{u_e \delta} \quad (4.151)$$

Inserting these relations into the momentum equation results in

$$\frac{C_f}{2} = \frac{\nu}{u_e \delta} = \frac{\nu}{u_e \delta \theta} = \frac{d\theta}{dx} + \left(2 + \frac{\delta^*}{\theta}\right) \theta \frac{u_e}{u_e} \quad (4.152)$$

Multiplying this equation by 2θ produces a linear, first-order equation in θ^2 ,

$$\frac{d\theta^2}{dx} + \left(10 \frac{u_e}{u_e}\right) \theta^2 = \frac{\nu}{3u_e}$$

where $u_e(x)$ is given. Recall the solution for this linear equation,

$$\frac{dy}{dx} + yP(x) = Q(x) \quad (4.153)$$

$$y = e^{-\int P dx} \int_0^x Q e^{\int P dx} dx \quad (4.154)$$

$$e^{\int P dx} = e^{\int n(u_{ex}/u_e) dx} = e^{\ell n u} e^n = u_e^n \quad (4.155)$$

$$\int Q e^{\int P dx} dx = \int \frac{B\nu}{u_e} u_e^n dx = B\nu \int u_e^{n-1} dx \quad (4.156)$$

Hence,

$$\theta^2 = \frac{B\nu}{u_e^n} \int_0^x u_e^{n-1} dx \quad (4.157)$$

where the approximate values are $n = 10$ and $B = 0.333$. The similarity values are $n = 6$ and $B = 0.47$.

Once $\theta(x)$ is known, C_f can be obtained,

$$\frac{C_f}{2} = \frac{d\theta}{dx} + (2 + H) \theta \frac{u_{ex}}{u_e}, \quad H = \frac{\delta^*}{\theta} \quad (4.158)$$

St can be obtained in a similar fashion. More elaborate relationships for the velocity profile can be used, but the procedure is similar. Numerical integration of the resulting ODE in x is then required, however.

Boundary-layer numerical methods. Although similarity solutions and integral methods have historical significance and provide considerable understanding of the boundary-layer phenomenon, they are not currently used in high technology. Digital computers have advanced greatly during the last two decades, so that numerical solutions can be obtained for the entire boundary layer in only a few seconds.

The transformed equations developed in the previous section are used without assuming similarity,

$$(CF_\eta)_\eta + VF_\eta - \beta(F^2 + S - 1) = 2\xi FF_\xi \quad (4.159)$$

$$(CS_\eta)_\eta + VS_\eta = 2\xi FS_\xi \quad (4.160)$$

where

$$F = u/u_e, \quad S = (H/H_e) - 1 \quad (4.161)$$

$$V \equiv g\Psi_\xi, \quad \Psi_\eta = gF \quad (4.162)$$

Hence

$$(1/g)V_\eta = \Psi_{\xi\eta} = \Psi_{\eta\xi}(gF)_\xi \quad (4.163)$$

or

$$V_\eta = g(gF)_\xi = F + 2\xi F_\xi \quad (4.164)$$

These three partial differential equations contain three unknowns, V , F , and S . The boundary conditions are

$$V(\xi, 0) = 0$$

$$F(\xi, 0) = 0 \quad S(\xi, 0) = S_w$$

$$F(\xi, \infty) = 1 \quad S(\xi, \infty) = 0$$

$$F(0, \eta) = 1 \quad S(0, \eta) = 0$$

The first and second derivatives in η and first derivatives in ξ must be approximated by finite differences,

$$F_\eta = \frac{F_{n+1} - F_{n-1}}{2\Delta\eta} \text{ (central)}, \quad F_\xi = \frac{F_n^m - F_{n-1}^{m-1}}{\Delta\xi} \text{ (backward)} \quad (4.165)$$

$$F_{\eta\eta} = \frac{F_{n+1} - 2F_n + F_{n-1}}{\Delta\eta^2} \text{ (central)} \quad (4.166)$$

Hence,

$$-a_n F_{n+1} + b_n F_n - c_n F_{n-1} = d_n \quad (4.167)$$

where

$$a_n = 1 + V_n (\Delta\eta/2) \quad (4.168)$$

$$b_n = 2 + \left[\beta + \frac{2\xi}{\Delta\xi} \right] F_n^* \Delta\eta^2 \quad (4.169)$$

$$c_n = 1 - V_n (\Delta\eta/2) \quad (4.170)$$

$$d_n = \left[-\beta(S_n - 1) + \frac{2\xi F_n^*}{\Delta\xi} F^{m-1} \right] \Delta\eta^2 \quad (4.171)$$

Similarly,

$$-A_n S_{n+1} + B_n S_n - C_n S_{n-1} = D_n \quad (4.172)$$

where

$$A_n = 1 + V_n \frac{\Delta\eta}{2} = a_n \quad D_n = \frac{2\xi F_n^*}{\Delta\xi} S_n^{m-1} \Delta\eta^2$$

$$B_n = 2 + \frac{2\xi}{\Delta\xi} F_n^* \Delta\eta^2 \quad V_n = \int_0^\eta (F + 2\xi F_\xi) d\eta$$

$$C_n = 1 - V_n \frac{\Delta\eta}{2} = c_n \quad \text{Trapezoidal rule integration}$$

Writing this relationship for every node in the grid results in N equations with N unknowns in F_n . Since only three elements exist in each equation, a tridiagonal matrix results,

$$\begin{bmatrix} b_1 & a_1 & 0 & 0 & 0 & 0 & \cdot \\ c_2 & b_2 & a_2 & 0 & 0 & 0 & 0 \\ 0 & c_3 & b_3 & a_3 & \cdot & 0 & 0 \\ 0 & 0 & 0 & \cdot & \cdot & \cdot & 0 \\ 0 & 0 & 0 & \cdot & \cdot & \cdot & 0 \end{bmatrix} \begin{bmatrix} F_1 \\ F_2 \\ F_3 \\ \vdots \\ F_n \end{bmatrix} = \begin{bmatrix} d_1 \\ d_2 \\ d_3 \\ \vdots \\ d_n \end{bmatrix}$$

For such a matrix, a standard “tridiagonal algorithm” solution procedure is available. This method is extremely efficient for solving boundary-valued problems and is the counterpart of the Runge-Kutta method for numerically solving initial-valued problems in ODE’s.

Once the profile is ascertained in y , we step to the next station in x and repeat the matrix solution procedure. Typically, only a few seconds are required to march down the entire configuration, since few iterations are necessary. Note that in this numerical procedure, no approximations to the original set of boundary-layer equations were required to obtain a solution. Hence, today we consider boundary-layer theory to be a "mature" field with little room for growth.

Theoreticians have, therefore, focused their attention on removing the original restrictions from the boundary-layer equations. Two major limitations exist: 1) the inability to compute separated flows (with subsequent reattachment) and 2) the fact that the inviscid field must be calculated independently and then coupled iteratively with the boundary-layer solution. An inefficient number of iterations can occur when strong interacting flowfields occur.

Both of these limitations are removed in numerically solving the Navier-Stokes equations. These are much more costly to compute and should be used only when either of the two limitations above are encountered.

4.4 AEROTHERMOCHEMISTRY

In this section, equations will be developed to deal with a gas undergoing dissociation.⁵ The original premise is that the gas can no longer be treated as perfect and so new relationships for the thermodynamic properties must be derived, but dissociated air can be treated as a *mixture* of perfect gases. Although the combination no longer satisfies the perfect-gas law (i.e., $p = \rho RT$), the individual species do obey such a law,

$$p = \frac{M}{V} \frac{\mathcal{R}}{\mathcal{M}} T = \text{pressure}$$

where M is the mass of substance, V the volume, \mathcal{M} the molecular weight, and T the temperature. Table 4.5 demonstrates this fact. Therefore, \mathcal{R} can be treated as a universal constant.

Table 4.5 Behavior of Gases under Perfect-Gas Law

Gas	\mathcal{M}	\mathcal{R}
H ₂	2	1536
H _e	4	1544
N ₂	28	1542
O ₂	32	1545
SO ₂	64	1543

Now, consider a mixture of perfect gases. The partial pressure of any species i is p_i ,

$$p_i = \frac{M_i}{\mathcal{M}_i} \frac{\mathcal{R}T}{V} \quad (4.173)$$

Dalton's law states that $p = \sum p_i$,

$$p = \sum_i p_i = \frac{\mathcal{R}T}{V} \sum_i \frac{M_i}{\mathcal{M}_i} \quad (4.174)$$

where $M = \sum M_i$ or $\sum_i (M_i/M) = 1$.

Defining

$$C_i = M_i/M = \text{mass concentration} \quad (4.175)$$

then $\sum C_i = 1$. Also note that

$$C_i = \frac{M_i/V}{M/V} = \frac{\rho_i}{\rho} \quad (4.176)$$

Thus,

$$p = \frac{\mathcal{R}TM}{V} \sum_i \frac{C_i}{\mathcal{M}_i} = \rho \mathcal{R}T \sum_i \frac{C_i}{\mathcal{M}_i} \quad (4.177)$$

First examine a case where $C_i = \text{const}$,

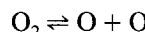
$$\sum \frac{C_i}{\mathcal{M}_i} = \frac{1}{\mathcal{M}} = \text{const} \quad (4.178)$$

Define

$$R = \mathcal{R}/\mathcal{M} \quad (4.179)$$

Thus, $p = \rho RT$, which is the equation for a mixture of perfect gases for which the concentration of each species does not change throughout the flowfield.

Now, consider a case where C_i varies. Take pure oxygen that is dissociating and composed of an O and O₂ binary mixture.



The mass balance is $\sum_i C_i = C_O + C_{O_2} = 1$. Also,

$$\sum \frac{C_i}{\mathcal{M}_i} = \frac{C_O}{\mathcal{M}_O} + \frac{C_{O_2}}{\mathcal{M}_{O_2}} = \frac{2C_O}{\mathcal{M}_{O_2}} + \frac{(1 - C_O)}{\mathcal{M}_{O_2}} \quad (4.180)$$

or

$$\sum_i \frac{C_i}{\mathcal{M}_i} = \frac{1 + C_O}{\mathcal{M}_{O_2}} \quad (4.181)$$

The equation of state becomes

$$p = \rho \mathcal{R} T \frac{(1 + C_O)}{\mathcal{M}_{O_2}} = (1 + C_O) \rho R T \quad (4.182)$$

Redefine

$$p = Z \rho R T \quad (4.183)$$

where $Z = 1 + C_O$. The value of Z depends upon the amount of O_2 dissociated in the field and for pure oxygen has the following limits:

$$1 < Z < 2$$

Now, consider an original mixture of 20% O_2 and 80% N_2 that is undergoing the following reactions (see Fig. 4.12):



Therefore,

$$\sum_i \frac{C_i}{\mathcal{M}_i} = \frac{C_O}{\mathcal{M}_O} + \frac{C_{O_2}}{\mathcal{M}_{O_2}} + \frac{C_N}{\mathcal{M}_N} + \frac{C_{N_2}}{\mathcal{M}_{N_2}} \quad (4.184)$$

$$= \frac{C_O}{16} + \frac{(0.2 - C_O)}{32} + \frac{C_N}{14} + \frac{0.8 - C_N}{28} \quad (4.185)$$

$$= \frac{0.2 + C_O}{32} + \frac{0.8 + C_N}{28} \quad (4.186)$$

$$\frac{1}{\mathcal{M}} = \frac{0.2}{32} + \frac{0.8}{28} = \frac{1}{28.71} \quad (4.187)$$

$$\bar{\mathcal{M}} \sum_i \frac{C_i}{\mathcal{M}_i} = 1.000 + 0.897C_O + 1.026C_N = Z \quad (4.188)$$

Note the limits: $0 < C_O < 0.2$, $0 < C_N < 0.8$, and $1 < Z < 2$. Thus,

$$P = Z(C_O, C_N) \rho R T \quad (4.189)$$

Knowing the amount of dissociation of each species permits the evaluation of the equation of state.

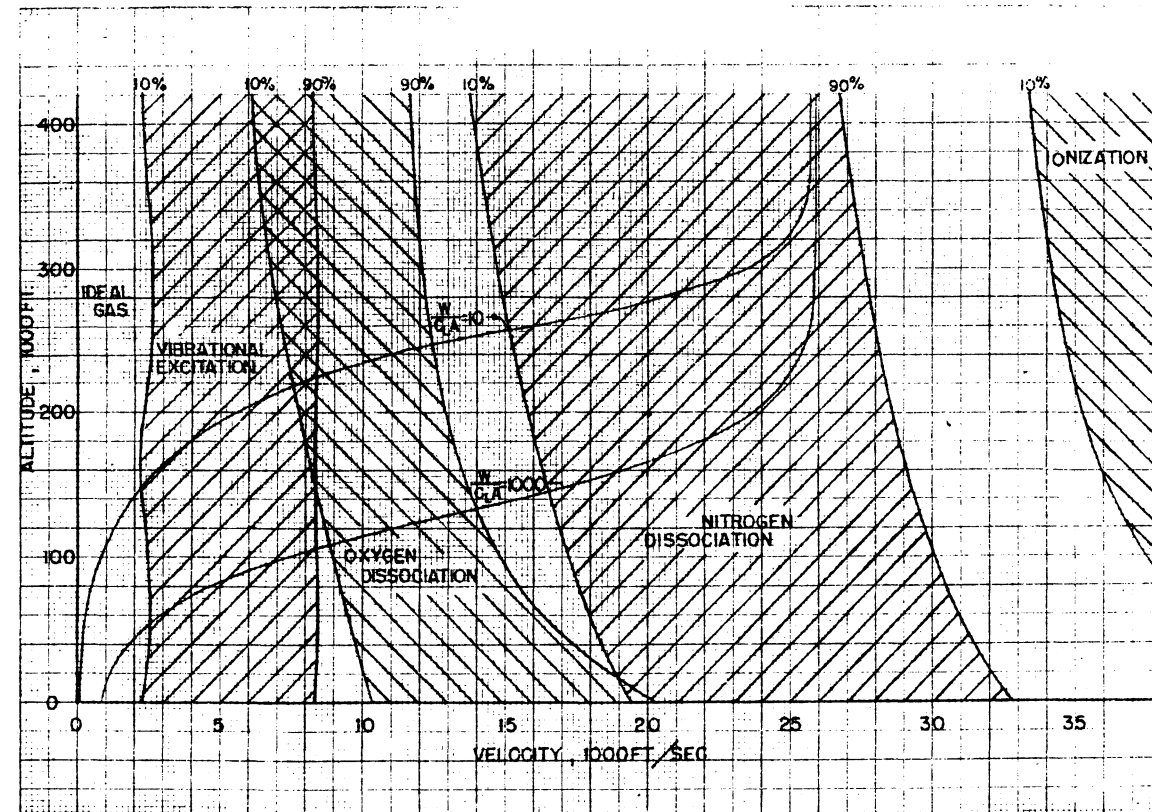


Fig. 4.12 Zones of energy excitations for stagnation point heating in equilibrium.

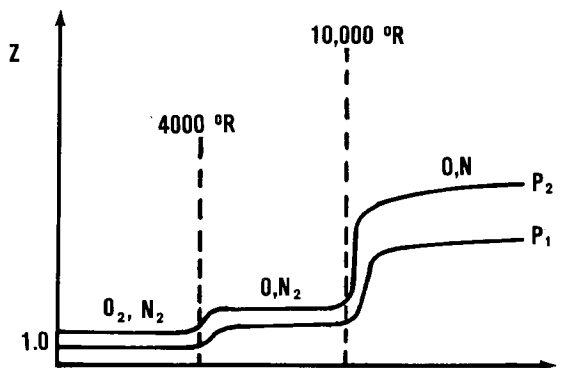


Fig. 4.13 Relation between enthalpy and compressibility factor Z at different pressures and temperatures (note that $Z = 1.0$ denotes an ideal gas).

Enthalpy

This section will evaluate the effects of enthalpy. Figures 4.13 and 4.14 show the relationship between enthalpy and compressibility factor Z . Figure 4.15 shows the relationship with temperature. The definition of specific heat is

$$C_p = \left[\frac{\partial h}{\partial T} \right]_p \quad (4.190)$$

Integrate the relationship

$$\int dh = \int C_p dT \quad (4.191)$$

$$h - h^0 = \int_0^T C_p dT \quad (4.192)$$

where h^0 is the integration constant called the heat of formation. For an ideal gas, $C_p = \text{const}$; thus,

$$h = C_p T + h^0 = \text{enthalpy} \quad (4.193)$$

where h^0 is arbitrarily set to zero. Now, consider a mixture of perfect gases,

$$h_i = \int_0^T C_{p_i} dT + h_i^0 \quad (4.194)$$

$$h = \sum_i C_i h_i = \sum_i C_i \int_0^T C_{p_i} dT + \sum_i C_i h_i^0 \quad (4.195)$$

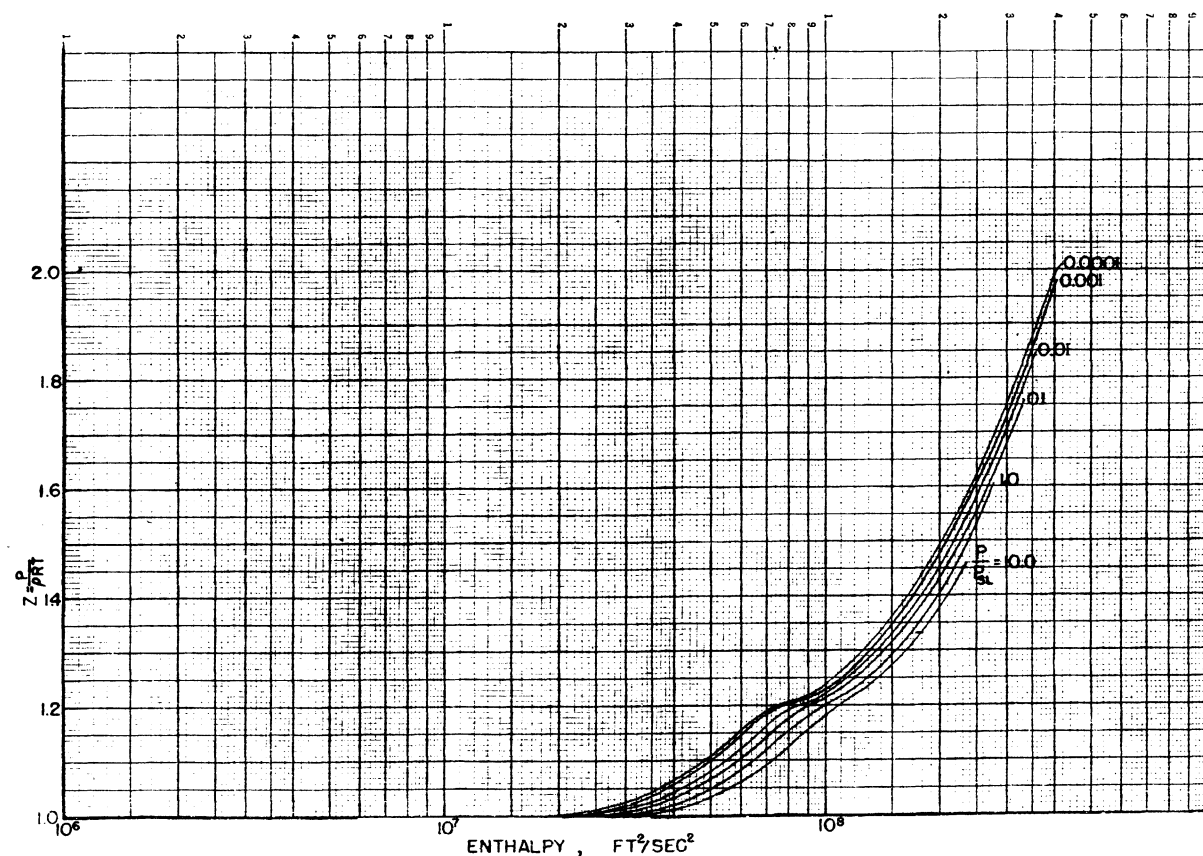


Fig. 4.14 Characteristics of real gases as a function of the flow enthalpy for various pressure ratios (compressibility factor Z).

RE-ENTRY HEATING

117

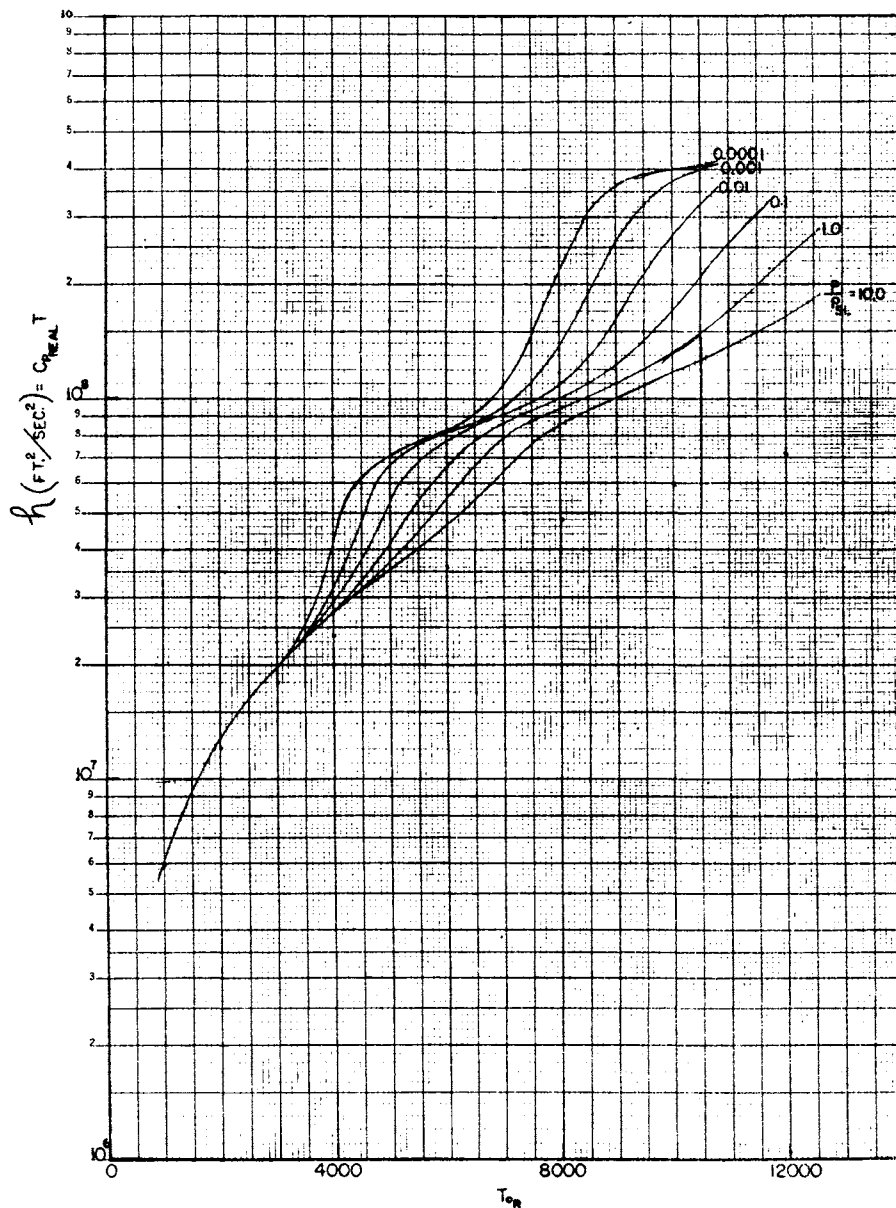
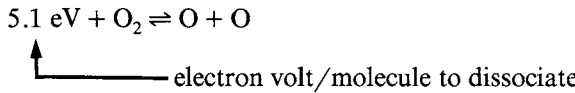


Fig. 4.15 Characteristics of real gases as a function of flow enthalpy for various pressure ratios (temperature).

and a binary mixture of oxygen,



Again,

$$C_{\text{O}} + C_{\text{O}_2} = 1$$

$$h = C_{\text{O}} \int_0^T C_{p_{\text{O}}} dT + C_{\text{O}_2} \int_0^T C_{p_{\text{O}_2}} dT + C_{\text{O}} h_{\text{O}}^0 + C_{\text{O}_2} h_{\text{O}_2}^0 \quad (4.196)$$

Let, $C_{p_{\text{O}}} = C_{p_{\text{O}_2}} = \bar{C}_p = \text{const}$. Thus,

$$h = (C_{\text{O}} + C_{\text{O}_2}) \bar{C}_p T + C_{\text{O}} h_{\text{O}}^0 + (1 - C_{\text{O}}) h_{\text{O}_2}^0 \quad (4.197)$$

$$h = \bar{C}_p T + C_{\text{O}} (h_{\text{O}}^0 - h_{\text{O}_2}^0) + h_{\text{O}_2}^0 \quad (4.198)$$

But, $h_{\text{O}}^0 - h_{\text{O}_2}^0 = 5.1 \text{ eV} = \Delta h^0 = \text{dissociation energy}$ and $h_{\text{O}_2}^0$ is arbitrarily set equal zero. Hence,

$$h = \bar{C}_p T + C_{\text{O}} (\Delta h^0) \quad (4.199)$$

For an air mixture of 20% O₂ and 80% N₂,

$$5.1 \text{ eV} + \text{O}_2 \rightleftharpoons \text{O} + \text{O}, \quad C_{\text{O}} + C_{\text{O}_2} = 0.2$$

$$9.7 \text{ eV} + \text{N}_2 \rightleftharpoons \text{N} + \text{N}, \quad C_{\text{N}} + C_{\text{N}_2} = 0.8$$

The enthalpy is

$$h = \sum C_i h_i = \sum C_i \int_0^T C_{p_i} dT + \sum C_i h_i^0 \quad (4.200)$$

$$\begin{aligned} h = & (C_{\text{O}} C_{p_{\text{O}}} + C_{\text{O}_2} C_{p_{\text{O}_2}} + C_{\text{N}} C_{p_{\text{N}}} + C_{\text{N}_2} C_{p_{\text{N}_2}}) T \\ & + C_{\text{O}} h_{\text{O}}^0 + C_{\text{O}_2} h_{\text{O}_2}^0 + C_{\text{N}} h_{\text{N}}^0 + C_{\text{N}_2} h_{\text{N}_2}^0 \end{aligned} \quad (4.201)$$

where C_{p_i} is assumed constant for these elements. Therefore,

$$h = \bar{C}_p T + C_{\text{O}} \Delta h_{\text{O}}^0 + C_{\text{N}} \Delta h_{\text{N}}^0 + (0.2 h_{\text{O}_2}^0 + 0.8 h_{\text{N}_2}^0) \quad (4.202)$$

Thus,

$$h = \bar{C}_p T + C_{\text{O}} (5.1 \text{ eV}) + C_{\text{N}} (9.7 \text{ eV}) \quad (4.203)$$

Collision Process

The dissociation process will be examined more closely in this section. Heat must be added to the molecule to cause it to dissociate. Generally, this requires a collision with another molecule possessing sufficient energy to cause dissociation (5.1 eV for O₂). See Fig. 4.16. Hence, dissociation requires a two-body molecular collision with heat addition.

A collision can also involve recombination. Figure 4.17 shows two atomic oxygen particles colliding and recombining. An O₂ molecule will be formed containing a 5.1 eV excess of energy, absorbed from the two oxygen atoms. Since this is the amount of energy for dissociation, the O₂ molecule will again dissociate. Thus, a *two-body* collision will not result in recombination of any extent. A third body is required to carry off the excess energy of recombination (5.1 eV). See Fig. 4.18. Thus,

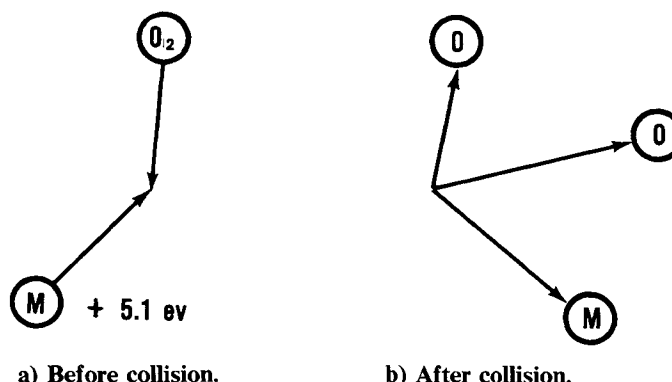
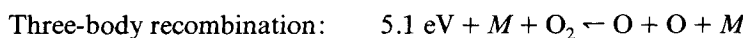
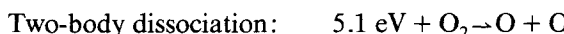


Fig. 4.16 Dissociation process.

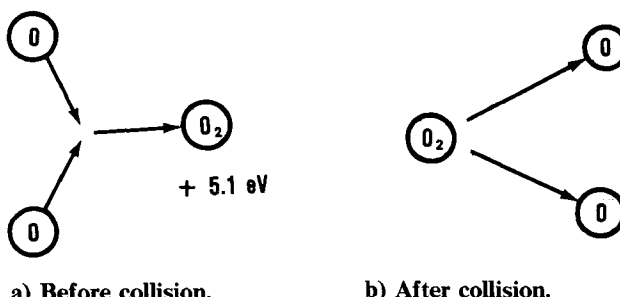


Fig. 4.17 Two-body collision involving recombination.

RE-ENTRY AERODYNAMICS

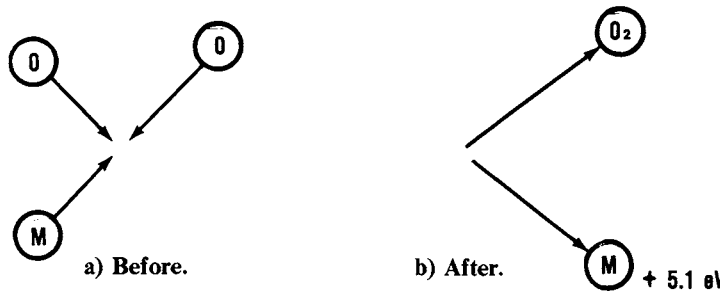


Fig. 4.18 Three-body recombination process.

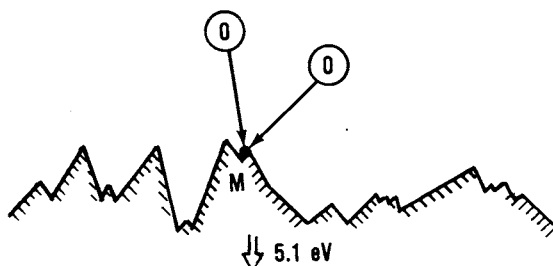


Fig. 4.19 Three-body collision on surface (wall molecular scale).

Obviously, recombination has a much lower probability of occurrence. The most likely location is at the wall where a third body is always present, as shown in Fig. 4.19. This recombination results in an additional form of heating to a surface over which high-temperature air is flowing. For example,

$$\text{Ideal-gas heating: } \dot{q} = k \left[\frac{\partial T}{\partial y} \right]_{\text{ideal}} \quad (4.204)$$

$$\text{Real-gas heating: } \dot{q} = k \left[\frac{\partial T}{\partial y} \right]_{\text{real}} + \sum \dot{m}_i \Delta h_i^0 \quad (4.205)$$

Conduction heat transfer Recombination heating

where

$$\dot{m}_i = \rho D \frac{\partial C_i}{\partial y} \quad (4.206)$$

which is Fick's law of diffusion.

Therefore,

$$\dot{q} = k \frac{\partial T}{\partial y} + \rho D \sum \frac{\partial C_i}{\partial y} \Delta h_i^0 \quad (4.207)$$

Replace the temperature with the enthalpy,

$$h = C_p T + \sum C_i \Delta h_i^0 \quad (4.208)$$

$$\frac{\partial h}{\partial y} = C_p \frac{\partial T}{\partial y} + \sum \frac{\partial C_i}{\partial y} \Delta h_i^0 \quad (4.209)$$

Therefore,

$$\dot{q} = \frac{k}{C_p} \frac{\partial h}{\partial y} + \frac{k}{C_p} \left[\frac{\rho D C_p}{k} - 1 \right] \sum_i \frac{\partial C_i}{\partial y} \Delta h_i^0 \quad (4.210)$$

where

$$\frac{k}{C_p} = \frac{\mu}{Pr} \sim \frac{\mu}{0.72} \quad (4.211)$$

$$\frac{\rho D C_p}{k} = Le \sim 1.4 \quad (4.212)$$

This heating rate equation is the only modification to the previously derived Navier-Stokes equations for an ideal gas. However, a species equation must also be added to the system to determine C_i ,

$$\frac{\partial C_i}{\partial t} + (C_i u)_x + (C_i v)_y = \dot{w}_i = \text{creation of species} \quad (4.213)$$

An interesting case occurs when $Le = 1$, as shown in the following:

$$\dot{q} = \frac{k}{C_p} \frac{\partial h}{\partial y} + \frac{\mu}{Pr} (Le - 1) \sum \frac{\partial C_i}{\partial y} \Delta h_i^0 \quad (4.214)$$

$$\dot{q}(Le = 1) = \frac{k}{C_p} \frac{\partial h}{\partial y} \quad (4.215)$$

Since $h \equiv (C_p T)_{\text{ideal}}$, then

$$\dot{q}(Le = 1) = k [\partial T / \partial y]_{\text{ideal}} \quad (4.216)$$

The fortuitous result occurs when $Le = 1$, in that the real-gas heating rate is *identical* to the ideal-gas heating rate. Since Le is near unity for air, little

difference between the calculations for ideal and real gases can be anticipated.

Chemical Kinetics

The reaction rates of the dissociation and recombination processes are important because the particles are in motion over the body. The residence time of the particle in the vicinity of the body compared to the time for the chemical reaction to occur is a key factor in real-gas phenomena.

The equation for the relaxation rate of molecular oxygen is determined by the difference between the amount of molecular oxygen dissociating into atomic oxygen through a two-body collision process and the amount of atomic oxygen recombining through a three-body process, i.e.,

$$\frac{d}{dt} C_{O_2} = -K_D C_{O_2} C_M + K_R C_O C_O C_M \quad (4.217)$$

Early in the reaction, the recombination is much less than the dissociation, i.e.,

$$\frac{dC_{O_2}}{C_{O_2} dt} \cong -K_D C_M \quad (4.218)$$

This equation can be integrated as

$$\ln C_{O_2}/(C_{O_2})_1 = -K_D C_M t \quad (4.219)$$

The half-life for this reaction is

$$\tau_{\frac{1}{2}} = -\frac{\ln \frac{1}{2}}{K_D C_M} = \text{relaxation time} \quad (4.220)$$

The residence time for the particle flowing over the body is

$$\Delta t = L/V \quad (4.221)$$

The ratio of this residence time to the relaxation time is an important parameter, as

$$\Delta t/\tau_{\frac{1}{2}} \gg 1 \quad \text{chemical equilibrium} \quad (4.222)$$

In this situation, the relaxation time is very rapid and the chemical reaction proceeds to its equilibrium value. Tables are available for this case.

The other extreme is

$$\Delta t/\tau_{\frac{1}{2}} \ll 1 \quad \text{chemically frozen} \quad (4.223)$$

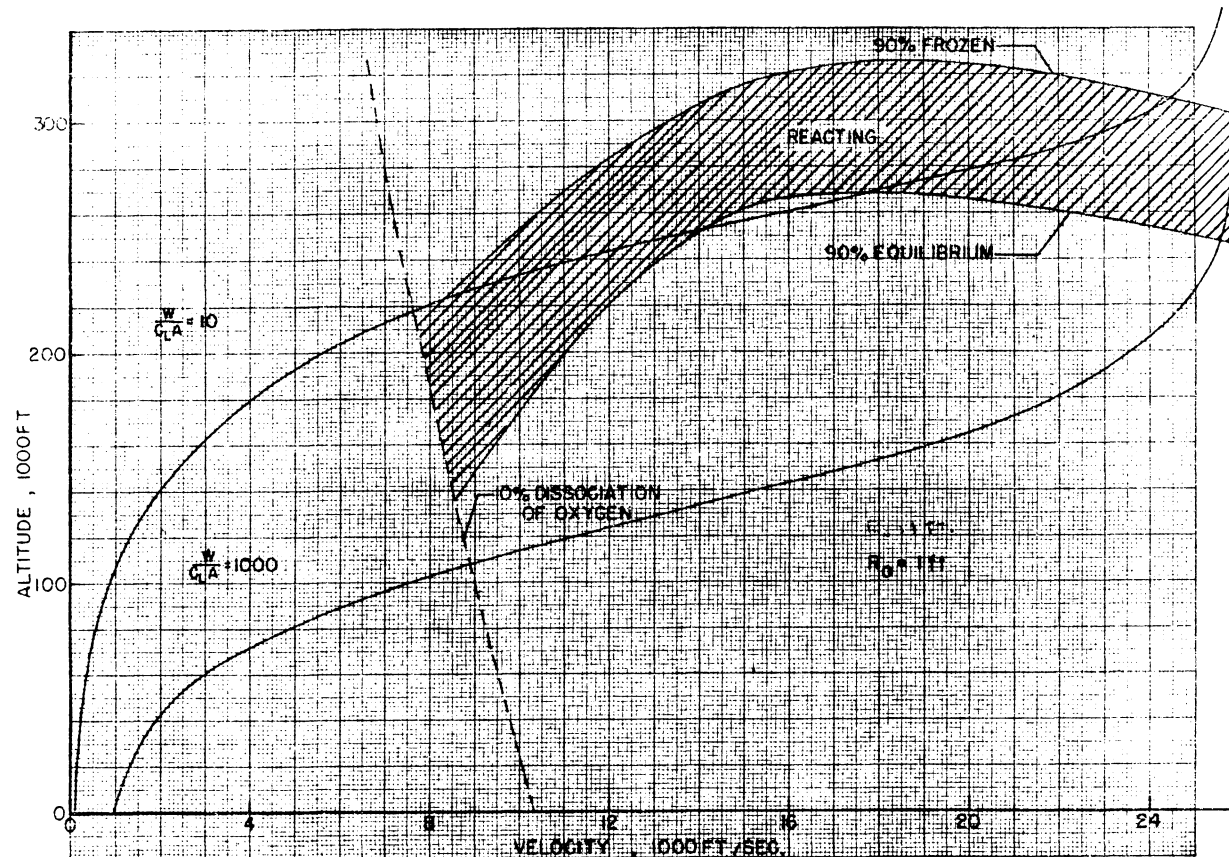


Fig. 4.20 Character of gas flow.

For this case, the particle moves rapidly compared to the relaxation time, so that no chemical reaction can occur. Therefore, C_i is a constant and perfect-gas relations can be used from the frozen point throughout the downstream stations.

Figure 4.20 is a chart made of the flow near the stagnation point to identify the chemical domains of interest. As noted, most of the stagnation region will be in the equilibrium range, with only a small portion in the reacting range.

In the next section, the stagnation point heating rate will be computed for both the equilibrium and chemically frozen limits.

4.5 FAY-RIDDELL SOLUTION

The equation derived for stagnation heating in an ideal gas is

$$\dot{q}_s = \left[\frac{S'(0)}{-S(0)} \right] \sqrt{(1 + K) \rho_s \mu_s \frac{du_e}{dx}} (H_e - H_w) \quad (4.224)$$

in which $Pr = 1$, $Cw = 1$, and $Le = 1$ are assumed.

Fay and Riddell⁶ conducted a more thorough analysis including the effects of Pr , Cw , and Le variations. They obtained very simple corrections to Eq. (4.224) to account for these variations. The final result is

$$\begin{aligned} \dot{q}_s = & \left[\frac{S'(0)}{-S(0)} \right] \sqrt{(1 + K) \rho_s \mu_s \frac{du_e}{dx}} (H_e - H_w) \\ & \times \frac{Cw^{0.1}}{Pr^{0.6}} \left[1 + (Le^a - 1) \sum C_i \frac{\Delta h_i^0}{H_e} \right] \end{aligned} \quad (4.225)$$

where

$$a = 0.52 \quad \text{equilibrium,}$$

$$= 0.63 \quad \text{frozen}$$

$$\frac{S'(0)}{-S(0)} = 0.570, \quad S(0) = 0, \quad \beta = 1$$

$$\frac{S'(0)}{-S(0)} = 0.494, \quad S(0) = -1, \quad \beta = \frac{1}{2}$$

An appreciation for the magnitude of the real-gas corrections can be obtained as follows:

$$\text{Equilibrium: } 1 + (Le^a - 1) \frac{H_D}{H_e} = 1 + (1.4^{0.52} - 1)0.5 = 1.095$$

$$\text{Frozen: } 1 + (Le^a - 1) \frac{H_D}{H_e} = 1 + (1.4^{0.63} - 1)0.5 = 1.118$$

$$Cw^{0.1} = 5^{0.1} = 1.175, \quad Pr^{0.6} = 0.72^{0.6} = 0.821$$

A difference of only 2% (for the most extreme case) between the equilibrium and frozen situations is observed. Thus, the effects of real gas are minimal.

One situation where the real-gas effects can be appreciable, however, is with the noncatalytic wall influence. For recombination heating at the surface, the wall is assumed to be catalytic. If the surface turns out to be *noncatalytic*, then recombination will not occur on the surface. Thus, a dramatic reduction in heating will result. Information is lacking in this area, but a catalytic surface is a more probable and safer assumption. Recall that in Eq. (4.205),

For N₂ dissociation in air, half of the heat transfer is from recombination heating. This term would be eliminated if the surface is noncatalytic. (Space Shuttle data indicate the possibility of a noncatalytic wall effect reducing lower surface peak heating by about 40%. More information is necessary to substantiate this observation.)

4.6 INTERFERENCE HEATING

The most feared form of heating encountered during re-entry is that experienced in a shock-wave/boundary-layer interaction. In such an interaction, the heating rate can suddenly jump an order of magnitude. One such case was encountered by the X-15. A dummy ramjet model was attached to the lower surface of the X-15 to evaluate the flying qualities prior to installing the actual ramjet. The shock wave from the ramjet inlet impinged upon its own support pylon causing a "burn-through." The ramjet detached from the pylon and crashed to Earth, fortunately without serious damage to the X-15. This was a classic lesson to the technologists on interference heating.

In this section, the major features of shock/boundary interaction will be discussed, along with the cause of interference heating.

Separation and Reattachment of the Boundary Layer

The basis for understanding interference heating is involved in the process of the boundary layer. This can best be demonstrated by reviewing the entire class of similar laminar boundary layers. For boundary-layer flows in which

$$u_e = cx^m \quad (4.226)$$

exact solutions are possible (see Fig. 4.21).

A plot of $F_n(0)$ vs β is representative of τ_w vs $-dp/dx$ (Fig. 4.22). At $dp/dx = 0$, the classic Blasius solution exists. For a favorable pressure

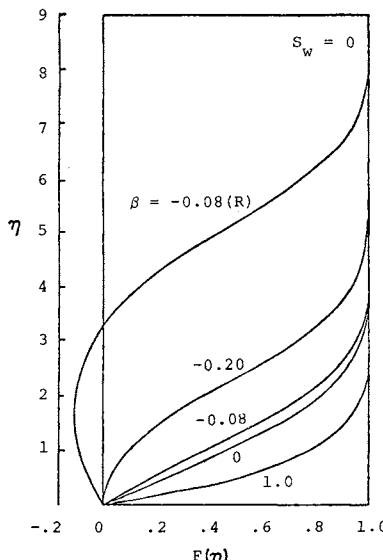


Fig. 4.21 Similar velocity profiles.

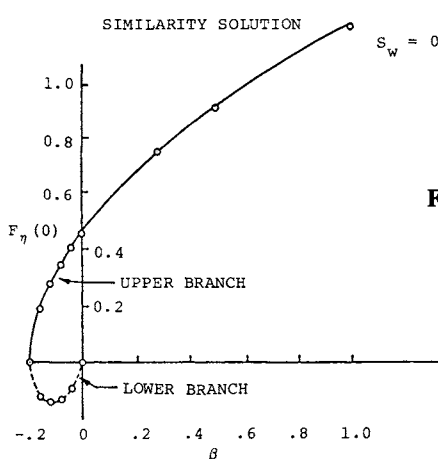


Fig. 4.22 Wall shear vs β for similar flow.

gradient ($d p / dx < 0$), no separation occurs. For an adverse pressure gradient, there are two solutions, i.e., the upper and lower branches. The lower branch has reversed flow profiles. No solutions are possible for β values below a minimum value of $\beta = -0.2$. Incipient separation occurs at this minimum value.

The next step is to examine the inviscid flowfield. The inviscid flow solution produces $u_e(x)$ or β and drives the boundary-layer solution. As an example, consider the incompressible inviscid flow over a cylinder. The solution for the stream function is

$$\Psi = u_\infty \left(r - \frac{a^2}{r} \right) \sin \theta \quad (4.227)$$

from which the velocity on the surface may be computed,

$$u_e = \left(\frac{\partial \Psi}{\partial r} \right)_{r=a} = 2u_\infty \sin \theta \quad (4.228)$$

where $x = a\theta$. One may now compute the local value of β ,

$$\beta = \frac{2\xi u_{e\xi}}{u_e}, \quad \xi = \rho \mu \int u_e dx \quad (4.229)$$

or

$$\beta = \frac{2 \cos \theta (1 - \cos \theta)}{\sin^2 \theta} \quad (4.230)$$

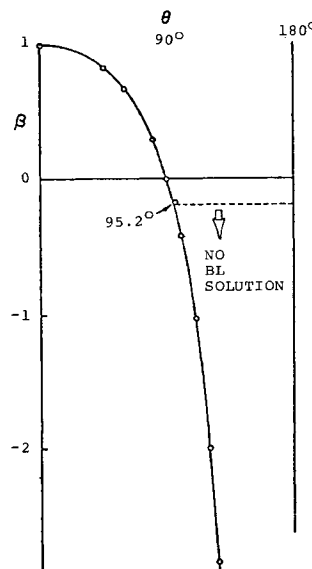
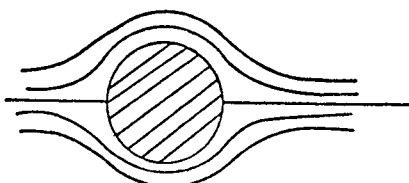
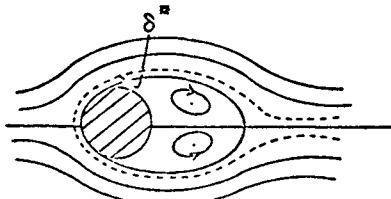


Fig. 4.23 Local β distribution over a cylinder.



a) Inviscid body.



b) Effective viscous body.

Fig. 4.24 Streamline pattern over a cylinder.

This value of β is plotted as a function of θ in Fig. 4.23. Note that for $\theta > 95.2$ deg, $\beta < -0.20$ no boundary-layer solutions are possible. Therefore, an incompatibility exists between the inviscid and viscous solutions. In nature, these flows "interact" to eventually find a mutual solution.

The effective shape of the inviscid body must be modified by the boundary-layer thickness δ^* , so that the new pressure distribution *avoids* large negative β values (Fig. 4.24). Conceptually, one could iterate the body shape until a compatible inviscid solution exists with the boundary layer. However, for large interactions, this is seldom practical. Simultaneous solution of the inviscid and viscous fields is preferred. Either an interacting boundary-layer program coupled with an inviscid routine or a complete Navier-Stokes code may be used.

An example of shock-wave/boundary-layer interaction is a flat plate with a after-body wedge in supersonic flow. The inviscid pressure distribution is a step function with the freestream value existing on the plate and the oblique shock value on the wedge (Fig. 4.25). The discontinuous pressure gradient parameter β is zero on the plate and wedge, but is negative infinity at the corner junction. Experiments indicate that the flow separates under this extreme situation and modifies the adverse pressure gradient to bring β within an acceptable range for the boundary layer. The experiment shows that a pressure plateau exists at the corner and that an inflection point in the pressure distribution occurs at both the separation and reattachment points. Therefore, the pressure gradient attains a local maximum at both separation and reattachment with a corresponding local minimum occurring in β . The interpretation of this result is that the boundary layer, originating from Blasius flow, progresses from the upper branch solution to the lower branch at the first minimum β location (separation) and returns to the upper branch solution at the second minimum β value (reattachment). See Fig. 4.25.

RE-ENTRY HEATING

129

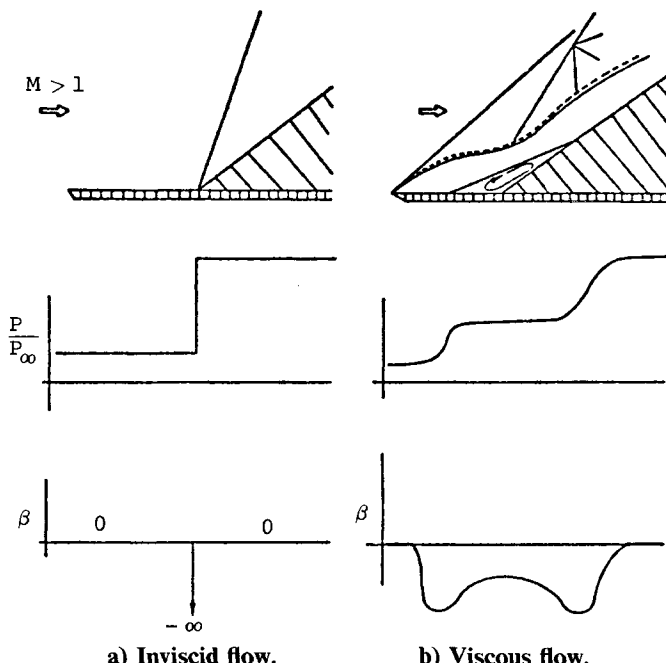


Fig. 4.25 Supersonic interaction on a compression ramp.

Let us examine the flowfield over the corner for this case. A separation bubble with a dividing streamline will connect the separation and reattachment points. Inside this region, streamlines will be closed and, hence, fluid will be trapped. (Unsteady or three-dimensional effects will fill and purge this bubble, but in the mean it can be considered a "dead water" region.) The outer edge of the boundary layer will turn gradually at both the separation and reattachment points, creating a series of weak shocks that coalesce into a lambda shock. The overall strength will produce a pressure equal to the inviscid single oblique shock value. Along the edge of the boundary layer, the flow can be considered isentropic. A streamline passing through the oblique shock will not be isentropic, nor will the lower streamlines in the boundary layer. All of the streamlines will eventually attain the same oblique shock pressure level, however. This is an essential point in the analysis.

Compute the heat transfer in this shock/boundary-layer interaction region,

$$\dot{q} = St \rho_e u_e (H_e - H_w) \quad (4.231)$$

The usual method is to compare this heating rate to a *reference* level from a location outside of the interaction region. By dividing these two heating

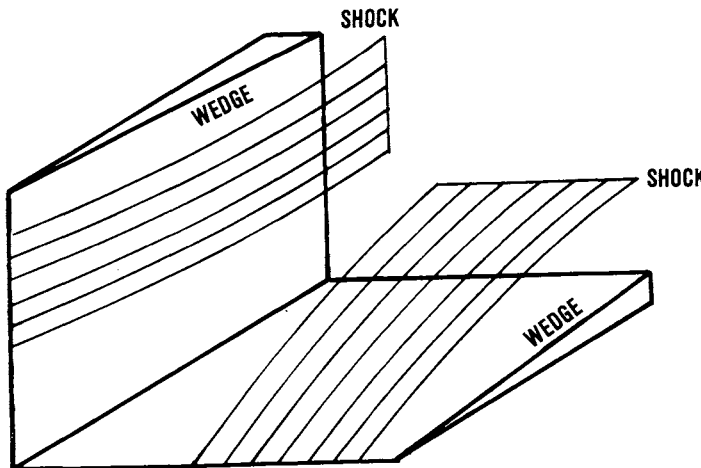


Fig. 4.26 Three-dimensional interaction: an axial corner produced by the interaction of two wedges.

rates, we obtain

$$\frac{\dot{q}}{\dot{q}_{\text{ref}}} = \frac{St \rho_e u_e (H_e - H_w)}{(St)_{\text{ref}} (\rho u)_{\text{ref}} (H_e - H_w)} \cong \frac{\rho_e u_e}{(\rho u)_{\text{ref}}} \quad (4.232)$$

where the St number is assumed to differ only slightly between the two stations.

Recall that isentropic flow was presumed for the edge quantities. Therefore,

$$\frac{\rho_e}{\rho_{\text{ref}}} = \left(\frac{P_e}{P_{\text{ref}}} \right)^{1/\gamma} \quad (4.233)$$

$$\frac{u_e^2}{2} + h_e = \frac{u_{\text{ref}}^2}{2} + h_{\text{ref}} \quad (4.234)$$

or

$$\frac{u_e}{u_{\text{ref}}} = \sqrt{1 - \frac{2}{(\gamma - 1) M_{\text{ref}}^2} \left[\left(\frac{P_e}{P_{\text{ref}}} \right)^{(\gamma-1)/\gamma} - 1 \right]} \approx 1 \quad (4.235)$$

Hence,

$$\frac{\dot{q}}{\dot{q}_{\text{ref}}} \cong \left(\frac{P_e}{P_{\text{ref}}} \right)^{1/\gamma} = \left(\frac{P_e}{P_{\text{ref}}} \right)^{0.71} \quad (4.236)$$

This is a simple approximation of a very complex phenomenon. Correlations have been accomplished between the peak heating ratio and the pressure ratio to improve the value of the exponent. For turbulent flow, good correlation with an exponent of 0.8 has been obtained. Greater variation has been observed for laminar flow.¹

Consider a Mach number of 14.5 over a flat plate with an 18 deg wedge. The pressure ratio for this case is 36, based upon an oblique shock calculation. The corresponding heat transfer ratio for this case is

$$\dot{q}/\dot{q}_{\text{ref}} = (36)^{1/\gamma} = 13 \quad (4.237)$$

This prediction is in good agreement with the data of Ref. 7, which shows a heating ratio of 12 (see Figs. 105 and 106 of that reference). The peak heating occurs at the reattachment point where the boundary layer is the thinnest and the isentropic pressure recovery is appropriate. Farther downstream, the heat-transfer level decays.

Three-Dimensional Interaction

The previous example of interference heating on a wedge was for a two-dimensional interaction. Greater complexity arises in a three-dimensional interaction. The shock-wave/boundary-layer interaction will be examined for the axial corner region produced by the intersection of two wedges. See Fig. 4.26.

The two shock waves generated by these wedges cannot intersect directly at right angles because the flow alignment would be incompatible along the axis of symmetry. An additional conical shock wave forms in the plane of symmetry, creating two *triple points* at the shock intersections. See Fig. 4.27. The extended shock from the triple point strikes the surface and forms a three-dimensional shock/boundary-layer interaction. A conical-shaped separation region occurs beneath the shock wave scavenging the boundary layer from the surface (Fig. 4.28). Note that no closed streamlines exist in the three-dimensional case, due to the fact that the separation region is

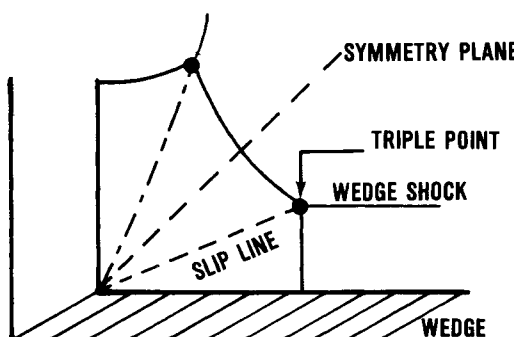


Fig. 4.27 Cross section of the conical flowfield in a three-dimensional corner (the wedge).

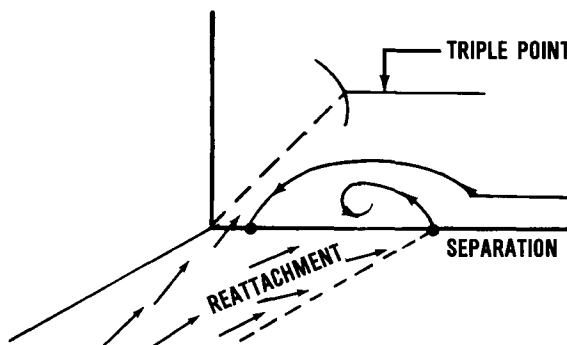


Fig. 4.28 Conical flowfield in a three-dimensional corner: conical-shaped separation region occurs beneath the shock wave.

continually fed by boundary-layer fluid. The reattaching streamlines are of high energy and total pressure and, therefore, create high heating.

Again, the power law relationship is used to estimate heat transfer from the pressure ratio,

$$\frac{\dot{q}}{\dot{q}_{\text{ref}}} = \left(\frac{P}{P_{\text{ref}}} \right)^{1/\gamma} \quad (4.238)$$

Navier-Stokes calculations of the interaction can be accomplished to obtain the complete heat-transfer and pressure distribution when required for development projects.

4.7 ABLATION

Consider the physical process of a surface ablating under a severe heat load, such as shown in Fig. 4.29. The surface will absorb heat, combust, char, melt, sublime, and radiate while undergoing a phase change. These effects can be evaluated by a static test under laboratory conditions.

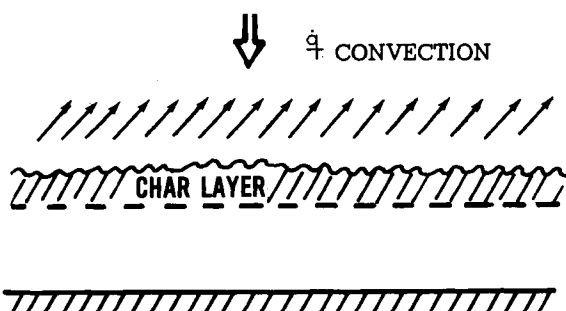


Fig. 4.29 Ablating surface under a severe heat load.

However, in a dynamic case, with hot air rushing over the surface, an additional phenomenon occurs. When a solid material undergoes a phase change and becomes a gas, a large increase in the volume of this material occurs. The outgassing of this substance at a colder temperature (3000°R) than the total temperature of the air ($20,000^{\circ}\text{R}$) creates a cooling film over the surface. This "blockage" influence is a major factor in the effectiveness of the ablator. The blockage factor can be several times larger than the phase change heat-absorbing capability of the material.

The total heat-absorbing effectiveness is called Q^* (see Fig. 4.30).

To determine the amount of material ablated, a heat energy balance is performed,

$$\text{Heat input} = \text{heat absorbed}$$

$$\dot{Q}_{\text{in}} = Q^* \dot{m} \quad (4.239)$$

or

$$\dot{q}A = Q^* \rho_m A \dot{b} \quad (4.240)$$

Rearranging

$$\dot{b} = \dot{q}/\rho_m Q^* \quad (4.241)$$

This simple relationship can be used to estimate the amount of ablation material required during re-entry.

4.8 HOT-GAS RADIATION

In addition to the convective heat input to the vehicle, another source of heat transmission exists in the form of hot-gas radiation. During re-entry, the temperature of the gas after the shock in the stagnation region may reach temperatures as high as $10,000^{\circ}\text{R}$. The black-body radiation from

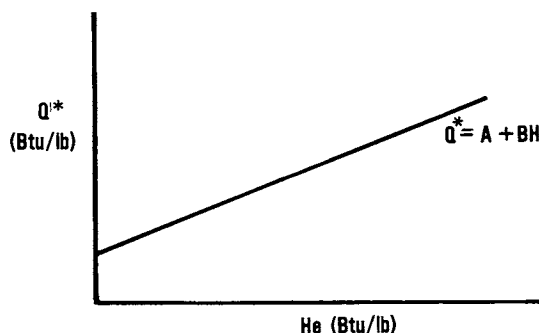


Fig. 4.30 Total heat-absorbing effectiveness Q (fiberglass, 1500°F , $A = 3000$ Btu/lb, $B = 0.5$).

such a source is of the order of 5000 Btu/ft²/s, which is much greater than that from convective heating. The emissivity of the gas at high altitudes is quite low (10^{-4}), however, so the gas radiative heating is also still low. Reference 2 presents a semiempirical curve for the Avco emissivity data. The resulting empirical equation is

$$\dot{q} = 7.5 R_0 \sigma^{1.5} \left(\frac{V_\infty}{10,000} \right)^{12.5} \quad (4.242)$$

More precise values of the hot-gas radiation may be obtained by using the Avco emissivity data directly rather than an empirical fit. Kivel and Bailey⁸ indicate that the emissivity is proportional to the gas thickness, which, for the stagnation point, becomes the shock detachment distance. Chester⁹ presents the following equations for the detachment distance:

$$\text{Cylinder: } \frac{\Delta}{R_{sh}} = \frac{1}{2} \varepsilon \ell n \frac{4}{3\varepsilon} + \frac{1}{4} \varepsilon^2 \ell n \frac{4}{3\varepsilon} - \frac{3}{8} \varepsilon^2 - \frac{\varepsilon}{M_\infty^2} \quad (4.243)$$

$$\text{Sphere: } \frac{\Delta}{R_{sh}} = \varepsilon - 1.633\varepsilon^{1.5} + 2.667\varepsilon^2 \quad (4.244)$$

where

$$\varepsilon = \rho_\infty / \rho_s \quad (4.245)$$

is the density ratio across the normal shock.

By using the normal shock, real-gas properties obtained in Fig. 4.31 together with the appropriate detachment distance for a sphere, the gas radiation may be determined as a function of velocity and altitude (Fig. 4.32). This figure shows that the hot-gas radiation in the region of interest for the glide-type vehicle is small compared with the convective heating; however, it may not necessarily be negligible. Particularly, large blunt bodies used at extremes of the glide parameter will cause an increase in radiation heating, although for normal aerodynamic re-entry the increase is less than 1 Btu/ft²/s.

Although hot-gas radiation was shown to be negligible for glide re-entry, for ballistic re-entry it becomes a more important factor. The hot-gas radiation rates from Fig. 4.32 are plotted on an altitude vs velocity graph in which lines of equal magnitude of turbulent convective and gas radiation are shown for radii of 1 and 10 ft in Fig. 4.33. The effect of hot-gas radiation on the entry of vehicles with high ballistic coefficients is readily apparent.

Distribution of this radiation about the nose of a hypervelocity vehicle is a strong function of the temperature ($T^{12.5}$ according to Ref. 2). The following equation is an approximation of this distribution:

$$\left(\frac{\dot{q}_\theta}{\dot{q}_s} \right)_{rad} = \frac{\Delta \delta}{\Delta} \left(\frac{\rho_\delta}{\rho_s} \right)^{1.5} \left(\frac{T_\delta}{T_s} \right)^{12.5} \quad (4.246)$$

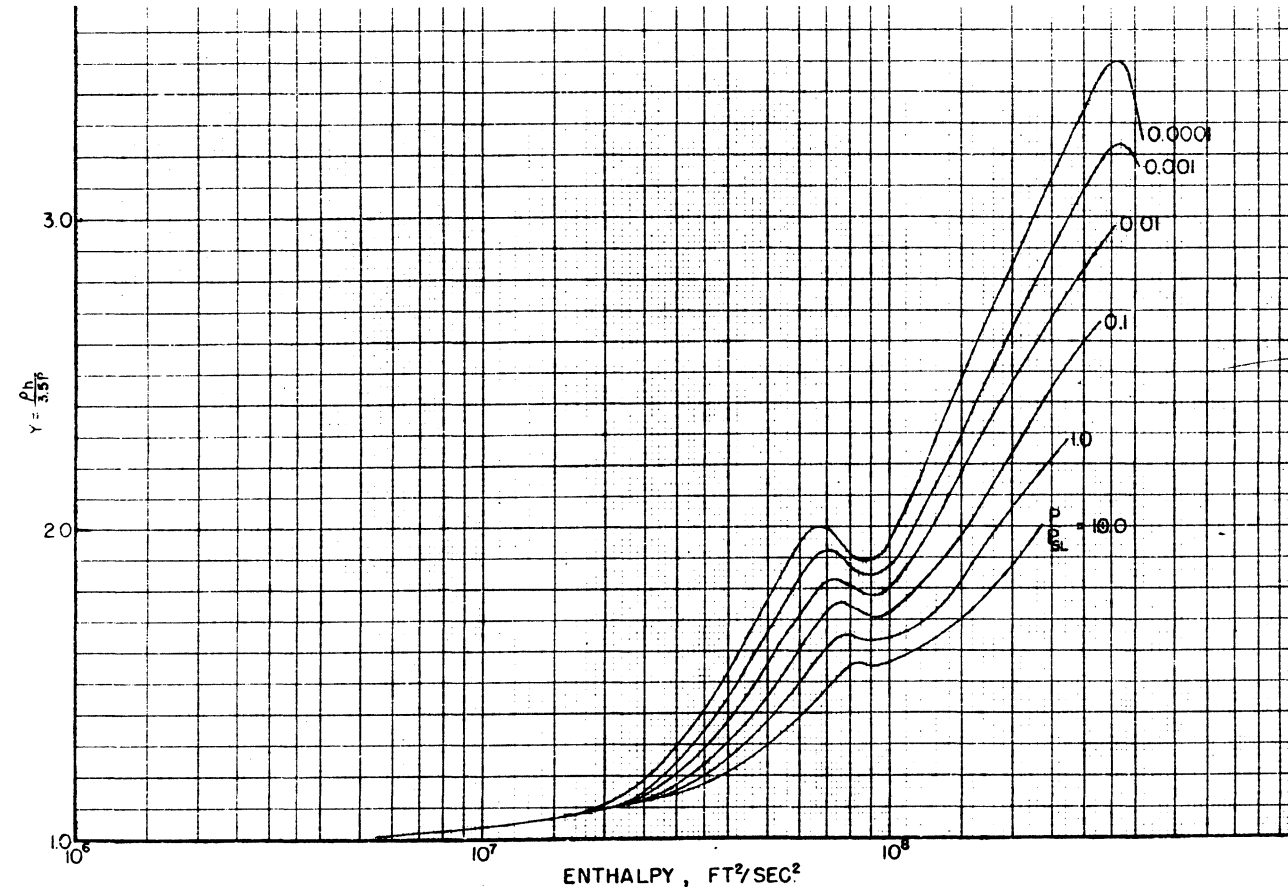


Fig. 4.31 Real-gas properties.

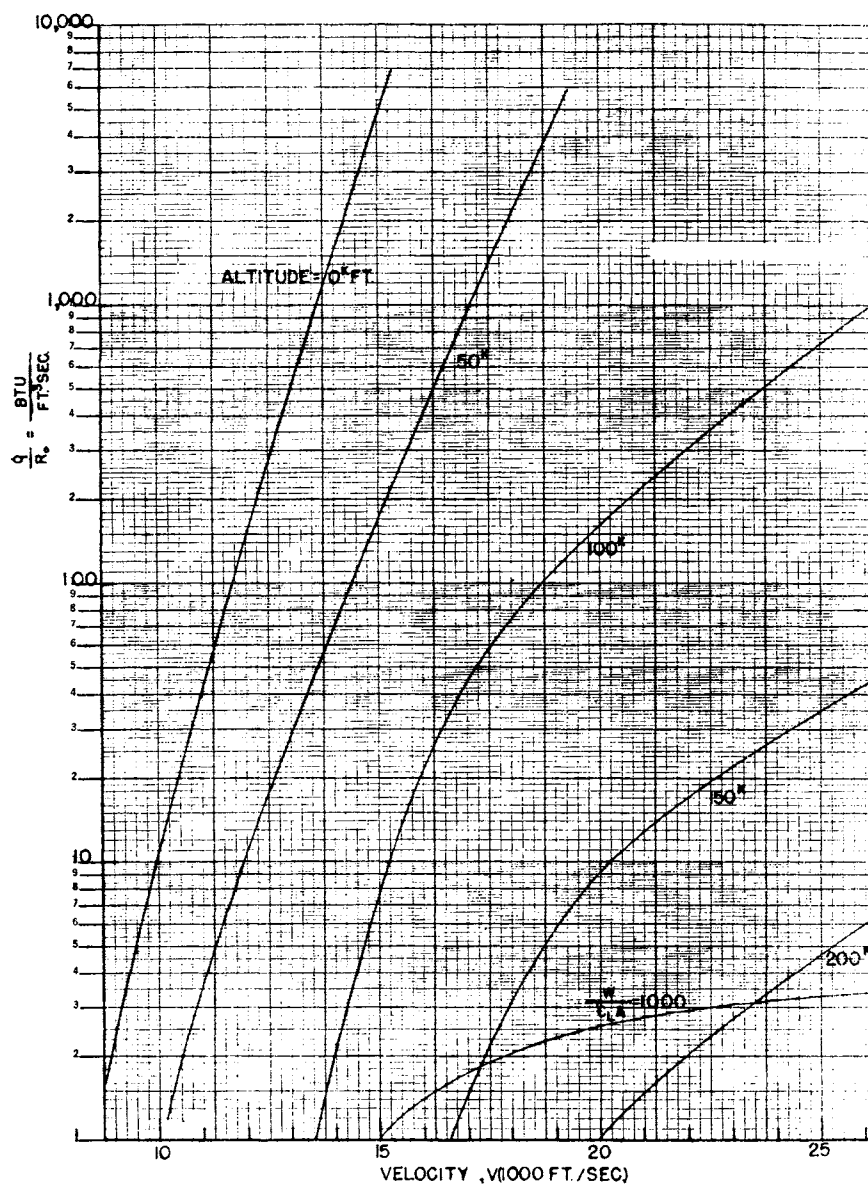


Fig. 4.32 Equilibrium stagnation point of hot-gas radiation for a flight spectrum.

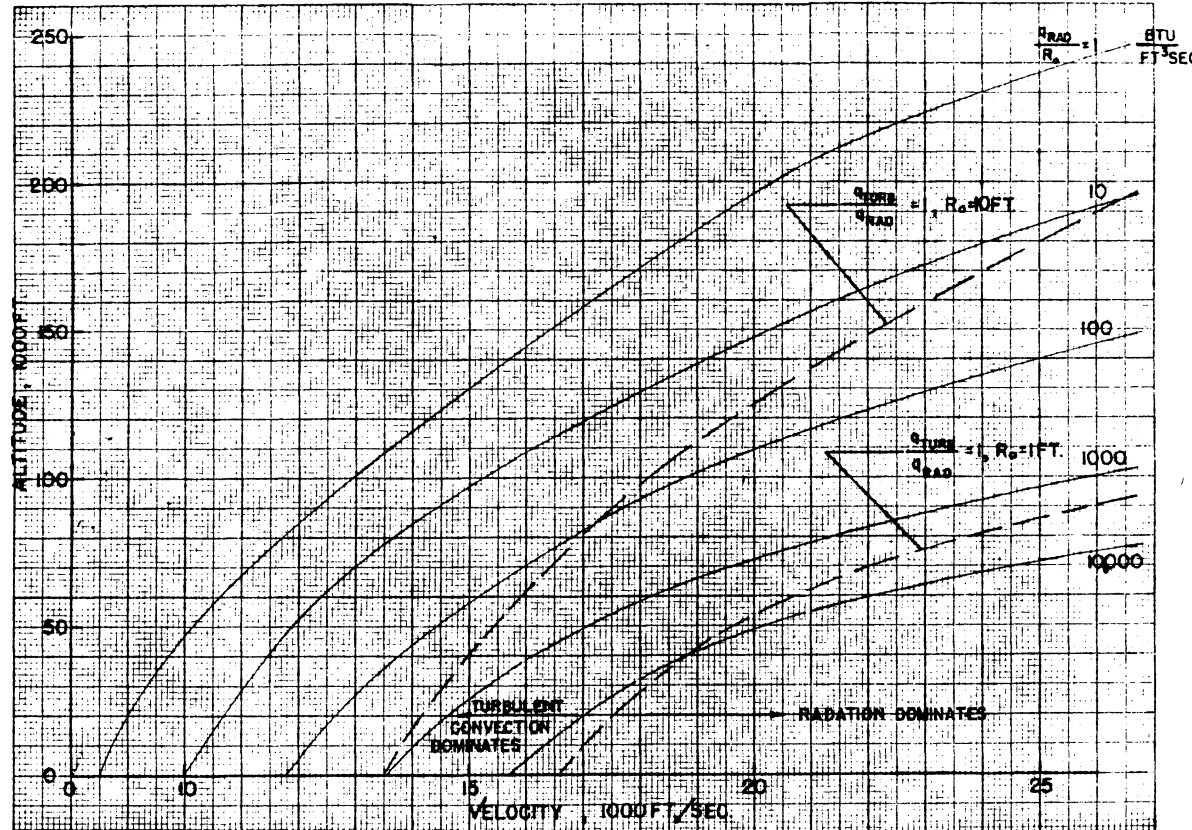


Fig. 4.33 Effect of hot-gas radiation on total heating at the stagnation point for ballistic re-entry.

Using the gas property approximation [Eq. (4.242)] and an empirical fit for the shock thickness, an equation for the distribution as a function of the angular position results,

$$\left(\frac{\dot{q}_\theta}{\dot{q}_s}\right)_{\text{rad}} = (1 + 2.0\theta^{2.3}) \cos^3\theta (1 - \beta^2\theta^2)^{11} \quad (4.247)$$

where

$$\Delta\delta/\Delta = 1 + 2.0\theta^{2.3} = \text{empirical fit} \quad (4.248)$$

$$\beta = \sqrt{(\gamma - 1)/\gamma} = 0.408 \text{ for } \gamma = 1.2 \quad (4.249)$$

$$\theta = \text{polar angle, rad}$$

The radiation drops to 44% of the stagnation point value at the location of the peak turbulent heating ($\theta = 35$ deg). To determine the critical heating point on the nose, the sum of the turbulent convective and $0.44\dot{q}_{\text{rad}}$ must be compared with the stagnation point radiation \dot{q}_{rad} in the flight region where radiation becomes important.

4.9 COMBINED FORMS OF HEATING

In a practical heating problem, all forms of heating are generally present, i.e., conduction, convection, and radiation. In the previous sections, these were examined separately. Now we shall indicate the procedure for solving problems with combined forms of heating. The only practical way to accomplish this is by numerical techniques. A standard procedure employed in industry is the "lumped parameter" method. The structure is decomposed into a number of elements with lumped averaged properties and finite differences are used to solve the heat energy equation. A statement of the heat energy balance is

$$\text{Heat input} = \text{change in internal energy}$$

$$\dot{Q}_{\text{in}} = \oint \dot{q} \cdot dA = \frac{\partial}{\partial t} \int \int \int \rho C_v T dV \quad (4.250)$$

where

$$\dot{q} = \dot{q}_{\text{conduction}} + \dot{q}_{\text{convection}} + \dot{q}_{\text{radiation}} \quad (4.251)$$

The flow of heat in a rod demonstrates the finite-difference procedure, (Fig. 4.34)

$$\dot{q} = k \nabla T = k \frac{\partial T}{\partial x} \quad \text{conduction only} \quad (4.252)$$

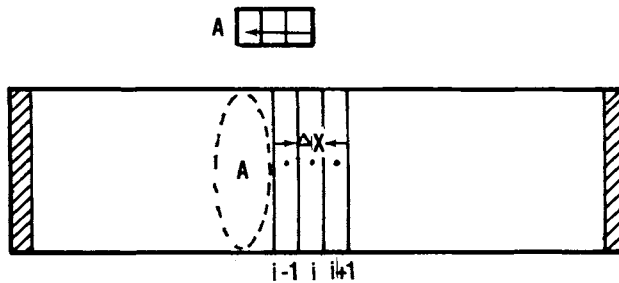


Fig. 4.34 Finite-difference elements for computation of heat flow in a rod.

$$\dot{Q}_{\text{in}} = \left(Ak \frac{\partial T}{\partial x} \right)_{i+1} + \left(Ak \frac{\partial T}{\partial x} \right)_{i-1} = \left(\rho C_v V \frac{\partial T}{\partial t} \right)_i \quad (4.253)$$

$$\dot{Q}_{\text{in}} = Ak \frac{(T_{i+1}^n - T_i^n)}{\Delta x} + Ak \frac{(T_{i-1}^n - T_i^n)}{\Delta x} = \rho C_v A \Delta x \frac{(T_i^{n+1} - T_i^n)}{\Delta t} \quad (4.254)$$

or

$$T_i^{n+1} = T_i^n + d(T_{i+1}^n - 2T_i^n + T_{i-1}^n) \quad (4.255)$$

where

$$d = \frac{\alpha \Delta t}{\Delta x^2}, \quad \alpha = \frac{k}{\rho C_v} = \text{thermal diffusivity} \quad (4.256)$$

and d is the numerical diffusion number. A series of these equations may be written for each grid point along the rod. Starting with an arbitrary initial temperature distribution and end point boundary conditions, these equations are marched in time to solve for the temperature distribution history.

Numerical Stability

One word of caution at this point. It might appear in the above analysis that the grid size of the element Δx and the time step Δt are completely arbitrary, depending upon the resolution accuracy desired. This is not the case in that numerical difficulties may be encountered in finite-difference schemes if certain time-step limits are exceeded. To examine this feature, a stability analysis should be performed. A common method, credited to Von Neumann, uses a Fourier analysis of small temperature perturbations. Let

$$T(x, t) = \hat{T}(t) e^{i\beta x} \quad (4.257)$$

Inserting this representation into the finite-difference equation produces

$$\hat{T}^{n+1} e^{i\beta x} = \hat{T}^n e^{i\beta x} + d [\hat{T}^n e^{i\beta(x+\Delta x)} - 2\hat{T}^n e^{i\beta x} + \hat{T}^n e^{i\beta(x-\Delta x)}] \quad (4.258)$$

or

$$\frac{\hat{T}^{n+1}}{\hat{T}^n} \equiv G = 1 + d(e^{i\beta\Delta x} - 2 + e^{-i\beta\Delta x}) \quad (4.259)$$

or

$$G = 1 - 2d(1 - \cos \beta \Delta x) \quad (4.260)$$

For stability of the numerical difference scheme, $|G| < 1$.

This must be true for any wavenumber β or phase angle $\beta \Delta x$. The extreme limitation occurs when $\cos \beta \Delta x = -1$. Hence,

$$|1 - 4d| < 1$$

or

$$d < \frac{1}{2} \quad (4.261)$$

The stability condition produces a limit in step size of

$$\Delta t < \frac{\Delta x^2}{2\alpha}, \quad \alpha = \frac{k}{\rho C_v} \quad (4.262)$$

Therefore, a maximum allowable time step must be honored for stability. An improved differencing scheme, entitled the Crank-Nicolson method, eliminates this stability restriction while maintaining accuracy and is recommended for this application.

General Case

A more general case is one in which combined forms of heating occur for an arbitrary geometry. See Fig. 4.35.

The energy balance equation for a single element is

$$\dot{Q}_{in} = \sum \dot{q}A = \rho C_v V \frac{\partial T}{\partial t} \quad (4.263)$$

For element i, j five different heat-transfer rates must be included,

$$\begin{aligned} \dot{Q}_{in} = & \Delta x \dot{q}_{conv} - \Delta x \dot{q}_{rad} + \Delta y k \frac{(T_{i+1,j}^n - T_{i,j}^n)}{\Delta x} \\ & + \Delta y k \frac{(T_{i-1,j}^n - T_{i,j}^n)}{\Delta x} + \Delta x k \frac{(T_{i,j-1}^n - T_{i,j}^n)}{\Delta y} \end{aligned} \quad (4.264)$$

RE-ENTRY HEATING

141

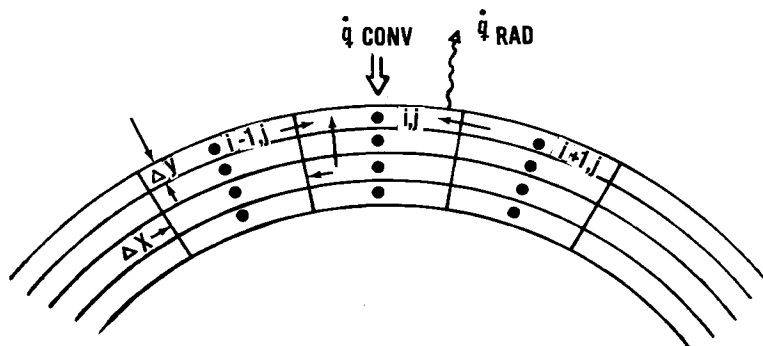


Fig. 4.35 Finite-difference grid for heat flow analysis.

$$\dot{Q}_{\text{in}} = \rho C_v \Delta x \Delta y \frac{(T_{i,j}^{n+1} - T_{i,j}^n)}{\Delta t} \quad (4.265)$$

Solving for the new temperature level,

$$\begin{aligned} T_{i,j}^{n+1} &= T_{i,j}^n + \frac{\alpha \Delta t}{\Delta x^2} (T_{i+1,j}^n - 2T_{i,j}^n + T_{i-1,j}^n) \\ &+ \frac{\alpha \Delta t}{\Delta y^2} (T_{i,j-1}^n - T_{i,j}^n) + \frac{\alpha \Delta t h_{i,j}}{\Delta y k} [T_{g_{i,j}}^n - T_{i,j}^n] + \frac{\alpha \Delta t \varepsilon \sigma}{\Delta y k} (T_R^4 - T_{i,j}^4) \end{aligned} \quad (4.266)$$

where

$$\dot{q}_{\text{conv}} = h(T_g - T_w) \text{ and } \dot{q}_{\text{rad}} = \varepsilon \sigma (T_w^4 - T_R^4) \quad (4.267)$$

Given an initial temperature distribution, the temperature history of all elements in the structure can be established by this numerical procedure.

References

¹Hankey, W., Neumann, R., and Flinn, E., "Design Procedures for Computing Aerodynamic Heating at Hypersonic Speeds," WADC TR-59-610, June 1960.

²Lees, L., "Laminar Heat Transfer Over Blunt Bodies at Hypersonic Speeds," *Jet Propulsion*, April 1956.

³Schlichting, H., *Boundary Layer Theory*, McGraw-Hill, New York, 1960.

⁴Christian, J., Hankey, W., and Petty, J., "Similar Solutions of the Attached and Separated Compressible Laminar Boundary Layer with Heat Transfer and Pressure Gradient," ARL 70-0023, Feb. 1970.

⁵Dorrance, W., *Viscous Hypersonic Flow*, McGraw-Hill, New York, 1962.

⁶Fay, J. and Riddell, F., "Theory of Stagnation Point Heat Transfer in Dissociated Air," *Journal of the Aeronautical Sciences*, Feb. 1958.

⁷Hankey, W. and Holden, M., "Two Dimensional Shock Wave Boundary Layer Interactions in High Speed Flows," AGARDograph 203, June 1975.

⁸Kivel, B. and Bailey, K., *Tables of Radiation for High Temperature Air*, AVCO Research Rept. 21, Dec. 1957.

⁹Chester, W., "Supersonic Flow Past a Bluff Body with a Detached Shock," *Journal of Fluid Mechanics*, Vol. 1, 1956.

Problems

- 4.1** Compute the laminar and turbulent peak heating in the stagnation region for the following conditions: $R = 1$ ft, $x = 0.8$ ft, altitude = 200,000 ft, and $M_\infty = 20$.
- 4.2** Determine the heating rate for the conditions of Problem 4.1 for a 70 deg swept leading edge at a 30 deg angle of attack.
- 4.3** Determine the ratio of two heating rates at the same flight conditions as Problem 4.1, but one with an H_w/H_{S_e} of 0.1 while the other is at 0.9.
- 4.4** Determine the temperature for both chemically frozen and chemical equilibrium air at the stagnation point for $M_\infty = 20$ at 200,000 ft altitude.
- 4.5** Determine the ratio of the hot-gas radiation and convection heating for a 1 ft radius sphere at $M_\infty = 20$ and 100,000 ft altitude.

Index

- Ablation, 6, 132
Accommodation coefficient, 19
Aerodynamic characteristics, 70
Aerothermochemistry, 111
Allen, H., 22
Angle of attack, 87, 90
Atmosphere, 9
 air properties, 9
Axial corner, 130

Binary mixture, 112
Boundary conditions, 60, 61, 95
Boundary layer, 58, 93, 98

Chapman, D., 49
Chemical equilibrium, 122
Chemical kinetics, 122
Chemically frozen, 122
Chester, W., 142
Christian, J., 141
Collision frequency, 12, 119
Concentration, 112
Conical flowfield, 132
Constant, F., 49
Curvilinear coordinates, 97
Cylinder, 64, 128

Dalton's law, 112
Deceleration:
 peak re-entry value, 36
Dimensional analysis, 18
Dissociation, 113
Divergence form, 56
Dorrance, W., 142
Drag coefficient, 45, 76
Dutch roll, 47
Dyadic, 52
Dynamic equations, 46
 lateral, 46
 longitudinal, 46

Emissivity, 134
Energy balance, 140
Energy equation, 55
Enthalpy, 115, 116
Etkin, B., 49
Euler angles, 43

Fay-Riddell, 124, 142
Free molecule flow, 19

Gas properties, 17
Gazley, C., 22
Generalized configuration, 71
Glenn, J., 3
Gyroscopic stability, 47

Hankey, W., 80, 141, 142
Hayes, W., 80
Heat of vaporization, 6
Heat sink, 6
Heating:
 combined forms, 138
 conduction, 120
 interference, 125
 leading edge, 86
 lower surface, 89
 peak re-entry value, 35
 recombination, 120
 re-entry, 81
Hirshfelder, J., 22
Hypersonics, 60, 74

Induced pressures, 67
Integral methods, 105
Inviscid equations, 58

Kennard, E., 22
Kepler's laws, 28
Kinetic theory, 10
Kivel, B., 142
Knudsen number, 18

Lees, L., 80, 141
Lewis number, 18, 121
Lift coefficient, 45
Linearized equation, 59
Loh, W., 48

Mach number, 18
Materials, 4
 refractory, 7
Moment coefficient, 45
Momentum equation, 54

Navier-Stokes equations, 51, 53
Newtonian flow, 62, 83
Numerical methods, 109
Nusselt number, 18

Orbital mechanics, 25

- Parabolized Navier-Stokes, 57, 94
Patterson, G., 22
Perfect-gas law, 111
Phugoid, 36
Planform, 77
Potential flow, 59
Prandtl number, 18

Radiation, hot gas, 133, 137
Range modulation, 38
 lateral, 40
 longitudinal, 40
Real-gas effects, 92, 117, 135
Reattachment, 126
Recovery factor, 92
Reference enthalpy, 92
Relaxation time, 122
Reynolds' analogy, 6, 81, 102
Reynolds number, 18

Schlichting, H., 141
Separation, 126
Shapiro, A., 80
Shock/boundary-layer interaction, 129
Similarity solutions, 101
Skin friction, 68, 82
 laminar, 68
 turbulent, 69
Slip flow, 20

Sphere, 64
Stability, 42, 78
Stagnation region, 83, 105
Stephan-Boltzmann constant, 7
Stress tensor, 52, 93
Subsonic aerodynamics, 74
Substantial derivative, 52
Sweep angle, 87, 91
Tangent wedge theory, 65
Temperature:
 adiabatic wall, 92
 radiation equilibrium, 7
 stagnation, 5
Thermal barrier, 3, 79
Thermal protection, 6
Three-dimensional interaction, 131
Trajectory:
 ballistic, 31
 lifting, 29
 orbital decay, 33
Transformation, 99
Transport phenomena, 14
Transport properties, 10, 14
Trapezoidal rule, 110
Tridiagonal algorithm, 110
Triple point, 131

Vector analysis, 51